6-1-2021

Characterization of Proteostasis Mechanisms in Chlamydia trachomatis

Amanda M. Blocker
Southern Illinois University Carbondale, a.blocker23@yahoo.com

Follow this and additional works at: https://opensiuc.lib.siu.edu/theses

CHARACTERIZATION OF PROTEOSTASIS MECHANISMS IN CHLAMYDIA TRACHOMATIS

by

Amanda M. Blocker

B.S., Southern Illinois University, 2019

A Thesis
Submitted in Partial Fulfillment of the Requirements for the
Master of Science Degree

School of Biological Sciences
in the Graduate School
Southern Illinois University Carbondale
May 2021

THESIS APPROVAL

CHARACTERIZATION OF PROTEOSTASIS MECHANISMS IN CHLAMYDIA
TRACHOMATIS

by

Amanda M. Blocker

A Thesis Submitted in Partial

Fulfillment of the Requirements

for the Degree of

Master of Science

in the field of Molecular Biology, Microbiology, and Biochemistry

Approved by:

Dr. Derek J. Fisher, Chair

Dr. Bethany A. Rader

Dr. Lahiru N. Jayakody

Graduate School
Southern Illinois University Carbondale
April 6, 2021

AN ABSTRACT OF THE THESIS OF

Amanda M. Blocker, for the Master of Science degree in Molecular Biology, Microbiology, and Biochemistry, presented on April 6, 2021, at Southern Illinois University Carbondale.

TITLE: CHARACTERIZATION OF PROTEOSTASIS MECHANISMS IN CHLAMYDIA TRACHOMATIS

MAJOR PROFESSOR: Dr. Derek J. Fisher

Chlamydia trachomatis is a gram negative, obligate intracellular pathogen with a highly reduced genome of ~1 Mbp. It is the leading cause of the reportable sexually transmitted infection known as chlamydia in the United States and is the leading cause of preventable blindness (trachoma) worldwide. While treatment of infections is possible, weaknesses of current approaches include treatment failure, antibiotic-induced dysbiosis, and resistance development of bystander bacteria during chlamydial treatment. These weaknesses support the need for improved therapeutic approaches. *C. trachomatis* undergoes a biphasic developmental cycle with two forms, the infectious elementary body (EB) and replicative reticulate body (RB), that have unique protein profiles. Due to the differing proteomes of each developmental form, we hypothesized that mechanisms that facilitate protein turnover will be essential for progression of *C. trachomatis* through the developmental cycle making them ideal drug targets. This study focused on characterization of two caseinolytic protease (Clp) systems: the ClpX/P2/P1 system and the ClpC/P1/P2 / McsAB system. We predicted that ClpP1 and ClpP2 come together to form the proteolytic component, that ClpX and ClpC are unfoldases that unfold and linearize large substrates in an ATP dependent manner for ClpP-dependent proteolysis, and that McsAB are adaptor proteins with McsA activating the kinase McsB to tag proteins for degradation by the ClpC/P1/P2 complex. The Clp system has been

the focus of numerous studies as a target for novel antimicrobials and we hypothesized that the chlamydial Clp system would also be a druggable target. To assess the functionality of the Clp system, we successfully purified all components except McsB for use *in vitro* assays. Using oligomerization, peptide and protein degradation assays, and ATP hydrolysis assays, we characterized the activity of the ClpP1, ClpP2, and ClpX components individually and in complexes. We also measured the activity of a collection of ClpX mutants. In addition, we assessed the activity of ClpP-targeted activating compounds that were potent *in vivo* inhibitors of *C. trachomatis*. We demonstrated that ClpP2/P1 can form hetero-oligomers and degrade peptides and that ClpX has ATPase activity, can oligomerize, and can degrade an SsrA-tagged GFP when complexed with ClpP2/P1. While the activator studies did not support interactions with ClpP2/P1 under the conditions tested, assays were developed for further analysis of Clp-targeted compounds. Our *in vitro* results support that *C. trachomatis* possesses a functional Clp system. In addition, *in vivo* expression of ClpX mutants confirmed to lack activity in our *in vitro* assays led to reduced chlamydial fitness and alterations in development supporting our hypothesis that the Clp system is required for chlamydial development. Collectively, our results indicate that the Clp system is critical to *C. trachomatis* survival in cells and suggests that drugs altering Clp-function could be a novel approach for anti-chlamydial therapeutics.

ACKNOWLEDGMENTS

TABLE OF CONTENTS

LIST OF FIGURES

CHAPTER 1

INTRODUCTION

Organism Overview

Members of the family Chlamydiaceae are gram negative obligate intracellular bacteria characterized by a unique biphasic developmental cycle and reduced genome (~1 Mbp) (1, 2). This family contains the genus *Chlamydia*, which encompasses organisms responsible for a variety of serious diseases in both animals and humans. In general, these pathogens infect epithelial cells lining mucosal tissue and elicit damage through immunopathology. Many of the organisms in this genus are host restricted, including *Chlamydia suis* (swine), *Chlamydia muridarum* (rodents of the family Muridae), and *Chlamydia caviae* (guinea pigs) (1). However, other organisms within this genus are able to infect a variety of hosts and even cause zoonotic infections in humans (3). *Chlamydia felis* is endemic among household cats worldwide and *Chlamydia abortus* commonly infects ruminants, but both are also able to cause zoonotic infections in humans (1, 3). Of particular clinical importance to humans are the pathogens *Chlamydia pneumoniae, Chlamydia psittaci*, and *Chlamydia trachomatis*. *C. psittaci* is a zoonotic pathogen that is able to infect humans that come in contact with aerosolized bacteria from the respiratory tract or fecal material from infected birds causing the disease psittacosis (4). Although rare, failure to recognize the symptoms of psittacosis can result in severe respiratory disease or even death (4). *C. pneumoniae* is known to cause respiratory tract infections that can result in pneumonia and has also been implicated in chronic inflammatory diseases such as atherosclerotic cardiovascular diseases, Alzheimer's disease, and reactive arthritis (5). *C. trachomatis*, the focus of my research,

causes different forms of disease that have large public health implications, which are highlighted in the following pathology section.

Chlamydia trachomatis Pathology

      C. trachomatis has two different biovars: the oculogenital biovar with ocular tropic (serovars A-C) and genitourinary tropic strains (serovars D-K) and the lymphogranuloma venereum (LGV, serovars L1-L3) biovar which contains more invasive strains (6, 7). Serovars A-C of the ocular pathotype cause chronic ocular infections called trachoma that can lead to blindness (7). Trachoma is the leading cause of preventable blindness affecting over 1.9 million people worldwide (8). Serovars D-K of the genital pathotypes are responsible for the disease chlamydia, which is the leading cause of reportable bacterial sexually transmitted infections (STIs) world-wide and can infect the genital, oral, and rectal tissues (7). LGV serovars L1-L3 make up the minority of reported STIs, but unlike serovars D-K they can cause an invasive and systemic infection that moves from the initial site of infection to regional lymph nodes leading to lymphadenopathy (9). A major concern with chlamydia is that up to 50% of STI cases in men and up to 90% of cases in women can be asymptomatic resulting in failure to seek treatment (10). In women, untreated infections can allow *C. trachomatis* to ascend the reproductive tract and cause pelvic inflammatory disease, ectopic pregnancy, chronic pelvic pain, or even infertility (10). Despite its largely asymptomatic nature, chlamydia is the most commonly reported STI in the United States with 1.8 million reported cases in 2018 resulting in a national financial burden of over 600 million dollars (11). Despite the increasing prevalence of bacterial resistance to antibiotics amongst many important human pathogens, evidence of clinical resistance in *Chlamydia* isolates is rare with the

only known resistance marker being a tetracycline efflux pump found in *C. suis* (12).

Consequently, human infections can still be treated using tetracyclines (doxycycline),

macrolides (azithromycin), and fluoroquinolones (13, 14). While resistance is not

currently a clinical problem, there are weaknesses to the available chlamydia

therapeutic approach: 1) treatment failure can occur in 5-23% of the population (14),

and 2) the frontline drugs doxycycline and azithromycin are broad-spectrum antibiotics

that induce dysbiosis of the host's microbiome and increase the risk of resistance

development in other pathogens such as *Neisseria gonorrhoeae* (14-16). Novel,

Chlamydia-specific therapeutic targets could provide relief from treatment failure, drug-

induced dysbiosis, and non-chlamydial drug-resistance observed with current therapies.

Developmental Cycle

Chlamydia undergo a biphasic developmental cycle transitioning between the

infectious elementary body (EB) and the replicative reticulate body (RB) (fig. 1.1) (17).

Upon attachment to a mucosal epithelial cell, the EB is taken up into a host cell derived

vacuole via normal cellular endosomal-trafficking pathways (18). In a type III secretion

dependent manner, the EB will then transform its intracellular environment, known as

the inclusion, into a unique parasitophorous vacuole for two main reasons: 1) to avoid

normal trafficking through the host endocytic pathway so it is not degraded by

lysosomes and 2) to fulfill its nutritional needs via interaction with exocytic pathways

(17, 18). Within the inclusion, the small and compact EB (~0.3 µm in diameter)

transforms into the larger and less dense RB form (~0.9 µm) and around 12 hours post-

infection will begin replication and cell division to produce more RBs (19). Two models

are proposed for how *Chlamydia* divide: 1) binary fission, or 2) a recently proposed

budding model of division (19, 20). The RB then has two fates prior to commencing conversion into an EB: continued growth and division or transition into the persistent form. Persistence can result from unfavorable conditions within the host cell, such as in the case of exposure to antibiotics, cytokines (i.e. interferon-γ), or a nutrient-deficient environment including tryptophan or iron deprivation (21). If cellular conditions favorable for bacterial growth and replication remain in place, or once unfavorable conditions have subsided, the RBs will continue to grow and divide until 18-40 hours post-infection, when the RB population will asynchronously differentiate into EBs (17, 19). Finally, infectious EBs are released from the host cell to infect other host cells or new hosts (17).

The two different developmental forms of *Chlamydia* are unique in both structure and function. Structurally, EBs are only ~0.3 μm in diameter and have a rigid outer membrane despite the presence of little to no peptidoglycan. The rigid structure is likely due to highly cross-linked outer membrane protein complexes that are rich in cysteine residues. The presence of multiple cysteines is significant as EBs are oxidized compared to the RB form, which suggest that *Chlamydia* may use redox in conjunction with protein cysteine content to both stabilize the bacterial envelope and as a regulatory mechanism (22, 23). The EB form of *Chlamydia* is considered metabolically restricted due to its DNA being highly compacted by the bacterial histone-like proteins HctA and HctB hindering transcription and therefore translation. This developmental form of *Chlamydia* has been likened to be the "spore-like" form of the species with minimal energy processes maintained to support infection. The RB form is larger than an EB with a diameter of ~0.9 μm. The membrane structure is not as rigid as EBs and RBs

have the characteristic inner membrane and outer membrane as seen in other gram negative bacteria. In contrast to typical gram negative bacteria, *Chlamydia* are peptidoglycan-poor, with the cell wall localized to rings at the site of cell division (24). The highly compacted DNA as seen in EBs is relaxed to allow for initiation of transcription and translation allowing for metabolic and physiological processes in the RBs that promote growth and division within the host cell. The distinct physiological differences between the EB and RB forms are conferred by divergent protein profiles between the two forms, which is supported by multiple proteomic studies (25-27). One group that set out to examine the differing proteomic profiles of the two forms concluded that the proteome of EBs is primed for generating bursts of energy via glucose catabolism to fuel the developmental transition from EB to RB while the proteome of RBs is specialized for robust protein synthesis, accumulation of ATP, and nutrient transport (26). Antibiotics that target transcription and translation, such as doxycycline and azithromycin, can block differentiation from EB to RB, suggesting that *de novo* protein expression, synthesis, and subsequent homeostasis of these proteins is going to be required for intracellular growth and continuation of the developmental cycle (28). Clearly, protein turnover is essential for chlamydial development making the process an ideal therapeutic target, but there is a significant gap in our knowledge of how the proteome shifts are regulated and carried out.
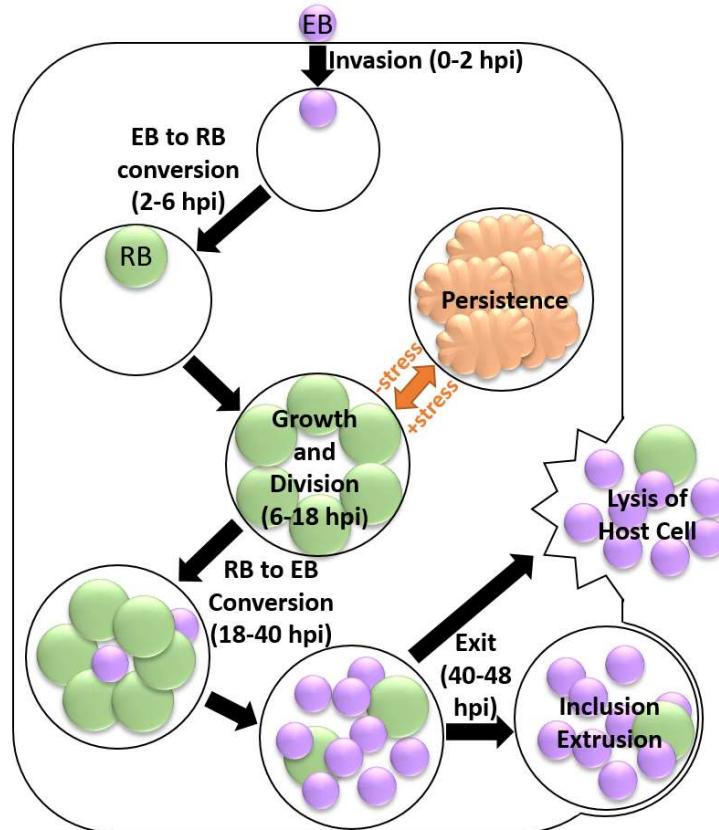
Figure 1.1. The chlamydial developmental cycle.

Protein Homeostasis

      Protein homeostasis, also referred to as proteostasis, is essential for bacteria to

survive in dynamic environments that support optimal growth or present stressors such

as temperature, osmotic shock, oxidation, immune factors, and toxics including

antibiotics (29, 30). Upon exiting the ribosome, the polypeptide is exposed to a highly

crowded cellular environment and it is essential that newly synthesized proteins are

able to fold into their functional, native state. If the protein is unable to fold unassisted,

then it will need the help of specialized proteins called chaperones (31, 32). Despite

extra help from chaperones, sometimes a nascent protein may find itself tangled in a

self-aggregate or with other proteins. In addition, proteins can become damaged

overtime, may lose their conformation due to environmental insults, or are no longer

6

needed due to physiological changes in the bacterium such as developmental changes as observed for the chlamydial RB/EB. To deal with these "protein problems" bacteria have a collection of chaperones that work independently or as complexes and are generally assigned into three categories based on function (with some overlap between them): folding, disaggregation, and degradation (fig. 1.2) (33).

The first type of proteins involved in protein homeostasis are those that perform protein folding and/or refolding. A common chaperone system used for protein (re)folding is the ATP-dependent GroEL/ES system (34, 35). The GroEL tetradecamer has hydrophobic amino acids, which bind and capture non-native proteins that need to be refolded. Upon association of the protein substrate with the GroEL barrel, the GroES "cap" will associate with the complex and drive the protein substrate farther into GroEL. Next, in an ATP-dependent manner, the protein is refolded and subsequently released in its native form (35). Uniquely, *Chlamydia* have three GroEL homologs, but with only one being essential for growth in cell culture and likely serving the role as the bona-fide GroEL-GroES chaperone (36).

The second type of chaperones involved in proteostasis are those that resolve aggregates. Aggregates typically arise from two scenarios. Under normal conditions, some proteins may require molecular chaperones to complete folding, but if these chaperones are not readily available, it can lead to the problematic presence of unfolded proteins in the cytoplasm that interact to form aggregates. Alternatively, under stressful conditions, a protein can lose its noncovalent interactions and have its secondary and tertiary structures disrupted, leading to unfolding of the protein. Often times, this loss of structure can cause the unfolded protein to assume a structure that

7

deviates from its functional state through the formation of non-native interactions to form aggregates (37). Protein aggregates can be cytotoxic to cells via trapping other cellular proteins or by physically blocking cellular processes (38), so the cell needs to have mechanisms to not only resolve aggregates, but also to prevent their formation. The DnaJK/GrpE and ClpB bichaperone machinery is one example of molecular chaperones working together to resolve protein aggregates. Within this system, small heat shock proteins bind the proteins within the aggregate and maintain them in a near-native state until displaced by DnaJ and DnaK. GrpE acts as a nucleotide exchange factor for DnaK, swapping ADP for ATP following DnaK ATP hydrolysis. DnaK will then recruit the ClpB disaggregase, which will activate its ATPase activity to extract substrates from the aggregate where they can then be refolded (such as by the GroEL/ES system) or degraded (37).

Before proteins are able to form these aggregates, bacteria can maintain a functional proteome by tagging proteins directly for degradation. In the bacterial periplasm, including *Chlamydia* is a protease designated as DegP. This protease functions upon initiation of the bacterium's heat shock response to degrade partially folded proteins denatured by elevated temperatures. Additionally, DegP is able to act as a "holding" chaperone to prevent the formation of aggregates within the periplasm (33, 39).

In the cytoplasm, bacteria can maintain functional proteomes by proteolytic families such as the Lon proteases or the caseinolytic proteases (Clp) (fig. 1.3) (40). Both of these degradation machineries fall into the AAA+ protein family (<u>A</u>TPases <u>a</u>ssociated with various cellular <u>a</u>ctivities) due to their similar ATP-driven degradation

mechanisms (40, 41). After binding of the substrate, the protease linearizes the target through the use of ATP, enabling the unfolded substrate to be fed into the proteolytic chamber and subsequently degraded (41). The Lon protease functions using a catalytic dyad of serine and lysine with a hypothesized structure of a three-tiered hexagonal cylinder (42-44). Unregulated protease activity is typically lethal for bacteria as seen with the overexpression of the Lon protease in *Escherichia coli* (45). To avoid improper protease activity, *E. coli* and other bacteria rely on the recognition of specific degradation tags, known as degrons, to keep proteolysis in check. In addition to Lon protease, the other cytoplasmic protease system commonly found in bacteria is the Clp protease, which is the focus of this thesis.
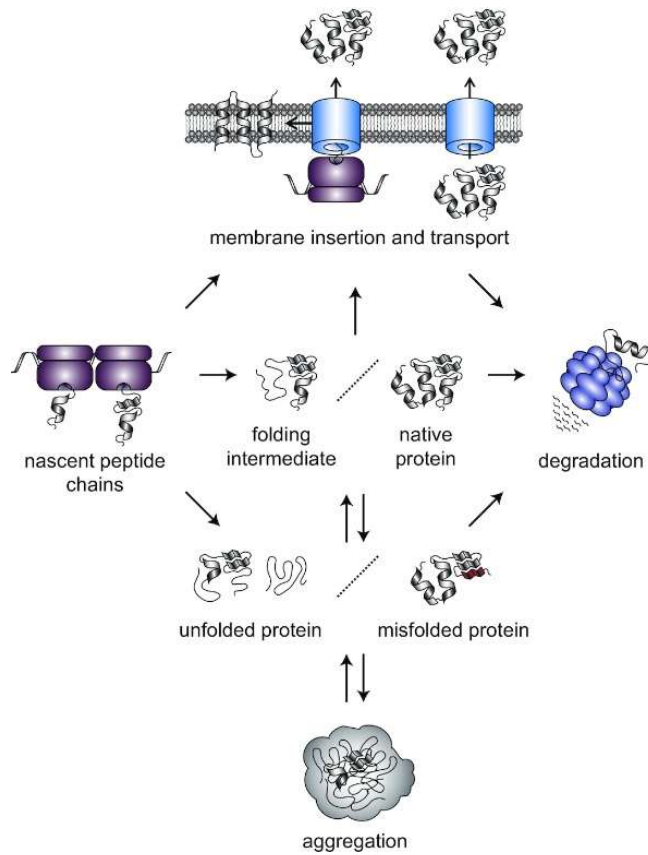
Figure 1.2. Overview of the major proteostasis processes in bacteria. Used with permission from Oxford University Press through Copyright Clearance Center's RightsLink® service (37).

9

Clp Proteases

The caseinolytic proteases (Clp) are a class of proteases that utilize a highly conserved serine protease core, ClpP, in conjunction with various adaptor proteins. The ClpP protease possesses a catalytic triad (active site) of a serine, histidine, and an aspartic acid (46, 47). Structurally, ClpP orthologs are similar in that they form two heptameric rings that come together to form the functional tetradecamer with each monomer containing its own active site. Some bacteria, such as *E. coli* and *Bacillus subtilis*, have homo-tetradecamers in which all of the monomers are from a single ClpP. However other bacteria, such as *Chlamydia*, *Mycobacterium tuberculosis*, and *Pseudomonas aeruginosa*, encode two orthologs of ClpP instead of one, so these orthologs can form homo-heptamers (ClpP1$_7$ or ClpP2$_7$) that come together to form a hetero-tetradecamer (ClpP1$_7$ plus ClpP2$_7$) (48, 49). The compartmentalized structure of the tetradecamer effectively shields the active sites of ClpP from the cytoplasm so they will not interact with unintended targets (50).

The ClpP complex itself is only able to degrade small substrates (<5 kDa), however it is able to interact and degrade larger substrates with the help of AAA+ (ATPases associated with various cellular activities) unfoldases such as ClpX, ClpA, and ClpC (51, 52). The unfoldases form homo-hexamers that interact with the ClpP tetradecamer protease complex. The unfoldase, in an ATP-dependent manner, recognizes the degron on a condemned protein, unfolds its tertiary structure, and translocates the unfolded substrate into the ClpP barrel for degradation into peptide fragments (53). Clp proteases have been shown to play essential roles in cells such as removing damaged, denatured, and aberrantly folded proteins that are harmful to the

cell and they are also important for bacterial virulence (52, 53). As such, efforts have

been made to develop drugs that target these systems as novel approaches for

treatment of bacterial infections. Typically, Clp-targeted drugs act as either inhibitors or

activators of the system. Inhibitors usually target unfoldases and inhibit the activity of it

so the system can no longer maintain homeostasis (54). Activators make the Clp

system hyperactive, such as increasing the size of the ClpP proteolytic barrel alleviating

the need for an unfoldase and leading to uncontrollably degradation of proteins within

the cell (55). *Chlamydia* encode two adaptors, ClpX and ClpC, and two proteases,

ClpP1 and ClpP2. We hypothesize that these systems are essential for chlamydial

development making them druggable targets. Furthermore, we hypothesize that a

ClpX/P2/P1 system is needed for *trans*-translation and cell division and that a

ClpC/P1/P2 / McsAB system is used to degrade phospho-arginine tagged proteins.
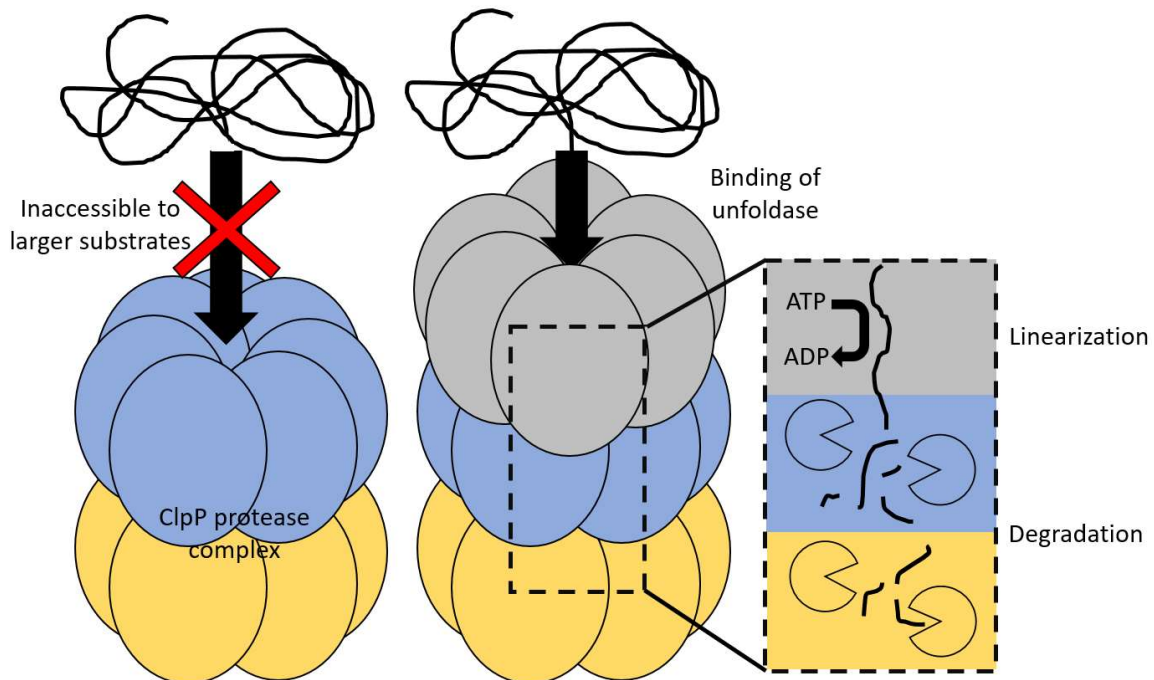
Figure 1.3. General structure and mechanism of Clp systems. ClpP can form homomeric barrels or heteromeric barrels as pictured where yellow would be ClpP1 and blue would be ClpP2.

ClpXP system

   The ClpXP system can serve various functions in cells. A common function of the

ClpXP is degrading tagged proteins produced by *trans*-translation. *Trans*-translation

occurs when a ribosome is stalled on a transcript lacking a stop codon and in general

resolves mRNA problems in the cell (56). Ribosome stalling on damaged mRNA results

in partially translated peptides, which can present a potentially dangerous situation to

bacteria as these truncated products can have a dominant negative effect on growth in

addition to trapping ribosomes on non-productive transcripts (57). Before the ribosome

can be rescued, a hybrid RNA called the tmRNA binds to SmpB and becomes

aminoacylated by alanyl-tRNA synthetase. GTP-bound EF-Tu binds this charged

tmRNA so that it is ready to interact with the stalled ribosome. Once charged, this

tmRNA complex recognizes and binds to the 3' end of the mRNA to enter the A-site of

the ribosome. Via transpeptidation, the truncated polypeptide transfers over to the

tmRNA. The tRNA that had the truncated polypeptide is displaced from the P site of the

ribosome utilizing the GTP from EF-TU so it can be replaced with the truncated

polypeptide now cross-linked to the tmRNA. The freed mRNA transcript that did not

contain a stop codon can then be degraded by RNases within the cell. Translation can

then resume using the tmRNA as a template, and this will result in addition of a C-

terminal SsrA degradation tag. Once the stop codon within the tmRNA is reached, the

tagged protein and the ribosome are released, and the tagged protein is degraded by

targeted proteolysis via the Lon protease, Tsp protease, or the ClpXP system (fig. 1.4)

(56, 58).

While degrading products of the *trans*-translation system is an important role of the ClpXP complex, it is not the only role that it can serve. The N-terminus of ClpX contains a zinc-binding domain (ZBD) important in binding adaptor proteins so that the ClpX can be tailored to degrade other types of °proteins based on their degradation tag (59, 60). In organisms with developmental forms such as *Caulobacter*, its essential ClpXP system can be modulated by the addition of a number of adaptor proteins and the more that bind, the narrower the specificity for substrates (61, 62). This demonstrates the potential range in substrates that the ClpXP system can degrade. In addition to the ZBD motif, *Chlamydia*'s ClpX contains other conserved motifs associated with AAA+ unfoldases including the Walker A and Walker B motifs associated with ATP binding and ATP hydrolysis respectively, the IGF loop important for ClpX binding to ClpP, and the RKH motif associated with substrate recognition (specifically SsrA tag recognition associated with *trans*-translation) (47, 53, 60). Mutation of these motifs can alter ClpX function and inhibit chlamydial growth as demonstrated *in vivo* by our group, in which an overexpressed ClpX Walker B motif mutant led to abnormal developmental forms that appeared multinucleated and having abnormally condensed intermediate forms (60). Further characterization of the ClpXP system in *Chlamydia* will be essential to delineate its role(s) in chlamydial growth and for future studies aimed at developing ClpX-targeted therapeutics.
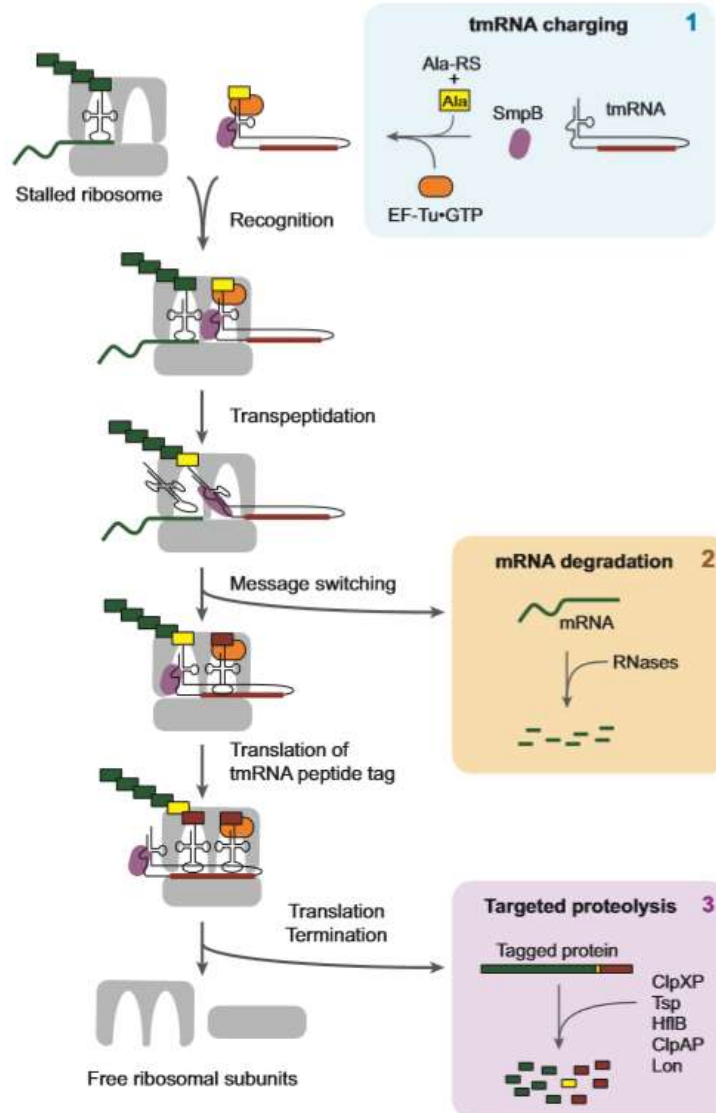
Figure 1.4. Process of *trans*-translation. Used with permission from Annual Review of Microbiology through Copyright Clearance Center's RightsLink® service (56).

McsAB and ClpCP System

The McsAB and ClpCP system, based on literature review, is almost exclusively a gram positive system, except for *Chlamydia* which is gram negative. It is best characterized in *B. subtilis*, where the McsAB and ClpCP system is involved in degradation of phosphoarginine-tagged proteins. The ClpCP complex functions similarly to the ClpXP in that ClpP serves as the proteolytic component and ClpC functions as

the unfoldase in an ATP-dependent manner (63). McsA is the activator of McsB, which functions as an arginine kinase in *B. subtilis*. Under normal, non-stress inducing conditions, ClpCP sequesters McsB rendering it inactive. Upon stress-inducing conditions such as increased temperature, McsB will be released from ClpCP and activated by McsA. In keeping with a heat-related stress response, the repressor CtsR will dissociate from DNA and be phosphorylated on conserved arginine residues by the activated McsB. The various arginine phosphorylation of CtsR by McsB prevents CtsR from rebinding to its target DNA allowing for transcription of heat stress response genes (64). McsB also serves as an adaptor protein, so it will deliver the arginine-phosphorylated CtsR to the ClpCP complex where it can be degraded. McsB can also phosphorylate damaged proteins targeting them to ClpCP for degradation. To return the McsB system back to the resting state in *B. subtilis*, one of two things can happen: 1) the phosphatase YwlE can dephosphorylate McsB to return it to its inactive state or 2) McsB can be degraded by the ClpCP complex (65). Interestingly, there is no annotated homolog of the YwlE phosphatase found in *Chlamydia*. This could mean that the McsB in *Chlamydia* is degraded once it is no longer needed, as is seen in *B. subtilis*. A second potential solution is that the YwlE homolog escapes annotation as *Chlamydia* are phylogenetically distinct from *B. subtilis*. Alternatively, since *Chlamydia* has a small genome of only 1 Mbp, it is possible that an already annotated phosphatase in *Chlamydia* also functions in dephosphorylating the system and returning it to a resting state. Dual functionality of proteins within *Chlamydia* is a common theme. One example is CppA, which is a PP2C-type phosphatase that can dephosphorylate P-serine, P-threonine, and unexpectedly P-tyrosine (66). Another examples is the Npt1 ATP/ADP

translocase which is also able to transport NAD$^+$ (67). A fourth solution is that McsB will function as both a kinase and its own phosphatase, such as seen in *Geobacillus stearothermophilus* (68). Along with the chance of missing a YwlE, another missing component of this system is the transcriptional regulator CtsR, although this is only one target protein of the system and may simply reflect differing physiological needs between *Chlamydia* and *Bacillus*. The exact function and mechanisms of action of the McsAB and ClpC proteins in *Chlamydia* remain to be determined.

Statement of the Problem

Chlamydia is the most commonly reported bacterial STI in the United States and its negative impact on both human health and healthcare costs are highly significant. *Chlamydia* undergoes a biphasic developmental cycle alternating between two different forms and the protein profiles between the two forms varies dramatically (26). We hypothesize that the mechanisms that drive the differentiation of protein profiles, such as protein degradation systems, are essential for *Chlamydia*'s progression through the developmental cycle. The McsAB / ClpC/P1/P2 system and ClpX/P2/P1 systems of *Chlamydia* are excellent candidates for both proteostasis and development, are largely uncharacterized, and their actions represent a significant gap in our understanding of basic chlamydial biology. Further understanding of these systems could provide new therapeutic targets for improved treatment of chlamydial infections.

CHAPTER 2

MATERIALS AND METHODS

Bacterial Culture Conditions

All strains constructed and used in this study are listed in Appendix A. *E. coli*

cloning strains DH5α and XL-1 blue (except those containing pHT08) and *E. coli* protein

production strain BL21 (DE3) were routinely grown and maintained using Luria-Bertani

(LB) broth and agar plates containing either 100 µg/mL ampicillin (Amp) or 20 µg/mL

chloramphenicol (Cm) as dictated by vector usage. *E. coli* cloning strains containing

pHT08 clones were grown and maintained on 2xYT broth and agar plates containing 50

µg/mL ampicillin. All *E. coli* BL21 (DE3) ΔPAX protein production clones (parent strain

provided by Dr. Peter Sass, University of Tuebingen) were grown using LB broth and

agar plates supplemented with 100 µg/mL ampicillin, 20 µg/mL chloramphenicol, and 50

µg/mL kanamycin (Kan). All *B. subtilis* clones were grown and maintained using 2xYT

media. *B. subtilis* clones with the vector pHT08 were grown in the presence of 5 µg/mL

chloramphenicol and if pHT08 was in a mutant *B. subtilis* (such as *B. subtilis* 168

Δ*mcsA* and *B. subtilis* 168 Δ*mcsB*), then kanamycin was also added to a final

concentration of 5 µg/mL.

Strain Construction

E. coli Strain Construction

Gene sequences were obtained from the NCBI database using genome

sequences for *C. trachomatis* 434/Bu (LGV serovar L2 strain, NC_010287.1), *E. coli*

K12 (NC_000913.3), or *B. subtilis* 168 (NC_000964.3). All clones containing either

pLATE31 or pLATE52 were generated using the Ligation Independent Cloning (LIC)

17

method as directed (Thermo Scientific). Genes were amplified by PCR using Phusion High-Fidelity PCR Master Mix with their respective primers (listed in Appendix C). Upon amplification, products were run on an agarose gel, visualized using ethidium bromide staining and UV transillumination, and then extracted and purified using the GeneJET Gel Extraction Kit (Thermo Scientific). The PCR/pLATE product was then used for chemical transformation into the respective *E. coli* cloning strain. Transformants were subject to colony PCR using Fermentas Master Mix (Thermo Scientific) and the respective primers (Appendix C) to confirm insertion of the gene into the vector. PCR confirmed clones were struck out for isolation onto 100 μg/mL ampicillin LB plates, grown in LB broth supplemented with ampicillin, and the plasmid isolated using the GeneJET Plasmid Miniprep kit (Thermo Scientific). Upon sequence verification of the insert (performed by Psomagen), plasmids were transformed via electroporation into either *E. coli* BL21 (DE3) or *E. coli* BL21 (DE3) ΔPAX.

All clones containing pACYCDuet-1 were generated via restriction digestion of the vector with either multiple cloning site (MCS) #1 using FastDigest Restriction Enzymes BamHI and NotI or MCS#2 using FastDigest Restriction Enzymes NdeI and XhoI (Thermo Scientific). Gene inserts were amplified by PCR using Phusion High-Fidelity PCR Master Mix with their respective primers (listed in Appendix C). Upon amplification, products were run on an agarose gel, and then extracted and purified using GeneJET Gel Extraction Kit (Thermo Scientific). PCR products were digested with the respective restriction enzymes and then cleaned up using the GeneJET PCR Purification Kit. The digested PCR products and vector were ligated at a 3:1 free-ends ratio overnight at 4°C in T4 ligation buffer using T4 DNA ligase (Thermo Scientific). The

next day, ligation reactions were chemically transformed into XL-1 Blue *E. coli* and plated onto LB plates containing 20 µg/mL chloramphenicol. Transformants were subject to colony PCR using Fermentas Master Mix (Thermo Scientific) and the respective primers (Appendix C) to confirm insertion of the gene into the vector. Confirmed clones were struck out for isolation and grown in LB broth containing chloramphenicol so the plasmid could be isolated using the GeneJET Plasmid Miniprep kit (Thermo Scientific). Upon sequence verification, clones that had only one gene insert were transformed via electroporation into *E. coli* BL21 (DE3). For clones that were to contain genes in both MCS#1 and MCS#2, the digestion process was repeated so the other gene that was not already in the pACYCDuet-1 could be inserted. All clones were sequence verified and transformed via electroporation into *E. coli* BL21 (DE3).

All clones containing pGex-6p-1 or pMAL-c5X were generated via restriction digestion and insertion. Genes were amplified by PCR using Phusion High-Fidelity PCR Master Mix with their respective primers (listed in Appendix C). Upon amplification, products were run on an agarose gel, and then extracted and purified using GeneJET Gel Extraction Kit (Thermo Scientific). For pGex-6p-1 clones, the vector and PCR products were digested at 37°C for 1 hour using the FastDigest Restriction Enzymes BamHI and XhoI (Thermo Scientific). For clones containing pMAL-c5X, DNA was digested at 37°C for 1 hour using the FastDigest Restriction Enzymes BamHI and NotI (Thermo Scientific). Digested PCR products were cleaned up using the GeneJET PCR Purification Kit and vectors were agarose gel purified and isolated with the GeneJET Gel Extraction Kit (Thermo Scientific). The digested PCR products and vector were ligated at a 3:1 free-ends ratio overnight at 4°C in T4 ligation buffer using T4 ligase

(Thermo Scientific). The next day, ligation reactions were chemically transformed into *E. coli* XL-1 and plated onto LB plates with 100 µg/mL ampicillin. Transformants were subject to colony PCR using Fermentas Master Mix (Thermo Scientific) to confirm insertion of the gene into the vector. Confirmed clones were struck out for isolation and grown in broth culture so the plasmid could be isolated using the GeneJET Plasmid Miniprep kit (Thermo Scientific). All clones were sequence verified and then transformed via electroporation into *E. coli* BL21 (DE3) ΔPAX.

All pHT08 clones were generated via restriction digestion and insertion. Genes were amplified by PCR using Phusion High-Fidelity PCR Master Mix with their respective primers (listed in Appendix C). Upon amplification, products were run on an agarose gel, and then extracted and purified using the GeneJET Gel Extraction Kit (Thermo Scientific). The entire reaction mixture was then digested at 37°C for 1 hour using the FastDigest Restriction Enzymes BamHI and SmaI (Thermo Scientific). Digested products were cleaned up using the GeneJET PCR Purification Kit. The pHT08 vector was also digested at 37°C for 1 hour using the same restriction enzymes, incubated for an additional 15 minutes at 37°C upon addition of FastAP (Thermo Scientific), and then the product was isolated following extraction from the agarose gel. The digested PCR products and vector were ligated at a 3:1 free-ends ratio overnight at 4°C in T4 ligation buffer using T4 DNA ligase (Thermo Scientific). The next day, ligation reactions were chemically transformed into DH5α *E. coli* and plated onto 2xYT plates containing 50 mg/mL ampicillin. Transformants were subject to colony PCR using Fermentas Master Mix (Thermo Scientific) to confirm insertion of the gene into the vector. Confirmed clones were struck out for isolation and grown in broth culture so the

plasmid could be isolated using the GeneJET Plasmid Miniprep kit (Thermo Scientific).

Upon sequence verification, plasmids were transformed via either electroporation or

natural competence into the respective *B. subtilis* strains.

Bacillus subtilis Transformation via Electroporation

Strains were grown in 5 mL of 2xYT media and appropriate antibiotics when

necessary at 37°C with vigorous shaking overnight. The next day, 500 µL of the

overnight cultures were transferred to 50 mL of 2xYT media and grown with shaking at

37°C until an OD_{600} of 0.2 was achieved. The culture was then supplemented with 1%

w/v DL-threonine, 2% w/v glycine, 0.1% w/v tryptophan and 0.03% v/v Tween 80

prepared in 2xYT and allowed to continue shaking at 200 rpm for an additional hour at

37°C. The culture was cooled on ice for 20 minutes and then spun down at 5000 x g for

10 minutes at 4°C. The pellet was washed twice with 10 mL of electroporation buffer (all

buffers and their components are listed in Appendix B) with the final pellet being

resuspended in 100 µL of electroporation buffer. One µg of the desired plasmid was

added to the final resuspension mixture and transferred to an ice-cold 2 mm cuvette.

The cells were shocked using the BioRad GenePulser Xcell at 2500 V, 200 Ω, and 25

µF and immediately transferred to 1 mL of 2xYT media supplemented with 0.5 M

sorbitol and 0.38 M mannitol. The culture was recovered at 37°C for 3 hours with

shaking at 100 rpm. The entire culture was then spun down and all but 100 µL of

supernatant removed. The pellet was resuspended in the remaining supernatant, plated

onto selective media, and incubated at 37°C overnight.

Bacillus subtilis Transformation via Natural Competence

To prepare competent *B. subtilis* cells, an overnight culture of recipient cells was incubated at 37°C under vigorous agitation in 5 mL of HS medium. 50 mL of HS medium was inoculated to an OD_{600nm} of 0.05 using the overnight culture and then incubated under vigorous shaking at 37°C. The growth curve was recorded every 30 minutes and immediately upon transition from exponential to stationary phase (OD_{600nm} ~ 1), 10 mL samples were taken every 15 minutes for a total of 4 samples. One mL of sterile 87% v/v glycerol was added to each sample, mixed, and left on ice for 15 minutes. After the 15 minutes, samples were fractionated into 1 mL aliquots, snap frozen in liquid nitrogen, and stored at -80°C. The next day, an aliquot was thawed at 37°C and used to inoculate 20 mL LS medium. Cells were than shaken slowly in a 30°C water bath for 2 hours to obtain maximal competence. After 2 hours, 1 mL aliquots were transferred to plastic reaction tubes (Caplugs Evergreen sterile 5 mL polystyrene test tubes) containing 10 μL of 0.1 M EGTA (pH 7.2) and incubated at room temperature for 5 minutes. One μg of plasmid was added and the reaction mixture was incubated for 2 hours at 37°C with vigorous shaking. After 2 hours, the reaction mixture was spun down at 5,000xg for 3 minutes, all but 100 μL of supernatant was removed, the pellet was resuspended in the remaining supernatant, plated onto selective 2xYT medium containing 5 μg/μL of chloramphenicol, and finally incubated at 37°C overnight.

Bacillus subtilis Colony PCR

A single colony was resuspended in elution buffer (10 mM Tris-HCl, pH 8.5) from the Thermo Scientific GeneJET Plasmid Miniprep Kit in a 1.5 mL Eppendorf tube. The tube was wrapped with parafilm and a hole was made in the top to allow for ventilation.

The tube was then incubated for 5 minutes on ice followed by microwaving for 1 minute and then immediately returned to ice for 30 seconds. This was repeated for a total of three times in the microwave. Following the final microwave step, the tubes were incubated on ice for 5 minutes. Samples were spun down at 5000 x g for 5 minutes at 4°C so that 1 µL of the supernatant could be used immediately in the PCR reaction.

Codon Optimization

DNA sequences for *C. trachomatis* 434/Bu McsA and McsB were obtained from the National Center for Biotechnology Information (NCBI) database and entered into codon optimization tools offered by both NovoPro and Integrated DNA Technologies (IDT). NovoPro generated graphs to show improvement in codon selection compared to the targeted expression system preferred codon usage (*E. coli* or *B. subtilis*). The optimized IDT sequences were also entered into the NovoPro optimization tool to assess improvement of the IDT optimized sequence and a double optimized sequence. NovoPro, IDT, and double optimized sequences were compared and codons that fell well below 20% of relative adaptiveness were replaced with codons that had a higher percent of relative adaptiveness as determined by NovoPro. After codon optimization, gBlocks were ordered from IDT and cloned into pHT08 or pLATE52 as previously described.

Confirmation of Protein Production

Bacillus subtilis SDS-PAGE Protein Sample Preparation

One mL of *B. subtilis* culture was resuspended in 100 µL of *B. subtilis* SDS Lysis Buffer and 3 µL of 50 mg/mL lysozyme was added. The sample was incubated at 37°C for 5 minutes. Twenty-five µL of *B. subtilis* 5X SDS Sample Buffer was added and mixed

well. The sample was heated at 95°C for 5 minutes. The sample was then centrifuged at 13,000 x g for 2 minutes and 10 µL of the supernatant was loaded onto SDS-PAGE gels.

<u>Urea Denaturing Purification</u>

C-terminal 8xHis-tagged *Bs* McsA and McsB, codon optimized gBlock *Ct* McsA and McsB, and N-terminal 6xHis-tagged codon optimized gBlock *Ct* McsB were purified from a 15 mL culture of either *Bs* ΔA (*Bs* McsA and *Ct* McsA), *Bs* ΔB (*Bs* McsB and 8xHis-tagged *Ct* McsB), or *E. coli* BL21(DE3) ΔPAX (6xHis-tagged *Ct* McsB). Cultures were induced for 2.5 hours at 37°C with 1 mM IPTG. After induction, cultures were pelleted by centrifugation and stored at -80°C overnight. The next day, pellets were resuspended in urea lysis buffer, sonicated, pelleted, and the supernatant was transferred to prepared HisPur Cobalt Resin and rotated end over end for 30 minutes. HisPur Cobalt Resin (Thermo Scientific) was prepared by washing it twice in 150 µL of urea lysis buffer. The proteins were then washed 3x with urea lysis buffer and eluted four times using urea elution buffer. Samples taken throughout the purification were then mixed with Laemmli buffer with BME and run on 12% SDS-PAGE gels and protein was detected using Coomassie Brilliant Blue Brilliant Blue Brilliant Blue staining. Note that urea treated samples were not heated prior to gel analysis. Images were acquired using a BioRad ChemiDoc MP Imaging System.

<u>*E. coli* Protein Induction and Solubility Trials</u>

Proteins expressed in *E. coli* were confirmed by western blot. Proteins were then tested for optimal solubility by altering three variables: isopropyl β-D-1-thiogalactopyranoside (IPTG) concentration, induction time, and induction temperature.

Strains to be tested were grown in 50 mL of the respective media and supplemented with appropriate antibiotics. Upon reaching OD_{600nm} between 0.6 and 0.8, cultures were induced with varying amounts of IPTG and subject to different incubation times and temperatures. Upon completion of the experimental induction conditions, cultures were split into 15 mL aliquots, spun down, and store at -80°C overnight. The next day, pellets were resuspended in 3 mL of the experimental lysis buffers and sonicated. Pre-induction, post-induction, non-soluble (pellet), and soluble (supernatant) samples were mixed with Laemmli containing BME, heated, and run on SDS-PAGE gels. Protein was detected using Coomassie Brilliant Blue Brilliant Blue Brilliant Blue staining.

Bacillus subtilis Induction Trials

Proteins expressed in _B. subtilis_ were also tested for optimal solubility using three variables: isopropyl β-D-1-thiogalactopyranoside (IPTG) concentration, induction time, and induction temperature. Strains to be tested were grown in 50 mL of the respective media supplemented with appropriate antibiotics. Upon reaching OD_{600nm} between 0.6 and 0.8, cultures were induced with varying amounts of IPTG and subject to different incubation times and temperatures. After induction, cultures were split into 15 mL aliquots, spun down, and suspended in 300 μL of urea lysis buffer. Samples were then sonicated, spun down, and the supernatant was transferred to 30 μL of pre-equilibrated HisPur Cobalt Resin. The resin and supernatant were mixed end over end for 30 minutes to allow protein binding. After 30 minutes, the resin was spun down and the supernatant was removed. The resin was washed twice with 60 μL of urea lysis buffer, resuspended in Laemmli with BME, and stored at -20°C until samples were assessed on 12% SDS-PAGE gels.

Protein Purification

<u>Purification of recombinant wild-type and mutant ClpP proteins</u>

C-terminal 6xHis-tagged *C. trachomatis* ClpP1, *C. trachomatis* ClpP2, and *E. coli* ClpP were purified from 500 mL cultures of *E. coli* BL21(DE3) ΔPAX containing the respective plasmids as described in Seleem *et al*. (55). Briefly, cultures were induced for 20 hours at 18°C with 0.5 mM IPTG. After induction, cultures were pelleted and stored at -80°C overnight. Samples were suspended in ClpP lysis / wash buffer, sonicated, spun down to separate the nonsoluble and soluble fractions, filtered using 0.45 μm filters, and rotated end over end for 1 hour with HisPur Cobalt Resin (Thermo Scientific). After binding, the resin was washed using the ClpP lysis / wash buffer to remove contaminating proteins. Proteins were then eluted from the resin using the ClpP elution buffer and collected. After four elution steps, the buffer was exchanged to ClpP storage buffer using a Millipore Amicon Ultra 15 filtration units (3 kDa cut-off). ClpP proteins were then quantified using the Bio-Rad Protein assay, assessed for purity on 12% SDS-PAGE gels with Coomassie Brilliant Blue staining, and identified using anti-His-tag western blot. Blotting was performed using a mouse monoclonal anti-6xHis antibody (1:1000; Millipore HIS.H8) and a goat anti-mouse IgG HRP conjugated secondary antibody (1:2000). Protein samples were aliquoted and stored at -80°C.

<u>Purification of Recombinant ClpX:</u>

C-terminal 6xHis-tagged *C. trachomatis* ClpX and ClpX mutants were purified from 500 mL cultures of *E. coli* BL21(DE3) ΔPAX containing the respective plasmids as described in Wood *et al*. (60). Briefly, cultures were induced for 20 hours at 18°C with 0.5 mM IPTG. After induction, cultures were pelleted and stored at -80°C overnight.

Samples were suspended in ClpX lysis / wash buffer, sonicated, spun down to separate the nonsoluble and soluble fractions, filtered using 0.45 µm filters, and rotated end over end for 1 hour with HisPur Cobalt Resin (Thermo Scientific). After binding, the resin was washed using the ClpX lysis / wash buffer to remove contaminating proteins. Proteins were then eluted from the resin using the ClpX elution buffer and collected. After four elution steps, the buffer was exchanged to ATPase assay buffer using a Millipore Amicon Ultra 15 filtration units (3 kDa cut-off). ClpX proteins were then quantified using the BioRad Protein assay, assessed for purity on 10% SDS-PAGE gels with Coomassie Brilliant Blue staining, and identified using anti-His-tag western blot. Blotting was performed using a mouse monoclonal anti-6xHis antibody (1:1000; Millipore HIS.H8) and a goat anti-mouse IgG HRP conjugated secondary antibody (1:2000). Protein samples were aliquoted and stored at -80°C.

Purification of Recombinant GFP

N-terminal 6xHis-tagged GFP was purified from a 500 mL culture of *E. coli* BL21 (DE3) ΔPAX containing the respective plasmids. Cultures were induced for 6 hours at room temperature with 0.5 mM IPTG. After induction, cultures were pelleted and stored at -80°C overnight. Samples were resuspended in GFP lysis buffer, sonicated, spun down to separate the nonsoluble and soluble fractions, filtered using 0.45 µm filters, and rotated end over end for 1 hour with HisPur Cobalt Resin (Thermo Scientific). After binding, the resin was washed using the GFP wash buffer to remove contaminating proteins. Proteins were then eluted from the resin using the GFP elution buffer and collected. After four elution steps, the buffer was exchanged to GFP storage buffer using a Millipore Amicon Ultra 15 filtration units (3 kDa cut-off). GFP proteins were then

quantified using the BioRad Protein assay, assessed for purity on 12% SDS-PAGE gels with Coomassie Brilliant Blue staining, and identified using anti-His-tag western blot. Blotting was performed using a mouse monoclonal anti-6xHis antibody (1:1000; Millipore HIS.H8) and a goat anti-mouse IgG HRP conjugated secondary antibody (1:2000). Fluorescence was confirmed by spotting samples on slides for fluorescence microscopy and in 96 well plates for analysis with a BioTek Synergy H1 plate reader at excitation λ = 465 nm and emission λ = 535 nm. Protein samples were aliquoted and stored at -80°C.

Purification of pACYCDuet-1 His-tagged McsA

N-terminal 6xHis-tagged *Ct* McsA was purified from a 50 mL culture of *E. coli* BL21(DE3). The culture was induced for 10 hours at 37°C with 1 mM IPTG. After induction, the culture was pelleted and stored at -80°C overnight. The pellet was suspended in pACYCDuet-1 McsA lysis buffer, sonicated, spun down to separate the nonsoluble and soluble fractions, filtered using 0.45 μm filters, and rotated end over end for 1 hour with HisPur Cobalt Resin (Thermo Scientific). After binding, the resin was washed using the pACYCDuet-1 McsA wash buffer to remove contaminating proteins. Proteins were then eluted from the resin using the pACYCDuet-1 McsA elution buffer and collected. After four elution steps, the buffer was exchanged to pACYCDuet-1 McsA storage buffer using a Millipore Amicon Ultra 15 filtration unit (3 kDa cut-off). The pACYCDuet-1 McsA protein sample was then quantified using the BioRad Protein assay and assessed for purity on 12% SDS-PAGE gels with Coomassie Brilliant Blue staining. Protein samples were aliquoted and stored at -80°C.

<u>Purification of MBP-tagged McsA</u>

N-terminal MBP-tagged *C. trachomatis* McsA was purified from a 500 mL culture of *E. coli* BL21 (DE3) ΔPAX. Cultures were induced for 2.5 hours at 37°C with 1 mM IPTG. After induction, cultures were pelleted and stored at -80°C overnight. Samples were suspended in McsA lysis buffer, sonicated, spun down to separate the nonsoluble and soluble fractions, filtered using 0.45 μm filters, and rotated end over end for 1 hour with Amylose Resin (New England BioLabs). After binding, the resin was washed using the McsA wash buffer to remove contaminating proteins. Proteins were then eluted from the resin using the McsA elution buffer and collected. After four elution steps, the buffer was exchanged to McsA storage buffer using a Millipore Amicon Ultra 15 filtration units (3 kDa cut-off). McsA proteins were then quantified using the BioRad Protein assay and assessed for purity on 10% SDS-PAGE gels with Coomassie Brilliant Blue staining.

<u>Pilot MBP-Tag Cleavage Trials for pMAL-c5X McsA</u>

Thirty μg of purified MBP-tagged McsA was diluted to 100 μL in cleavage buffer. Prior to addition of 0.6 μL of 1 mg/mL Factor Xa (New England BioLabs), 5 μL was taken from the protein sample to serve as the uncut control. Once the Factor Xa was added, the solution was split evenly so one could incubate at room temperature while the other incubated at 4°C. Samples were mixed once every hour and 5 μL samples were taken every 4, 7, and 24 hours. Samples were mixed with Laemmli with BME and heated so they could be assessed on 10% SDS-PAGE.

Clp Activity Assays

Fluorescent Peptide Degradation Assay

3 µM (monomeric concentration) of the *Ct* ClpP proteins were added to either buffer E or buffer F and incubated for 1 hour at 37°C as reported in Wood *et al*. (55). Upon addition of 500 µM Suc-Luc-Tyr-AMC (Boston Biochem) to give a final reaction volume of 50 µL, fluorescence due to peptide degradation was measured every 5 minutes for 6 hours at 37°C using a BioTek Synergy HT plate reader set at an excitation of 340/360 and an emission of 440/460.

FITC-casein Degradation Assay

Prior to use in assays, the FITC-labeled casein (Sigma-Aldrich C0528) was resuspended in buffer PZ to a stock concentration of 200 µM. To remove free FITC, the stock was passed through a Zeba 7K cutoff spin columns (Thermo Scientific) calibrated with ultrapure water and stored at 4°C. One or 0.1 µM (compound 40 only) of *E. coli* ClpP or 6 µM *Ct* ClpP1 and ClpP2 was incubated with 25 µg/µL compounds (provided by Dr. Martin Conda-Sheridan, UNMC) or DMSO solvent at 32°C for 30 min before adding FITC-casein. Upon addition of 20 µM FITC-casein to give a final reaction volume of 100 µL, the fluorescence resulting from FITC-casein degradation was measured for 3 hours with readings every 3 minutes at 32°C.

Kinase-GLO ATPase Assay for ClpX

Recombinant ClpX or mutant ClpX (1.5 µg) was incubated in up to 49.5 µL of ATPase assay buffer without ATP for 10 minutes at room temperature. To initiate the reaction, 1 µM of ATP dissolved in ATPase assay buffer was added to the reaction to give a final volume of 50 µL and incubated at 30°C for 1.5 hours. After the 1.5 hours, the

reactions were incubated for an additional 30 minutes at room temperature. Fifty µL of Kinase-Glo® reagent (Promega) was added to the reaction and it was incubated for 10 minutes at room temperature. Using a BioTek Synergy H1 plate reader, the luminescence of the reaction was measured (ATP not consumed by ClpX).

Malachite Green BioMol ATPase Assay for ClpX

Recombinant ClpX or mutant ClpX (1.5 ug) was incubated in up to 49 µL ATPase assay buffer without ATP for 10 minutes at RT. Upon addition of 1 mM ATP to give a 50 µL final reaction volume, the reaction was incubated for 2 hours at 32°C. After 2 hours, 200 µL of BioMol Green reagent (Enzo) was added to each reaction and then allowed to incubate for 20 minutes at RT. Inorganic phosphate released from ATP was colorimetrically quantified at OD_{620nm} using a BioTek Synergy H1 plate reader.

ClpX Oligomerization Native PAGE

Five ug of purified protein was incubated with oligomerization buffer at 37°C for 20 minutes. After 20 minutes, the reaction was mixed with 5X native sample buffer without heating and run on a BioRad MiniProtean 4-20% gradient gel for Native-PAGE. Protein was detected using Coomassie Brilliant Blue staining.

GFP Degradation Assay

ClpP1 and ClpP2 at 3.5 µM and 3 µM of ClpX were incubated with 4 mM ATP, 8 mM creatine-phosphate, 10X buffer PZ, and 1 U/mL creatine phosphokinase for 30 minutes at 32°C. GFP at 0.36 µM was then added to the reaction for a final volume of 100 µL, samples were mixed via pipetting, and fluorescence was read using a pre-warmed (32°C) BioTek Synergy H1 plate reader for 2 hours at excitation λ = 465 nm and emission λ = 535 nm using a flat bottom white plate.

Bacillus subtilis Thermotolerance Assay

The OD_{600nm} was measured for 5 mL 2xYT overnight cultures of *mcsA/B* strains grown at 37°C with 5 µg/mL chloramphenicol and kanamycin. Culture OD's were then standardized to 0.05 with fresh 2xYT broth containing 5 µg/mL chloramphenicol. Final volumes were 50 mL. If necessary, 0.2 mM IPTG was added to induce *mcsA/B* gene expression from the pHT08 vector. Cultures were then grown with shaking for eight hours in a 53°C water bath with OD_{600nm} readings taken every hour to track bacterial growth.

Statistics and Replicates

In general, all protein assays were performed using at least two independent protein purifications and assays were performed at least three times with replicates used for each individual assay. Data are reported with error as standard deviation or standard error, assay dependent. Statistics were calculated using GraphPad (Prism) and one-way ANOVA analysis using Tukey "honestly significant difference" test with a $p < 0.05$ considered significant.

CHAPTER 3

RESULTS

<u>*Chlamydia* Clp Proteins and Gene Organization</u>

Figure 3.1A depicts the gene organization for the chlamydial Clp system

components based on annotated *C. trachomatis* genomes. In a prior study, we

demonstrated that all components of the Clp systems in *Chlamydia* are expressed as

RB-specific gene products and that the proteins could also be detected during the RB

stage, supporting that the genes are functional and that the proteins could impact the

developmental cycle (40). Due to *clpP2* and *clpX* being present in the same operon, we

proposed a model of the chlamydial Clp system (fig. 3.1B) with the adaptor ClpX binding

to and interacting with the ClpP complex via the ClpP2 interface. This model is

supported by experiments done by Pan *et al*. in which they mutated the hydrophobic

pockets of ClpP1 and ClpP2 by which the ClpX would interact to form the protease

complex (48). The mutation in ClpP2, but not ClpP1, affected protease activity of the

ClpX/P2/P1 complex. In addition, the Pan *et al*. report found that ClpP2 and ClpP1 each

form homo-heptamers that then associate as a hetero-complex. Since ClpX

demonstrates preferential interaction with ClpP2, we hypothesize that the ClpC adaptor

protein will interact with the ClpP1 interface (fig. 3.1B).
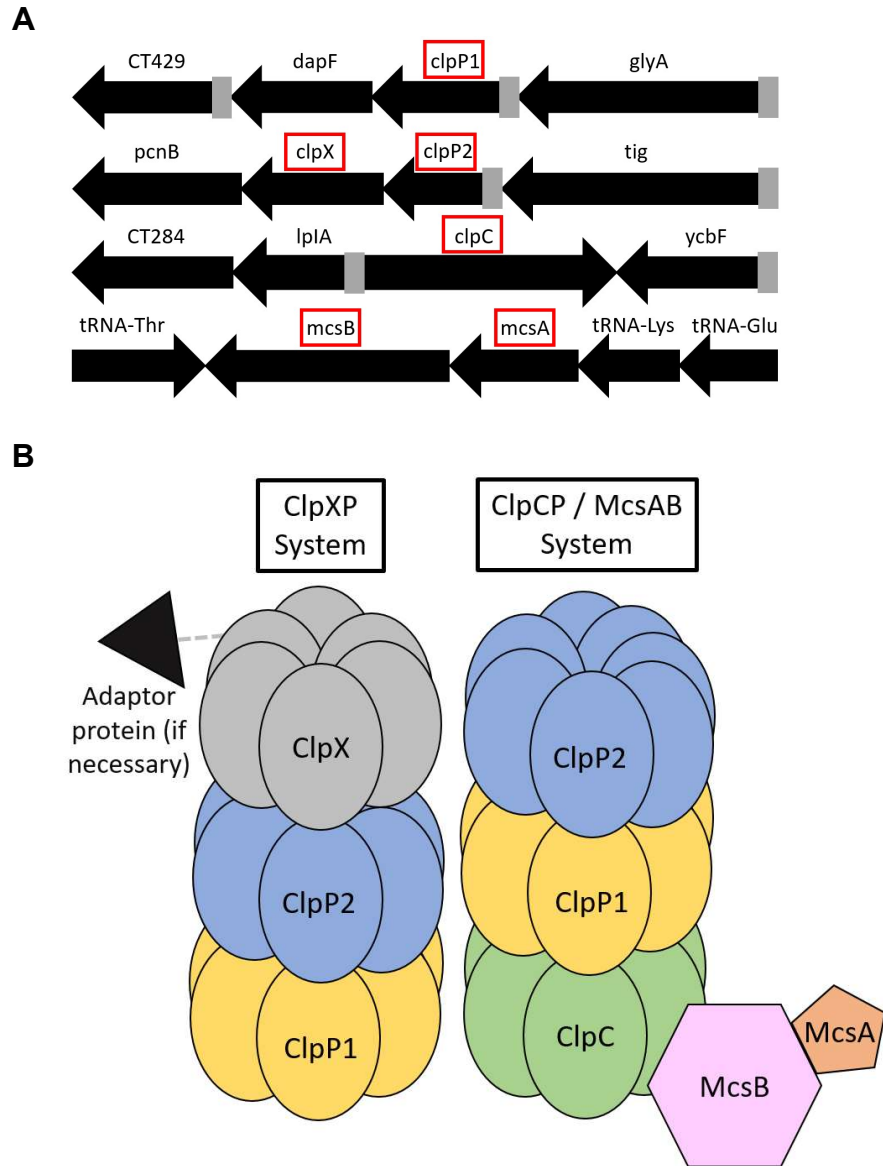
Figure 3.1. Gene organization and current model of the ClpX/P2/P1 and ClpC/P1/P2/ McsAB complexes. (A) Gene maps were generated using stdgen.northwestern.edu. Red boxes highlight the *clp* genes and grey boxes denote putative promoters (40). (B) The ClpX adaptor works with the ClpP2 interface of the ClpP2/P1 complex. Adaptor proteins may bind to ClpX to help facilitate degradation of differentially tagged substrates. The ClpC adaptor is hypothesized to work with the ClpP1 interface of the ClpP2/P1 complex. In its inactive state, we predict McsAB will bind to the complex via ClpC interaction.

To test our hypotheses regarding Clp complex structure and function(s) during

chlamydial growth and development, we took a two pronged-approach with our lab

focusing on *in vitro* characterization of the Clp proteins and the Scot Ouellette lab (with

PhD student Nicholas Wood) at the University of Nebraska Medical Center leading the *in vivo* aspects of the project. In general, *in vivo* results and their correlation with *in vitro* results will be reserved for the Discussion. To facilitate our *in vitro* studies, we needed to purify the Clp proteins along with protein substrates. The obligatory lifestyle of *C. trachomatis* and the difficulty in genetically manipulating it led us to use *E. coli* and *B. subtilis* as surrogate systems for protein production and purification. To assist in protein purification, we took a recombinant gene approach that used different affinity tags to aid in both protein solubility and purification. For the Clp proteins (*Ct* P1/P2/X/C, *Ec* P), C-terminal 6xHis tags were used (pLATE31, all constructs can be found in Appendix A) consistent with prior literature on Clp homologs supporting that the modification was not detrimental to oligomerization or protein function. Since the GFP construct carried a C-terminal ClpX degron tag, an N-terminal 6xHis tag (pLATE52) was used. All recombinant Clp proteins and substrates were expressed in an *E. coli* Δ*clpPAX* mutant to avoid contamination of protein preparations with the *E. coli* Clp homologs. The 6xHis-tagged proteins were purified via immobilized metal affinity chromatography (IMAC) on HisPur Cobalt Resin. Proteins were concentrated and stored in their respective storage buffer at -80°C, quantified using the Bradford assay, and 1 μg of each protein was assessed for purity on SDS-PAGE (fig. 3.2).
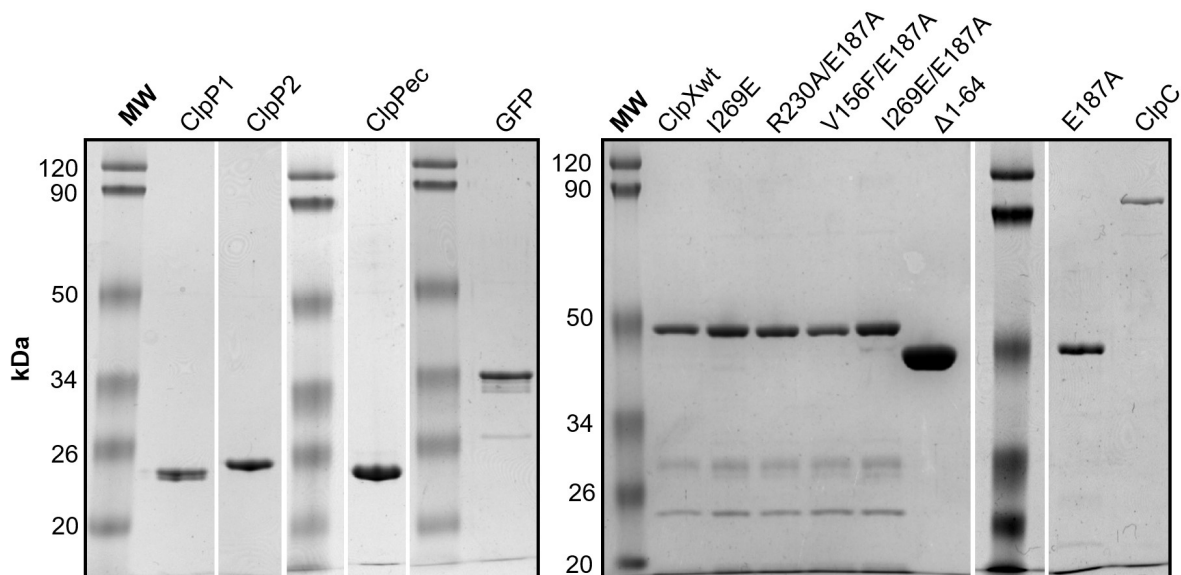
Figure 3.2. Assessment of protein purity. One µg of protein was run on SDS-PAGE gels under reducing conditions and protein was detected with Coomassie Brilliant Blue staining. The molecular weight ladder is on the left of each gel. Expected sizes in kDa are as follows: ClpP1 is 21 kDa, ClpP2 is 22 kDa, ClpPec is 23 kDa, ClpXwt and all ClpX mutants (except ClpXΔ1-64) are 47 kDa, ClpXΔ1-64 is 40 kDa, ClpC is 95 kDa, and GFP is 32 kDa.

In Vitro Studies of the ClpXP System

Confirmation of Protein Activity

With purified protein in-hand, we then used a number of assays to study the functions of the ClpXP components including fluorescent peptide and casein assays (for ClpP1/P2 protease activity), an oligomerization assay (ClpP1/P2/X), an ATPase assay (ClpX activity), and the GFP degradation assay (ClpX/P2/P1 activity). To assess ClpP1 and ClpP2 protease activity, the proteins were mixed and protease activity tested using the well-established Suc-Luc-Tyr-AMC fluorescent peptide degradation assay (fig. 3.3). While ClpP cannot degrade complex substrates without an adaptor, the protease can typically accommodate small peptides within the protease opening leading to degradation. ClpP1 and ClpP2 were incubated without the fluorescent peptide for one hour at 37°C to promote oligomerization. Upon addition of the fluorescent peptide,

fluorescence due to peptide degradation was measured. If the proteins were active,
then an increase in fluorescence should be detected upon cleavage of the peptide
which relieves quenching of the AMC fluorophore. ClpP from *E. coli* served as a positive
control.

The *Ec* ClpP had activity measuring over 150 RFU/min (fig. 3.3A and C). *Ct*
ClpP1/ClpP2 together had low level activity measuring at around 0.3 RFU/min.
However, when sodium citrate was added to the reaction, the activity of the
ClpP1/ClpP2 complex increased almost six-fold (fig. 3.3B and D). Some salts, such as
citrate, cause a "salting-out" effect that helps stabilize multimeric complexes which
subsequently leads to increased activity in the case of ClpP. Therefore, this assay was
successful in demonstrating the protease activity of the *Ct* ClpP1 and ClpP2 heter-
complex. In these assays, we did not detect activity when only *Ct* ClpP1 or Ct ClpP2
were used (data not shown). Since we also planned to test the affect of various
compounds on ClpP acitivity, we measured the impact of DMSO, used as a solvent for
the compounds, on protease activity. No significant differences were found for either *Ec*
ClpP or the *Ct* ClpP2/P1 in the presence or absence of DMSO.
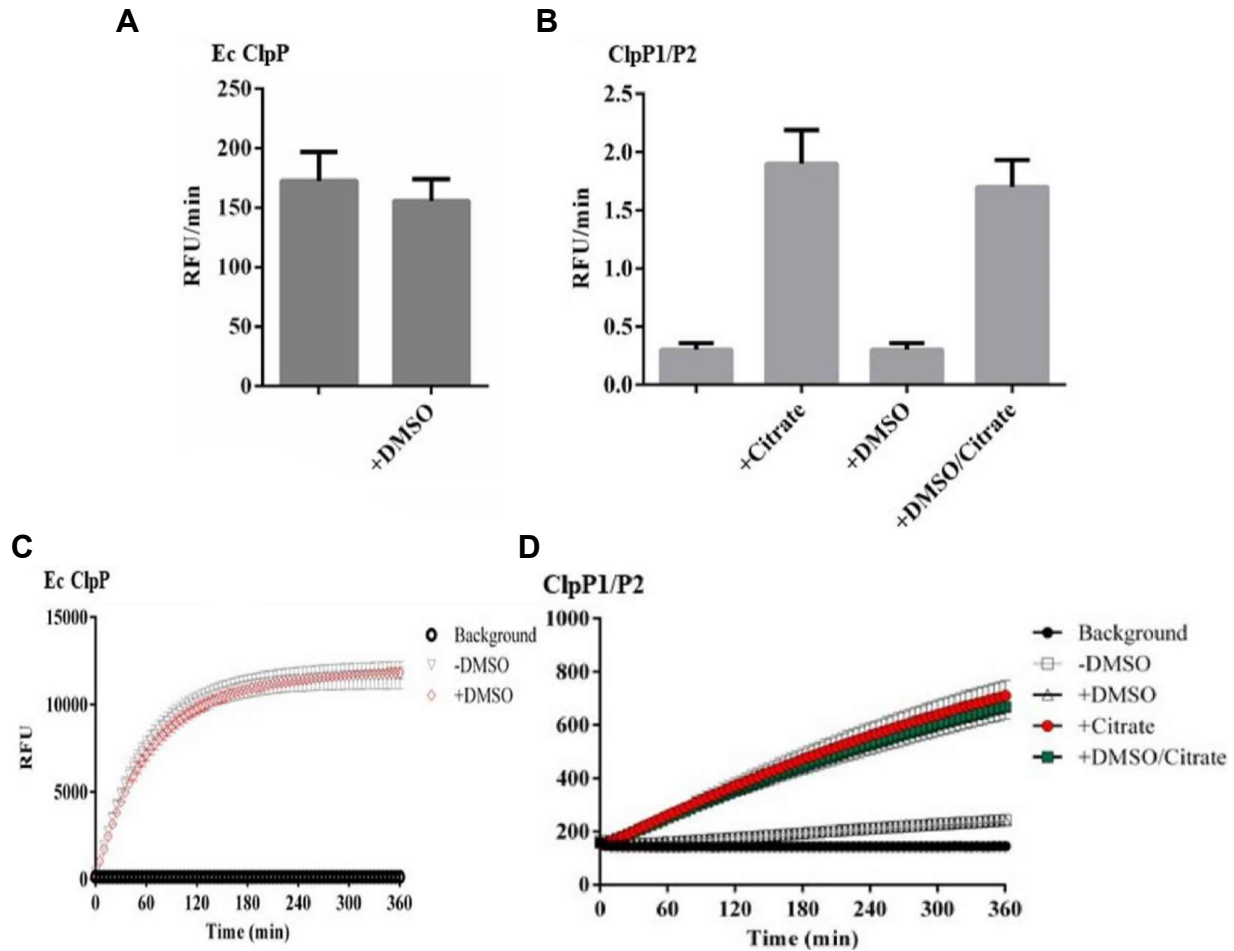
Figure 3.3. Assessment of ClpP1 and ClpP2 activity using the fluorescent peptide assay. 3 µM ClpP1 and ClpP2 were co-incubated with 500 µM Suc-Luc-Tyr-AMC at 37°C for 6 hours with (buffer F) or without (buffer E) 200 mM sodium citrate. Reactions were monitored using a BioTek Synergy HT plate reader set at an excitation of 340/360 and an emission of 440/460 with readings taken every five minutes. (A and B) Summary results for ClpPec and ClpP1/P2. Background was subtracted from each sample and the average values are reported with standard error. N = 3 for *Ct* ClpP1/P2, n = 2 for *Ec* ClpP; two different protein purification preparations were tested. (C and D) Original curve data averaged from all trials with error bars reported as standard error. Reported in figure S3 of (55).

The protease data (fig. 3.3) support that our purified ClpP2/P1 have activity and prior work with ClpP proteins indicates that oligomerization is required for proteolysis. To confirm that our *Ct* ClpP1 and ClpP2 proteins form a collaborative complex, native-PAGE gels were run to test for homo-oligomerization of the two heptamers and the formation of the functional tetradecamer (fig. 3.4). ClpP1 and ClpP2 were incubated

38

either alone or together in oligomerization buffer at 37°C to stimulate oligomer formation followed by complex analysis on native-PAGE. ClpP1 has a monomeric weight of 21 kDa, so the heptamer should be ~147 kDa. ClpP2 has a monomeric weight of 22 kDa, and heptameric weight of ~154 kDa. Together, the tetradecamer of ClpP1 and ClpP2 should yield a molecular weight of ~301 kDa. Both ClpP1 and ClpP2 formed homo-heptameric complexes at the expected molecular weight. When mixed together, they formed the tetradecamer (arrow) at the expected molecular weight of ~301 kDa (fig. 3.4). The native-PAGE results in conjunction with protease activity of the *Ct* ClpP1/P2 complex support that our ClpP preparations are functional, which we then leveraged for studies of activating compounds (fig. 3.5) and for later assessment of ClpX function.
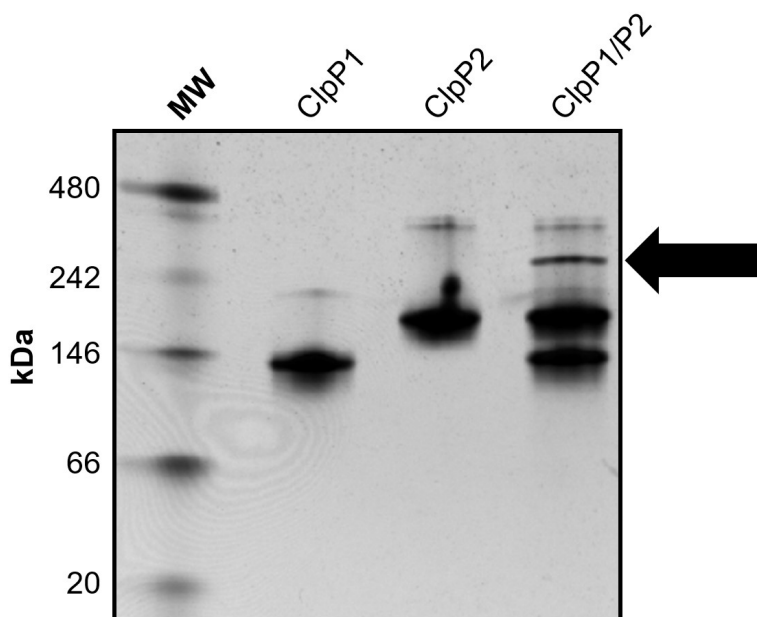

Figure 3.4. Native-PAGE of ClpP1, ClpP2, and ClpP1/ClpP2. 5 µg of ClpP1 and ClpP2 protein was incubated at 37°C for 20 minutes. The reaction was mixed with 5X native sample buffer and analyzed using native-PAGE followed by Coomassie Brilliant Blue staining. A native MW ladder is on the left of the gel. The arrow is pointing to the hetero-tetradecamer complex formed by combining ClpP1 and ClpP2. A representative gel is shown. Reported in figure S2 of (55).

Investigation of ClpP as a druggable target

Previous researchers have identified small molecule compounds that are toxic to ClpP-possessing bacteria by stimulating unregulated activity of ClpP. These activators work by opening the ClpP barrel so it can degrade large substrates that it would not otherwise be able to degrade on its own without the help of an adaptor protein. Since the activity of the ClpP1 and ClpP2 complex could be demonstrated using the fluorescent peptide assay, we could then test our proteins against various activators in a FITC-casein assay (fig. 3.5). In this assay, the fluorophore FITC is conjugated to casein, which is a substrate normally too large for the ClpP1 and ClpP2 complex to degrade. In the presence of activating compounds, the complex should be able to degrade the FITC-casein, which results in an increase in RFU. The activators, synthesized by the Martin Conda-Sheridan group at UNMC, were initially tested *in vivo* against *Chlamydia* and a number of compounds caused a decrease in inclusion size, altered inclusion morphology, and significant reductions in inclusion forming units approaching a 3-log drop (IFUs) (55). As the activators were designed based on previous drugs that targeted proteolytic enzymes, we hypothesized that these activators were targeting the ClpP2/P1 complex of *Chlamydia*. We tested the compounds *in vitro* using the FTIC-casein assay using *Ec* ClpP and *Ct* ClpP2/P1. Compound 40 had the greatest activation of the complex with over a 26-fold increase compared to the next highest activators 11 and then 16 versus the *Ec* ClpP (fig, 3.5A). Excepting compounds 9 and 11, which showed modest activation, no activation was detected with the *Ct* ClpP 2/P1 complex using the FITC-casein assay (fig. 3.5B), suggesting that these activators were not affecting chlamydial growth via activation of the ClpP2/P1 complex.
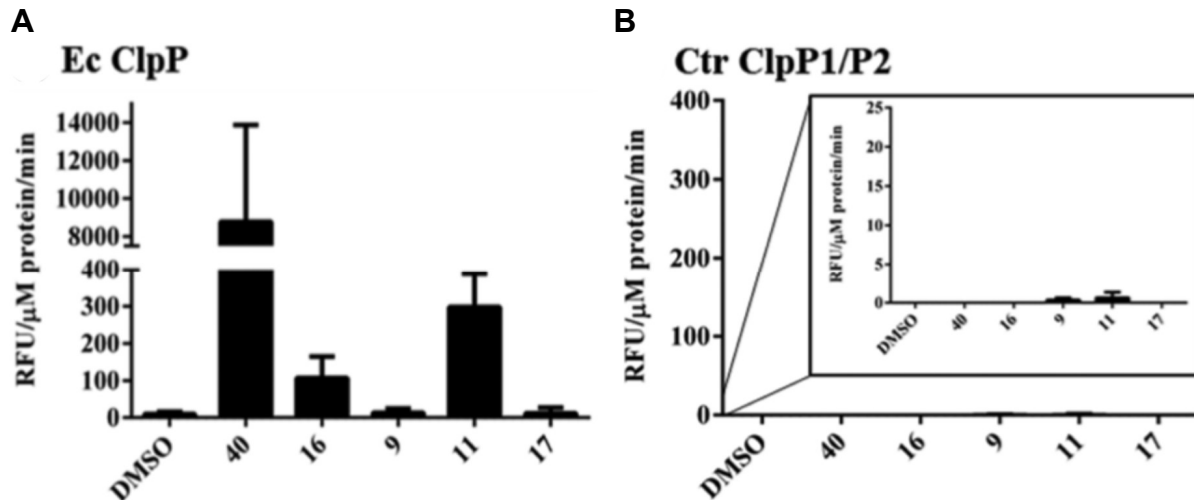
Figure 3.5. Effect of activating compounds against the *Ec* ClpP and *Ct* ClpP1/P2 complexes. Activators were incubated with *E. coli* ClpP or *Ct* ClpP2/P1 without FITC-casein for 30 minutes at 32°C. Upon addition of 20 µM FITC-casein, the fluorescence owning to FITC-casein degradation was measured for three hours with readings every three minutes. (A) Activators against the *Ec* ClpP complex. (B) Activators against the *Ct* ClpP2/P1 complex. Reported in figure 7 of (55).

ClpX-ClpP2/P1 interactions

After confirming we had functional ClpP1/P2 proteins, we turned our attention to studies on the protease-adaptor complexes. To dissect different ClpX "jobs" as highlighted in the introduction, we generated ClpX amino acid mutants with alterations in a number of task-specific motifs identified through sequence alignment with ClpX homologs from other bacteria (fig. 3.6). When compared to the ClpX of *E. coli*, *B. subtilis*, *Mycobacterium tuberculosis*, *Pseudomonas aeruginosa*, and *Staphylococcus aureus*, the *Ct* ClpX was found to possess key residues for ClpX function including: the Walker B motif for ATP hydrolysis (mutated E187A), IGF loops to bind to the ClpP complex (mutated I269E), the RKH motif for the SsrA-degron tag recognition (mutated R230A), pore 1 loop for substrate translocation from ClpX to the ClpP complex (mutated V156F), and the zinc-binding domain (ZBD) for binding of adaptor proteins to ClpX (deleted amino acids 1-64; ClpX adaptor proteins unknown for *Chlamydia*). *Ct* ClpX

41

retains other important motifs associated with ClpX function as highlighted in fig. 3.6.,

but not confirmed for function in this study. The amino acid mutants constructed and the

expected phenotypes are summarized in table 1.
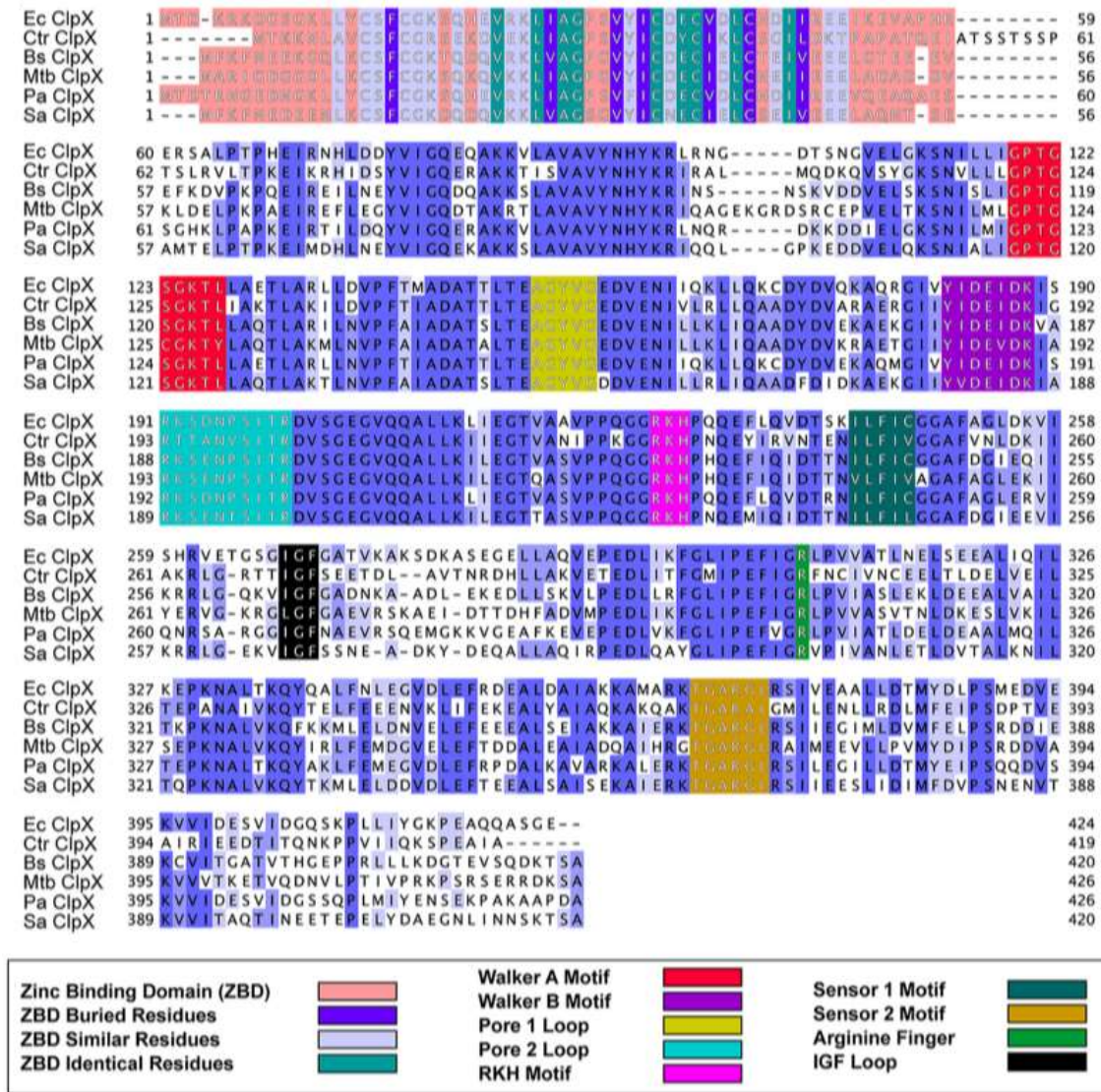
Figure 3.6. Bioinformatic analysis of chlamydial ClpX supports its role as an AAA+ ATPase. Multiple-sequence alignment of *Ct* ClpX with the ClpX orthologs of various other bacteria. *Ec*, *Escherichia coli*; *Ctr*, *Chlamydia trachomatis*; *Bs*, *Bacillus subtilis*; *Mtb*, *Mycobacterium tuberculosis*; *Pa*, *Pseudomonas aeruginosa*; *Sa*, *Staphylococcus aureus*. Alignment was performed using Clustal Omega with default settings and presented using Jalview version 2. Alignment was colored by percent identity in shades of blue or as indicated below the alignment. Reported in figure 1 of (60).

Following affinity purification of recombinant wild-type and mutant ClpX proteins,

Native-PAGE gels were used to test for the hexamer formation (fig. 3.7). ClpXwt has a

monomeric molecular weight of 47 kDa and the hexamer should have a molecular

weight of 282 kDa. All of the ClpX mutants, except ClpXΔ1-64, were expected to

migrate at a similar molecular weight as the wild-type since they only have one or two

point mutations. As ClpXΔ1-64 is missing the first sixty-four amino acids, its monomeric

size is 40 kDa and the hexameric complex should migrate at 240 kDa. All ClpX proteins

oligomerized and appeared at their expected molecular weight suggesting that the

proteins purified should be active (fig. 3.7).
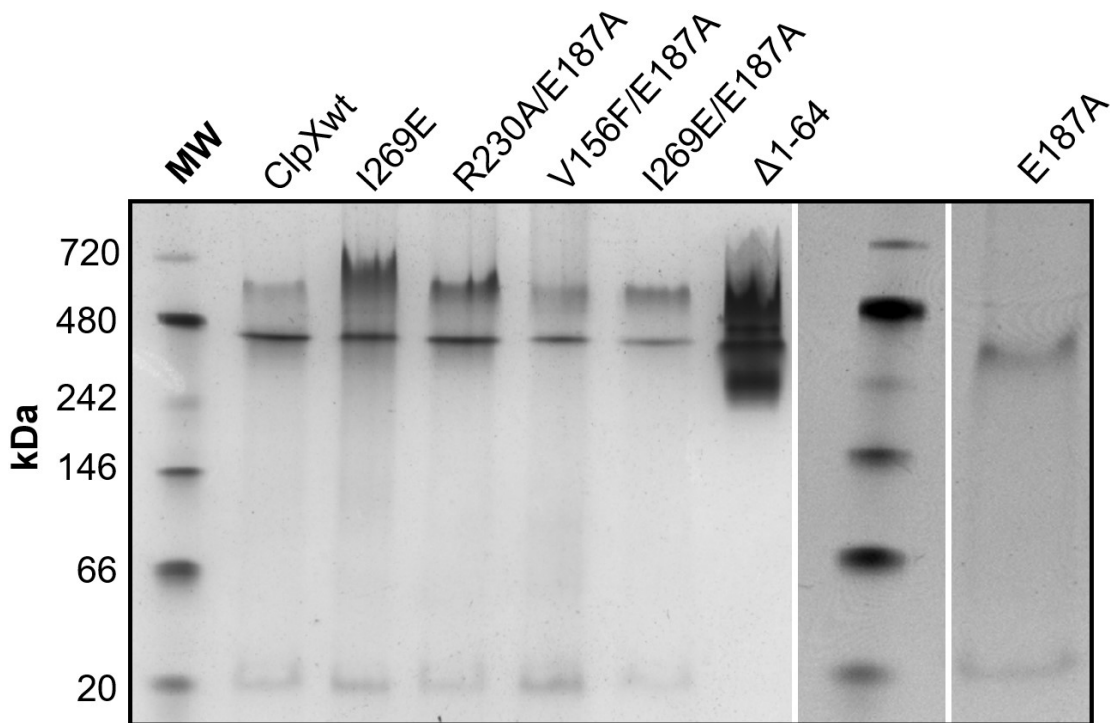
Figure 3.7. Native-PAGE of all ClpX clones. Five µg of the different ClpX clones were incubated at 37°C for 20 minutes to promote oligomerization. The reaction was mixed with 5X native sample buffer and analyzed using native-PAGE. The MW ladder is on the left of each gel.

As an AAA+ ATPase unfoldase, the adaptor ClpX utilizes ATP to unfold large

substrates that would not otherwise fit in the ClpP2/P1 complex for degradation. Since

all of the ClpX proteins were able to oligomerize into their functional state on the native-PAGE gels, we assessed the ATPase activity of each clone. We first used a malachite green-based assay (BioMol) to colorimetrically measure free phosphate released as ClpX hydrolyzed ATP to ADP (fig. 3.8). ClpX was incubated in ATPase buffer without ATP for 10 minutes. After addition of ATP, the reaction was incubated for 2 hours at 32°C. After the two hours, BioMol green reagent was added and allowed to incubate at room temperature for 20 minutes. The release of inorganic phosphate due to ATP consumption was colorimetrically quantified at Abs_{620nm}. ClpXwt had increased ATP consumption compared to the ClpX E187A mutant. Since the ClpX E187A mutant had a mutation in the walker B motif, it was expected to show reduced ability to hydrolyze ATP. While this assay effectively demonstrated the ATPase activity of ClpX, the small, although significant, difference in ATP consumption between the ClpXwt and ClpX E187A mutant along with the variability of the ClpXwt data led us to explore other approaches (fig. 3.8).

Table 1. List of ClpX mutants and their predicted phenotype.

E187A	Unable to hydrolyze ATP
I269E	Unable to interact with the ClpP1/ClpP2 complex
R230A / E187A	Unable to recognize SsrA-tagged substrates / unable to hydrolyze ATP
V156F / E187A	Unable to translocate substrates to the ClpP1/ClpP2 complex / unable to hydrolyze ATP
I269E / E187A	Unable to interact with the ClpP1/ClpP2 complex / unable to hydrolyze ATP
Δ1-64	Unable to interact with adaptor proteins
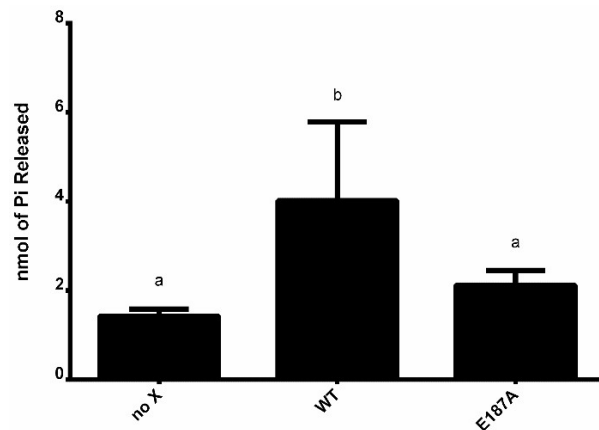
Figure 3.8. ATPase activity of ClpX clones as measured by the BioMol assay. Recombinant ClpX or mutant ClpX was incubated in ATPase assay buffer without ATP for 10 minutes at RT. Upon addition of ATP, the reaction was incubated for two hours at 32°C. BioMol Green reagent was added to each reaction and then allowed to incubate for 20 minutes at RT. Inorganic phosphate was colorimetrically quantified at Abs_{620nm}. The nmol of inorganic phosphate released was determined using a Pi standard curve. Error bars are standard deviation and the samples were tested at least three times with two independent protein purifications. Samples with no significant difference have the same letter and those with significant difference have different letters.

We next tested the kinase-GLO assay (fig. 3.9), which was expected to be more sensitive compared to the BioMol assay (fig. 3.8). ClpX and its various mutants were incubated in ATPase assay buffer without ATP for 10 minutes at room temperature. Once ATP was added, the reaction was allowed to incubate for 1.5 hours at 30°C and then for 30 minutes at room temperature. Upon addition of the kinase-GLO reagent, the level of ATP left in the reaction was measured as relative luminescence (RLU). If a protein is actively degrading ATP, then the luminescence of the reaction should be reduced compared to the "ATP only" control sample. ClpXwt, ClpX I269E, and ClpX Δ1-64 all demonstrated significant ATPase activity compared to the ATP only control. All other clones containing the E187A Walker B motif mutation showed little to no ATPase activity. The ATPase activity of ClpX is associated with the Walker A (ATP binding) and Walker B (ATP hydrolysis) motifs in the protein. The E187A mutation is in the Walker B motif, so all ClpX clones containing this mutation are still able to bind ATP, but are

45

unable to efficiently hydrolyze it. Although the clones with the E187A mutation were slightly decreased as compared to the "ATP only" sample, the difference is not significant. The kinase-GLO ATPase assay was more sensitive than the malachite green BioMol assay for demonstrating the differential ATPase activity of the various ClpX clones (figs. 3.9 vs 3.8).
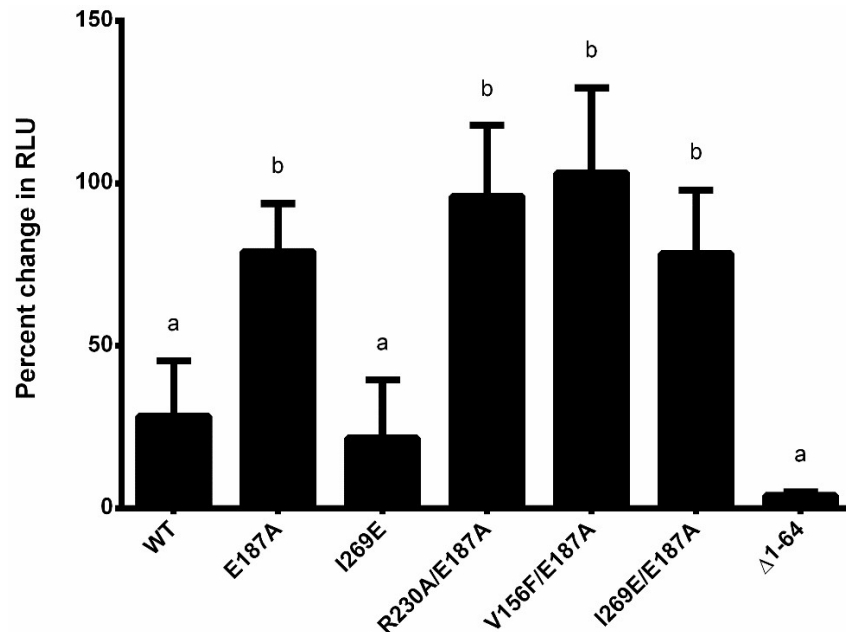

Figure 3.9. ATPase activity of ClpX clones as measured by the kinase-GLO assay. Recombinant ClpX or mutant ClpX was incubated in ATPase assay buffer without ATP for 10 minutes at RT. ATP was added to the reaction and incubated at 30°C for 1.5 hours. After the 1.5 hours, the reactions were incubated for an additional 30 minutes at room temperature. Kinase-GLO reagent was added to the reaction and it was incubated for 10 minutes at RT. The luminescence of the reaction (ATP not consumed by ClpX) was measured. Reactions were performed in duplicate at least three times with at least two independent protein preparations. Error bars report standard deviation. Samples with no significant difference have the same letter and those with significant difference have different letters.

As our previous assays demonstrated ClpP1/ClpP2 and ClpX activity independently, we next used the SsrA-tagged GFP degradation assay to measure proteolysis activity of the ClpX/P2/P1 complex (fig. 3.10). If the complex is able to recognize and degrade the SsrA-tagged GFP, then there should be a decrease in

fluorescence owing to degradation of GFP. ClpP1, ClpP2, and ClpX were incubated with creatine phosphokinase, ATP, and creatine phosphate for 30 minutes at 32°C. The creatine components were added as an ATP regeneration system, which proved essential for the assay. SsrA-tagged GFP was added to the reaction and the degradation of GFP or lack thereof was measured over two hours. ClpXwt and ClpX Δ1-64 were the only clones to demonstrate proteolysis activity, although the ClpX Δ1-64 showed reduced kinetics and lower overall activity than the ClpX wt. ClpX I269E carrying a mutation in the (I/L/V)-G-(F/L) motif (IGF loops) that is essential for interaction with the ClpP1/ClpP2 complex did not show any degradation of ATP. All other ClpX mutants have the E187A mutation, leading to reduced ATP hydrolysis and subsequent reduced degradation of the degron-tagged GFP.
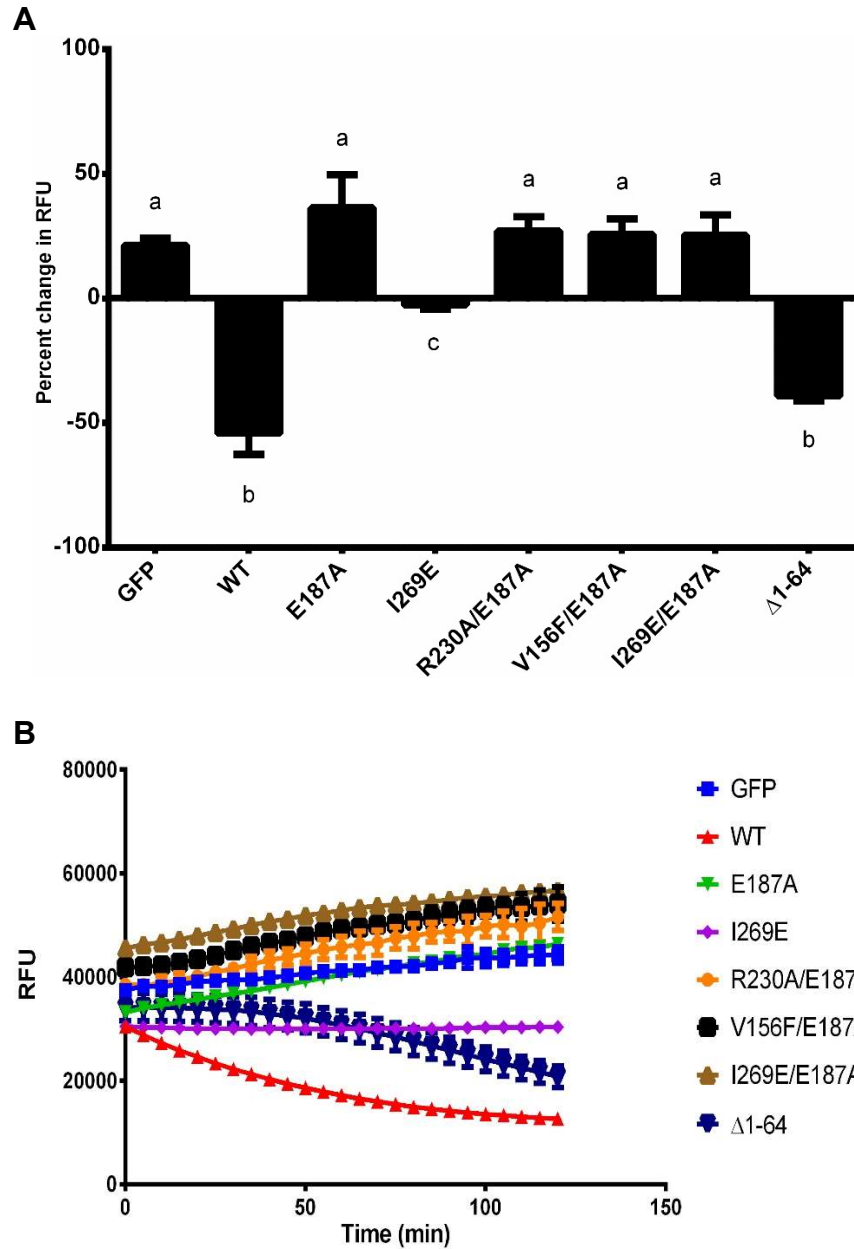
Figure 3.10. SsrA-tagged GFP degradation by the ClpXP complex. ClpP1, ClpP2, and ClpX were incubated with ATP, creatine-phosphate, 10X buffer PZ, and creatine phosphokinase for 30 minutes at 32°C. GFP was then added to the reaction and fluorescence was read for two hours at excitation λ = 465 nm and emission λ = 535 nm. Reactions were performed in duplicate at least three times with at least two independent protein preparations. (A) Percent change in GFP degradation with standard deviation. Samples with no significant difference have the same letter and those with significant difference have different letters. (B) Original curve data averaged from all trials with error bars reported as standard deviation.

ClpCP / McsAB

We hypothesize that the adaptor ClpC can also function with the ClpP2/P1 complex at the ClpP1 interface and that ClpC will be able to recognize and degrade proteins that have been phosphoarginine-tagged by McsAB. We speculate that tagging could be important for stress responses and developmental transitions. Based on the system in *B. subtilis*, McsA would act as the activator of the arginine kinase McsB and together they would be able to deliver doomed proteins to the ClpCP complex. We performed bioinformatic analysis of the *Ct* McsA and McsB to determine their similarity to the McsA and McsB proteins more typically found in gram positive bacteria. NCBI BLASTP was used to identify Mcs-homologs and multiple-sequence alignments were performed using MUltiple Sequence Comparison by Log- Expectation (MUSCLE) with default settings and edited using BioEdit. In fig. 3.11A, *Ct* McsA was compared against four other bacteria: *Chlamydia pneumoniae* (*Cpn*)*, Staphylococcus epidermidis* (*Sep*), *B. subtilis* (*Bs*)*,* and *Geobacillus stearothermophilus* (*Gst*). All McsA proteins contained a conserved UvrB/UvrC motif, which is associated with protein-protein interactions (69, 70). The *Ct* McsA retains all conserved cysteine residues (highlighted in blue) and shares an additional cysteine with its close neighbor *C. pneumoniae* (highlighted in green). As the EB (oxidized) and RB (reduced) have differing redox statuses, the high cysteine content of *Ct* McsA may have relevance for regulating McsA activity. Cysteines that are highlighted red (fig. 3.11A) and circled in red (fig. 3.11B) are those that were mutated for *in vivo* studies and will be further mentioned in the discussion. The sequence alignment and annotation suggests that the *Ct* McsA is similar to those of other bacteria and is likely to function as an activator of the partner McsB. *Ct* McsB was

49

also compared to the McsB proteins from the same organisms. Highlighted are motifs associated with McsB proteins: an ADP binding site (yellow), a phosphagen binding site (red), and substrate specificity loop (blue) as shown in fig. 3.11B. The sequencing alignment and annotation suggests that the *Ct* McsB is similar to those of other bacteria and would seem supportive of its role as an arginine kinase.

A

	Chlamydia trachomatis	100.00	52.66	22.58	22.58	28.39
	Chlamydia pneumoniae	52.66	100.00	22.08	25.32	26.62
	Staphylococcus epidermidis	22.58	22.08	100.00	29.78	30.34
	Bacillus subtilis	22.58	25.32	29.78	100.00	52.20
	Geobacillus stearothermophilus	28.39	26.62	30.34	52.20	100.00

B

C

ADP binding site

```
           10        20        30        40        50        60        70        80        90       100
          ....|....|....|....|....|....|....|....|....|....|....|....|....|....|....|....|....|....|....|....|
Ctr   1   -MLPNHILTAIATIKHSLRTETPRPICT-LSLSRNLSVSKFVPCLSKENK-RDVLETIAKQFSA--IEG-EEFFVLPLKDLPIWQRECLLEHYLFPYHLG  94
Cpn   1   MTLPNDLLETLVKRKESPQANKVWPVTT-FSLARNLSVSKFLPCLSKEQK-LEILQFITSHRNH--IEGFGEFIVLPLKDTPLWQKEFLLEHFLLPYDLV  96
Sep   1   ---MSNIHTNISEWMK-MSEETPVIISSRIRLARNLENHVHPLMFPSEQEGYRVINEVQDALPN--------LTLNRLDTMDQQSKMKLVAKHLVSPELV  88
Bsu   1   MSLKHFIQDALSSWMKQKGPESDIVLSSRIRLARNFEHIRFPTRYSNEEA-SSIIQQFEDQFSEQEIPGIGKFVLIRMNDAQPLEKRVLVEKHLISPNLT  99
Gst   1   MSFGKFFNTAVSAWMSQEGPNSDIVLSSRIRLARNIVDFRFPTLFSSEEA-KQIVALFERAFVHRPYGEAGRFELLKMSELQPIEKRVLVEKHLISPHLA  99
```

Phosphagen binding site

```
           110       120       130       140       150       160       170       180       190       200
          ....|....|....|....|....|....|....|....|....|....|....|....|....|....|....|....|....|....|....|....|
Ctr   95  SCLEGEFLIVNQAGTLLAGINLFDHVVIHGVDFVWQPEVLLQKLIDLDIRLQQSLSEAFSSDFGFLTAFPLRCGTALIARAFVHVPALKYGDALSELLVP  194
Cpn   97  GNPEGEFLVVSRSGDFLAAINFQDHLVLHGIDFQGNVEKTLDQLVQLDSYLHSKLSFAFSSEFGFLTNFPKNCGTGLKSQCFLHIPALLYSKEFTN-LID  195
Sep   89  K-QPASLVMLNDDESVSVMINEFDHIRIQALGTDLSLKDLYQRASKIDDELDKALDISYDEHLGYLTCFPTNLGTGMRASVMLHLFGLSIMKRMNR-IAQ  186
Bsu   100 E-SPFGGCLLSENEEVSVMINEFDHIRIQCLFPGFQLLEAMKAANQVDDWIEEKVDYAFNEQRGYLTSCPTNVGTGLRASVMMHLPALVLTRQINR-IIP  197
Gst   100 EDSPFGACLLSENEEISIMINEFDHIRIQCLFPGLQLAEALEAASELDDWIEGHVNYAFDERLGYLTSCPTNVGTGLRASVMMHLPALVLTQQINR-IIP  198
```

Substrate specificity loop

```
           210       220       230       240       250       260       270       280       290       300
          ....|....|....|....|....|....|....|....|....|....|....|....|....|....|....|....|....|....|....|....|
Ctr   194 --YQREFASSSLLPLSQESLGDILCLSNICSLGSLSEEQILSSIRLVVSKILSAEKEARNQLVKENPTEIKNRILRSVGMLTHSCCLDLQEALDATSWIQL  292
Cpn   195 --EEVEIITSSLLLGVTGFPGNIVVLSNRCSLGLTEELLLSSIRITASKLSVAEVAAKKRLSEENSGDLKNLILRSLGLLTHSCQLELKETLDALSWIQL  293
Sep   187 TINRFGFTIRGIYGEGSQVYGHIYQVSNQLTLGKTEEDIIDNLTEVVNQIINEEKQIRERLDKHNPVETLDRVYRSLGVLQNSRIISMEBASYRLSEVKL  286
Bsu   198 AINQLGLVVRGIYGEGSEAVGNIFQISNQITLGKSEQDIVEDLNSVAAQLIEQERSAREAIYQTSKIELEDRVYRSYGVLSNCRMIESKETAKCLSDVRI  297
Gst   199 AINQLGLVVRGTYGEGSEALGNIFQISNQITLGKSEEDIVADLHTIVEQLIAQERAARQALVKTLGIQLEDKVFRSYGILANCRVIDSKEAAQCLSDVRI  298
```

```
           310       320       330       340       350       360
          ....|....|....|....|....|....|....|....|....|....|....|....|....|....|
Ctr   293 GMSMQWIEDSENHPLWNPLFWDLRRGHLALYNQ---DTANRSIEKEVIAQIRAKATKPQOAERLIIRI--  356
Cpn   294 GIDLGLLKVTENHPLWNPLFWQIRRAHLALQKQ---AEDSRDLQKDTISHLRASVLKELTKGLSPESF-  358
Sep   287 GIDLNYLI-LLENFK-FNELMVAIQSPFLID------DDDNRTVNEKRADLLREHIK------------  334
Bsu   298 GIDLGIIKGLSSNI-LNELMILTQPGFLQQYSGGALRPNERDI--RRAALIRERLHLEMNGKRQEDESI  363
Gst   299 GIDLGYIKNVPRNI-LNELMILTQPGFLQQYAGGVLRPEERDV--RRAALIRERLRMETRRKMEGDER-  363
```

Chlamydia trachomatis	100.00	43.81	43.50	24.85	22.42
Chlamydia pneumoniae	43.81	100.00	70.99	22.51	24.01
Staphylococcus epidermidis	43.50	70.99	100.00	23.58	23.66
Bacillus subtilis	24.85	22.51	23.58	100.00	50.42
Geobacillus stearothermophilus	22.42	24.01	23.66	50.42	100.00

Figure 3.11. Bioinformatic analysis of the chlamydial McsA and McsB. Pairwise alignments were performed using NCBI BLASTP. The multiple-sequence alignment was performed using MUSCLE with default settings and edited using BioEdit. Organisms included are *C. trachomatis* (*Ctr*), *Chlamydia pneumoniae* (*Cpn*), *Staphylococcus epidermidis* (*Sep*), *B. subtilis* (*Bs*), and *Geobacillus stearothermophilus* (*Gst*). Conserved residues are highlighted. Black represents strongly conserved identical residues and gray represents partially conserved or similar residues. (A) Alignment of McsA. Red indicates cysteine residues mutated *in vivo*, blue indicates conserved cysteine residues across all organisms aligned, green indicates extra cysteines found only in *Chlamydia* species, and yellow indicates the conserved UvrB/UvrC motif found in McsA proteins. A percent identity matrix is listed underneath the alignment. (B) Predicted structure of *Ct* McsA. The structure was created using Phyre2. (C) Alignment of McsB. All highlighted regions indicate motifs conserved across all organisms aligned. Yellow indicates the ADP binding site, red indicates the phosphagen binding site, and blue indicates the substrate specificity loop for substrate binding. A percent identity matrix is listed underneath the alignments in A and C.

<u>Optimization of conditions for purifying *Ct/Bs* McsA and *Ct/Bs* McsB</u>

Since ClpP1, ClpP2, and ClpC can already be successfully purified (fig. 3.2), we focused on determining purification conditions for McsA and McsB. Previously, it was shown that co-expression of McsA and McsB from different plasmids in the same *E. coli* strain could rescue expression of McsB, possibly due to the predicted partnership of the two proteins (Michelle Malysa, Fisher lab; data not shown). However, it did not correlate with an increase in solubility for either partner. Therefore, *Ct* McsA and McsB were cloned into the two-gene expression plasmid pACYCDuet-1 to normalize expression levels to each other during co-expression as the cloning sites are encoded in an operon. After transformation into *E. coli* BL21 (DE3), each clone was tested for solubility in different lysis buffers. Cultures were then induced with varying amounts of IPTG and induced at different times and temperatures. Cell pellets were suspended in lysis buffers and sonicated to release soluble protein. Samples taken during the protein solubility trials were then assessed on SDS-PAGE and protein detected with Coomassie Brilliant Blue staining. While McsA was generally well expressed under conditions tested, solubility was poor (see example in fig. 3.12A). For McsB, all conditions tested for the pACYCDuet-1 clone with only *mcsB* exhibited both poor induction and solubility (fig. 3.12B). Rescue of McsB expression was seen when co-expressing McsA and McsB, but solubility was still too low to initiate purification (fig. 3.12C).
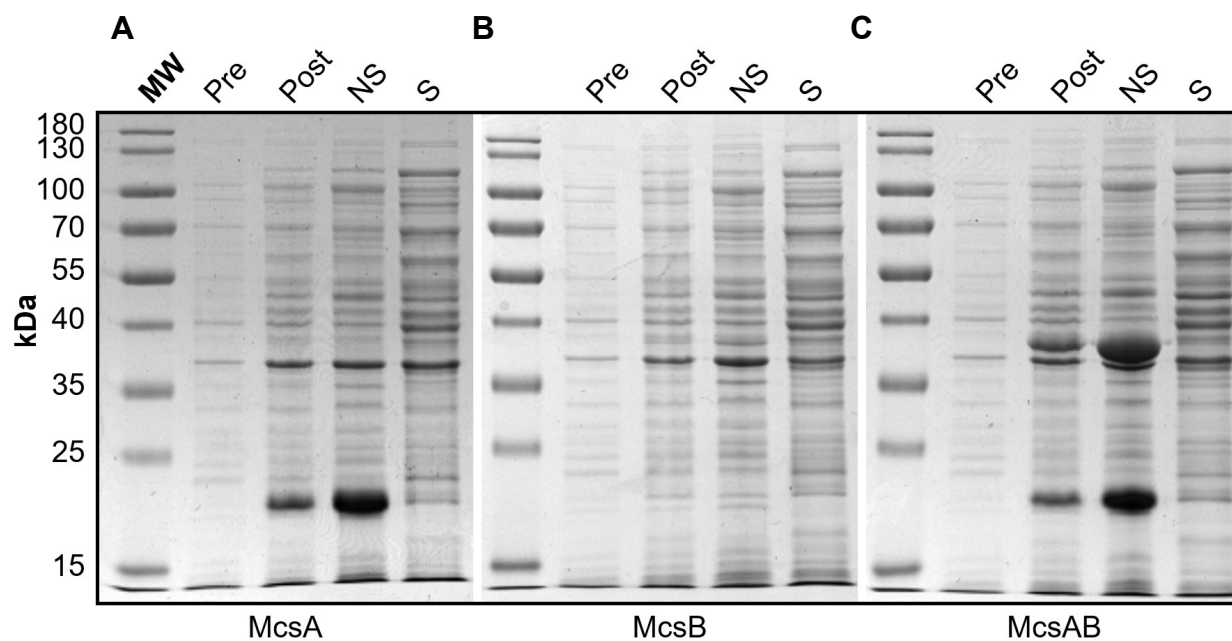
Figure 3.12. Representative SDS-PAGE gels of solubility trials for *Ct* McsA and McsB from the pACYCDuet-1 vector. The MW ladder is to the left of each gel. The first lane of each gel represents cultures prior to induction (Pre), the second lane represents cultures after induction (Post), the third lane represents the non-soluble protein fraction (NS), and the fourth lane represents the soluble protein fraction (S). (A) pACYCDuet-1 McsA alone, (B) pACYCDuet-1 McsB alone, and (C) pACYCDuet-1 McsA and McsB together. Expected protein molecular weights in kDa are: 21 kDa for McsA and 42 kDa for McsB.

The only condition for the pACYCDuet-1 McsA that demonstrated promising purification conditions was 1 mM IPTG for 10 hours at 37°C using the pACYCDuet-1 buffers listed in Appendix B. A 50 mL culture of pACYCDuet-1 *mcsA* strain was grown to an OD_{600nm} between 0.6-0.8, induced, and then spun down for storage overnight. The next day, McsA was purified via IMAC using HisPur Cobalt Resin. McsA was concentrated and stored in its storage buffer (Appendix B), quantified using the Bradford assay, and assessed on SDS-PAGE. Figure 3.13B is the quality control protein purification gel used to assess if the purification was successful or not. Although protein induction was strong, there was not a comparable amount of soluble protein as seen in the solubility trial gel in fig. 3.13A. This led to very little protein in the elution fractions

and a very dilute, unusable protein product. Based on the data in fig. 3.13B, we decided

to pursue other approaches for purifying McsA.
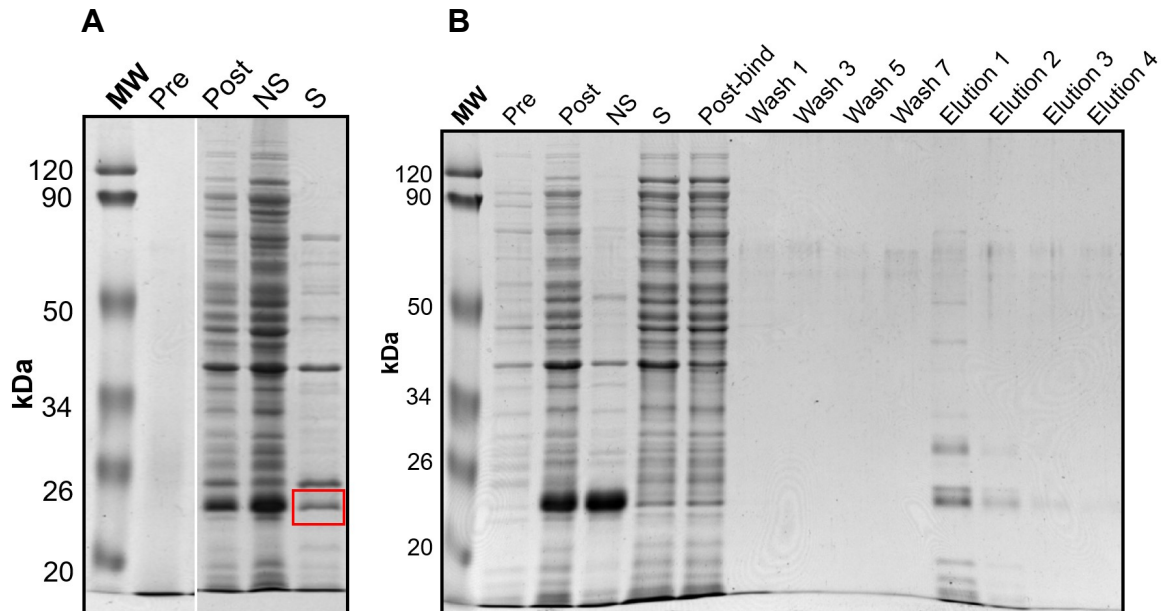
Figure 3.13. pACYCDuet-1 *mcsA* expression vector solubility trial and purification. (A) The boxed protein band represents the soluble McsA protein using the pACYCDuet-1 McsA lysis buffer. (B) The 6xHis-tagged McsA was purified via IMAC using HisPur Cobalt Resin.

Since the pACYCDuet-1 clones did not yield sufficient levels of soluble protein,

the proteins were next cloned into pLATE31 to generate C-terminal 6xHis-tagged

proteins. The advantage of this vector is the previous successes seen with the other

purified Clp proteins (fig. 3.2). However, this system would not allow co-expression of

McsA and McsB in a single protein expression strain from the same vector although

they could be transformed into the pACYCDuet-1 strain containing the other Mcs protein

as seen in fig. 3.12. *Ct* McsA and McsB were induced for 2.5 hours at 37°C so they

could be tested for basic expression via α-His western blot (fig. 3.14A). Following

confirmation of expression, pLATE31 *mcsB* was transformed into the strain carrying

pACYCDuet-1 *mcsA* to test if this method of co-expression would be successful in

rescuing McsB expression as previously seen in fig. 3.12. Unfortunately, expression and

solubility of both proteins was still suboptimal (fig. 3.14B).
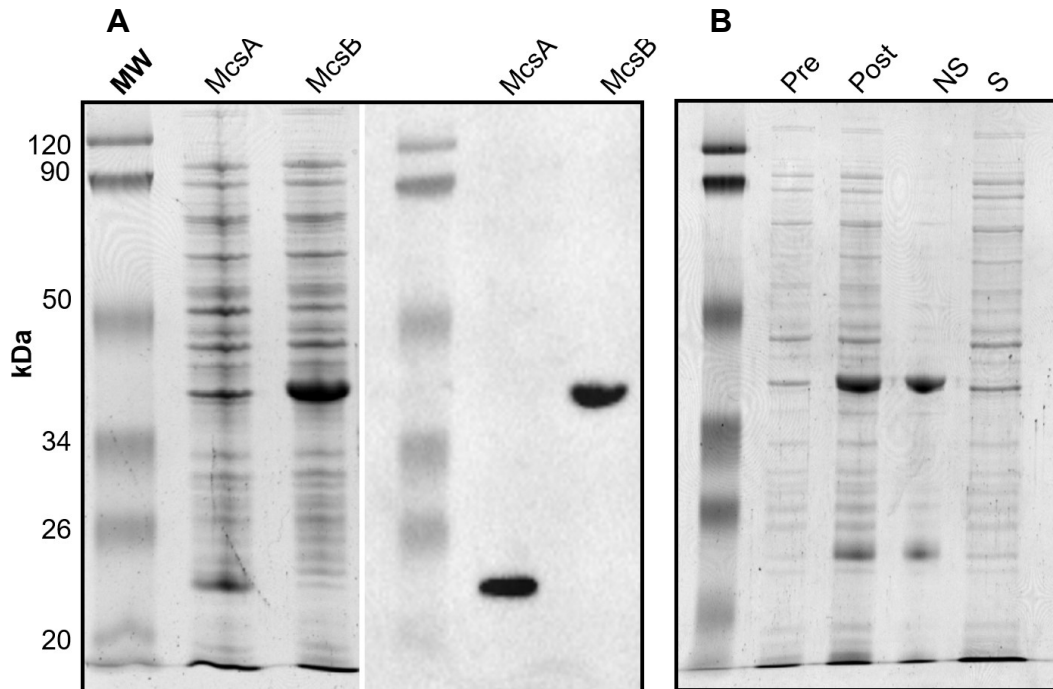
Figure 3.14. α-His western of from the pLATE31 *mcsA* and *mcsB* strains and a representative solubility trial for the pLATE31 *mcsB*/pACYCDuet-1 *mcsA* co-expression strain. (A) Left is the SDS-PAGE gel with the corresponding western blot on the right. (B) Co-expression solubility trial. The first lane of the gel represents the culture prior to induction (pre), the second lane represents the culture after induction (post), the third lane represents the non-soluble protein fraction (NS), and the fourth lane represents the soluble protein fraction (S). Expected product sizes in kDa are: 21 kDa for McsA and 42 kDa for McsB.

Since solubility was poor using the different combinations of pACYCDuet-1 and

pLATE31 vectors, clones containing new vectors and tags were created. *Ct mcsA* and

mcsB were cloned into pGex-6p-1 and pMAL-c5X vectors via restriction digestion and

transformed into the *E. coli* Δ*PAX* strain. Cultures were grown to an OD_{600nm} of 0.6-0.8

and induced with 1 mM IPTG for 2.5 hours at 37°C. After being spun down and stored

overnight, samples were resuspended in McsA lysis buffer, sonicated, and assessed for

protein production on 10% SDS-PAGE gels. The strain with pMAL-c5X *mcsA* produced

an abundance of soluble protein (fig. 3.15A). Neither of the pGex-6p-1 vectors nor the

pMAL-c5X containing *mcsB* were able to produce soluble protein in the lysis buffers tested (fig. 3.15B).

While the solubility profile of MBP-McsA was positive, a disadvantage of the MBP-construct was that MBP is a large tag at 42 kDa compared to the size of *Ct* McsA at 21 kDa. Since the MBP tag could interfere with the activity of McsA in future activity assays, an optimal MBP-tag cleavage protocol was determined (fig. 3.15C). After purification, the MBP-tagged McsA was subject to various tag cleavage conditions using factor Xa to determine optimal tag cleavage. Optimal cleavage was determined to be at room temperature for 24 hours as seen in fig. 3.15C. Compared to the control, almost all of the MBP-tagged McsA was cleaved into its separate parts of MBP and McsA alone, although McsA was buried in the dye front (arrow) due to the low percentage SDS-PAGE gel used. *Ct* McsA could now be successfully purified and the MBP tag cleaved in case it interfered in future activity assays.
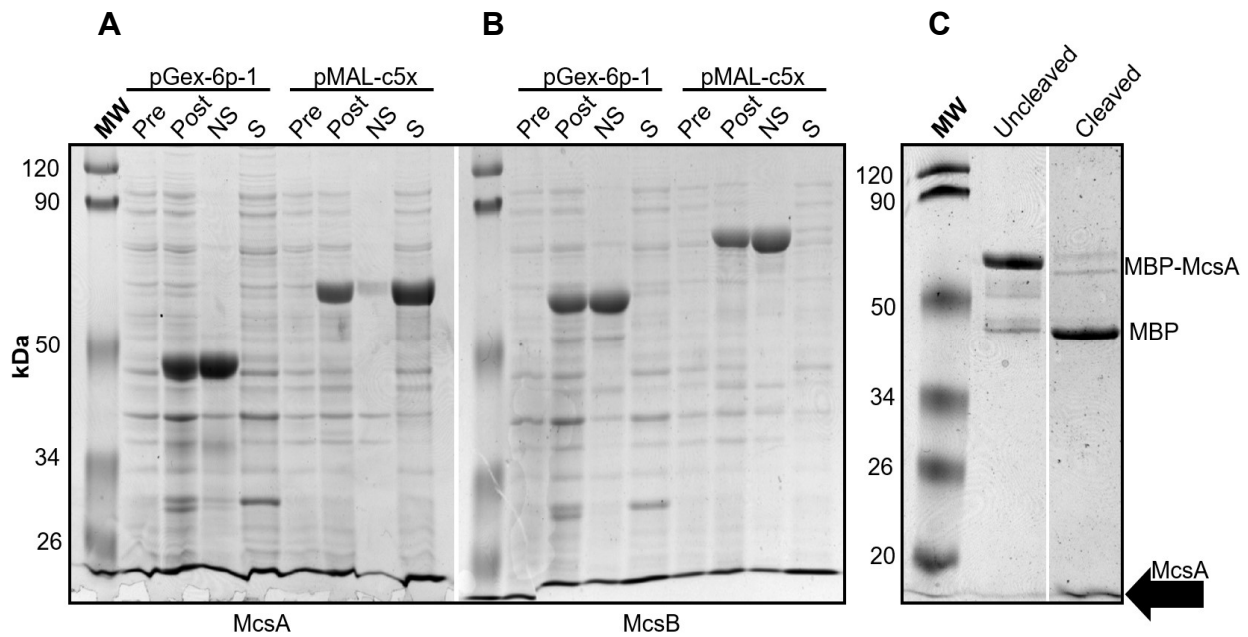
Figure 3.15. pGex-6p-1 and pMAL-c5X *Ct mcsA* and *mcsB* strain solubility trials and MBP-tag cleavage from MBP-McsA. SDS-PAGE gels of (A) McsA, (B) McsB, and (C) 24 hours at RT MBP-tag cleavage of McsA using factor Xa. Cleaved McsA is buried in the dye front represented by the arrow. Markers are shown to the left of each gel. Expected protein sizes for the pGex-6p-1 clones are: 46 kDa for McsA and 67 kDa for McsB. Expected protein sizes for the pMAL-c5x clones are: 63 kDa for McsA and 83 kDa for McsB.

Since many different conditions and tags tested in *E. coli* still did not yield a condition in which *Ct* McsB could be purified, a new expression system using *B. subtilis* was tested. This system was chosen because the McsAB system is an almost exclusively gram positive system, so perhaps *E. coli* is just unable to express *Ct* McsB at high levels and prior work by Suskiewicz *et al*. reported some toxicity when expressing McsB from *B. subtilis* in *E. coli* (71). Another reason for the switch was that as the system is most well-characterized in *B. subtilis*, we could purify and use *Bs* McsA and McsB as controls in future activity assays. *Ct* McsA/B and *Bs* McsA/B were PCR amplified from the respective genomic DNA of each organisms and cloned into the *E. coli, B. subtilis* shuttle vector pHT08 (fig. 3.16). The pHT08 vector is from the P*grac*01

expression system and has a C-terminally encoded 8xHis-tag. Based on the initial

vector publication, upon IPTG induction the tagged protein should account for 10-13%

of the total cellular protein (*Bacillus subtilis* Pgrac01 Expression Vectors manual from

MoBiTec).
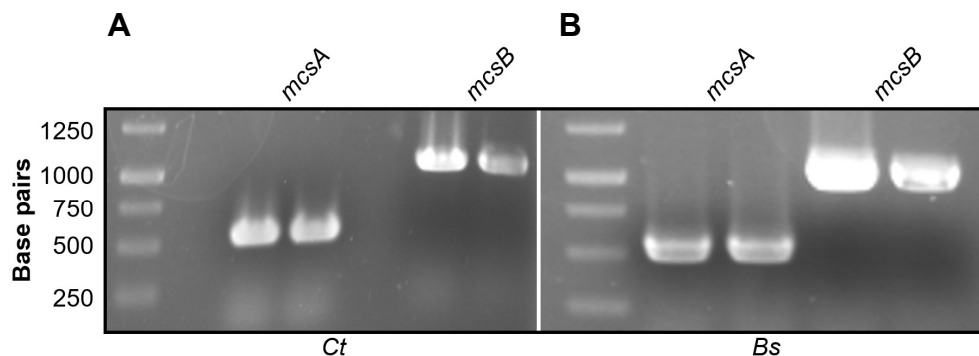
Figure 3.16. Amplification of *Ct* and *Bs mcsA* and *mcsB* from the respective gDNA. (A) *mcsA* and *mcsB* amplified from *Ct* L2 gDNA. (B) *mcsA* and *mcsB* amplified from *Bs* 168 gDNA. PCR products were run on an agarose gel and DNA visualized with ethidium bromide staining followed by UV transillumination.

After the *Ct mcsA/B* and *Bs mcsA/B* clones were created and transformed into *B.*

subtilis, protein expression was assessed. Protein expression was first tested with the

Ct gene clones. Upon growth to an OD_{600nm} between 0.6-0.8, cultures were induced

with 1 mM IPTG for 2.5 hours at 37°C. Previous work in *E. coli* utilized Laemmli buffer to

visualize proteins on SDS-PAGE. However, when Laemmli was used with *B. subtilis*,

little to no protein was seen on the SDS-PAGE gel (fig. 3.17A). Two different methods of

B. subtilis sample preparation were then tested. The first and selected method is

described in the materials and methods. The second method lysis buffer (50 mM Tris

[pH 7.2], 15% w/v sucrose, 2.5 mg/mL lysozyme) and 3X sample buffer (135 mM Tris,

30% glycerol, 3% w/v SDS, 150 mM DTT, and 0.03% bromophenol blue) were not

effective and showed streaking on the SDS-PAGE gels as seen in fig. 3.17B and C.
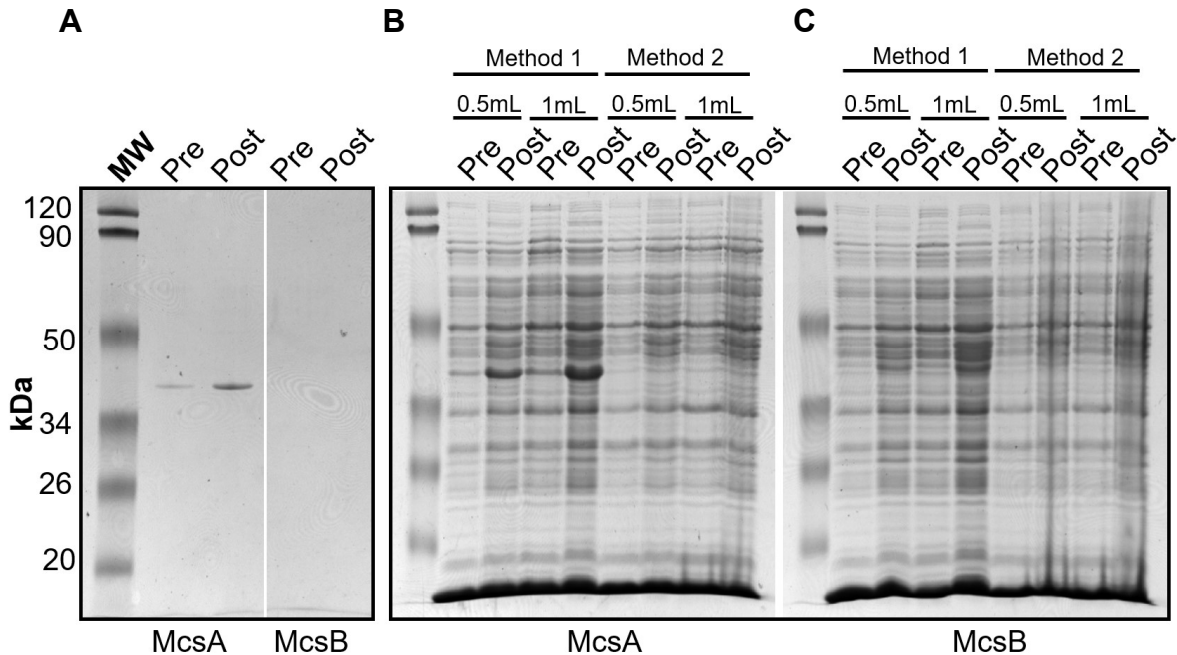
Figure 3.17. *B. subtilis* sample lysis experiments. (A) SDS-PAGE with the pre- and post-induction samples of *Ct* McsA and McsB lysed using Laemmli. (B) McsA sample lysis using method one and two. (C) McsB sample lysis using method one and two. Method one was selected for further use.

Prior to testing for optimal induction and solubility conditions, post-induction samples of *Ct* McsA and McsB were subject to an α-His western to determine if they were being expressed in *B. subtilis*. Westerns were done using a mouse monoclonal α-6xHis antibody and a goat anti-mouse IgG HRP conjugated secondary antibody. As shown in fig. 3.18B, neither *Ct* McsA nor McsB were detected. However, this same blot was reprobed using mouse α-*Ct* McsA antibody (provided by Dr. Gaungming Zhong, UT San Antonio) and *Ct* McsA was detected at the expected molecular weight of 21 kDa (fig. 3.18C). Although a band appeared just above the expected molecular weight of *Ct* McsB (42 kDa), this was suspected to be non-specific binding of the antibody since it was present in both lanes.
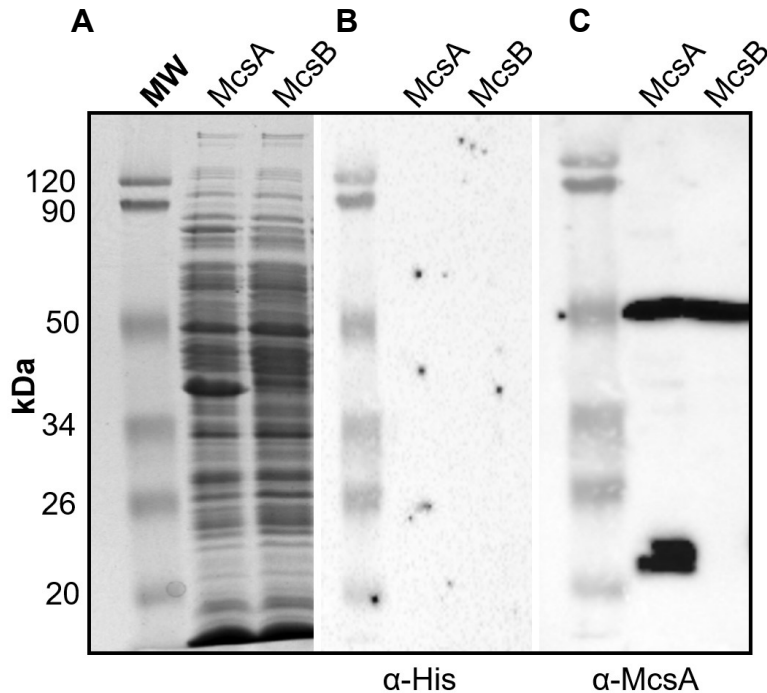
Figure 3.18. α-His and α-McsA western blots of *Ct* McsA. (A) Coomassie Brilliant Blue stained SDS-PAGE control for western showing total protein. (B) α-His western blot of *Ct* McsA and McsB. (C) α-His western blot was reprobed with α-McsA.

Failure of the α-His western blot could have been due to at least three reasons: 1) the His tag of the pHT08 vector was not exposed in my *Ct* proteins, 2) the α-6xHis antibody could not bind to an 8xHis tag although there was no evidence from other studies to suggest this would be a problem, or 3) the western failed as a bona-fide His-tagged positive control protein was not run in the previous western in fig. 3.18B. To trouble-shoot the anti-His western blotting, the pre-induction and post-induction samples from *Ct* McsA, *Bs* McsA, and the post-induction sample of a previous ClpX purification were used. ClpX has a 6xHis-tag that had been previously detected by our antibody, but the 6xHis-tag would not allow us to rule out that the α-6xHis antibody is unable to bind to an 8xHis tag. Again, the α-6xHis antibody did not detect the *Ct* McsA or *Bs* McsA (fig. 3.19). However, the α-6xHis antibody was able to detect the positive control ClpX, so the failure of the western could be due to reason one or two as stated above. Reason

60

one would be problematic because if the tag is buried in the protein, then the His-Pur

cobalt resin would also fail to bind to the tagged proteins, so purification via IMAC would

not be possible.
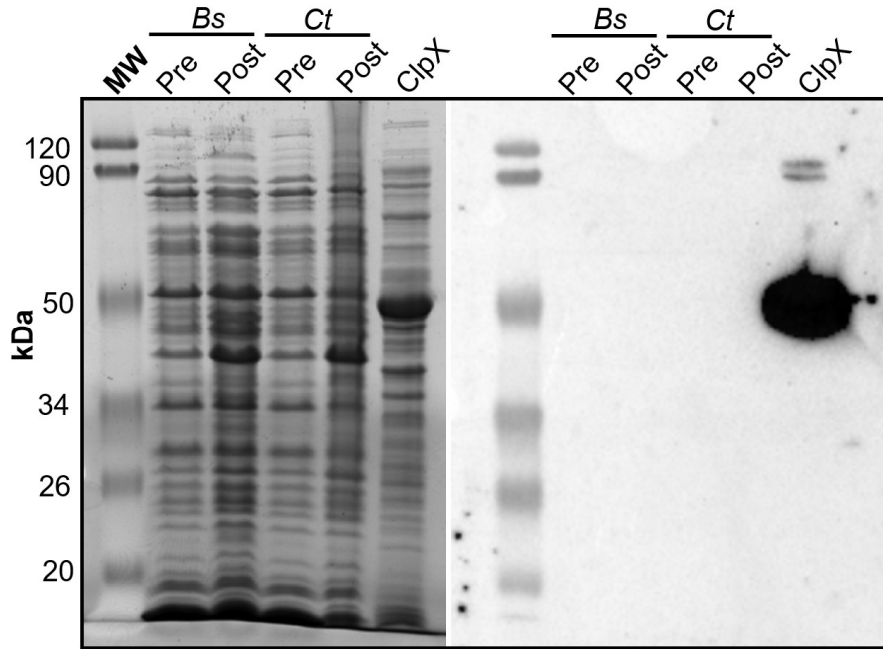
Figure 3.19. α-His western blot of *Ct* McsA, *Bs* McsA, and ClpX. Left is the Coomassie Brilliant Blue stained SDS-PAGE control for the western and right is the western blot. Protein sizes should be 21 kDa for *Bs* McsA, 21 kDa for *Ct* McsA, and 47 kDa for ClpX.

Although the α-His western blots failed, the α-McsA western blot was successful

in detecting the pHT08-expressed *Ct* McsA, so further induction trials were performed

for McsA without continued trouble-shooting for detection. Since *Ct* McsB could not be

detected, induction trials were performed in tandem with *Ct* McsA to see if the *Ct* McsB

could be visually confirmed using Coomassie Brilliant Blue staining under more optimal

induction conditions. Fifty mL cultures were grown to an OD_{600nm} between 0.6-0.8 in

2xYT media and then split into 5 mL aliquots that received either 0.1, 0.5, or 1 mM IPTG

and were incubated for either 3 hours at 37°C, 10 hours at 37°C, or 20 hours at 18°C.

Samples were assessed on 12% SDS-PAGE gels (fig. 3.20). Arrows represent the

expected location of each protein. For both proteins, there were no obvious changes in

expression levels despite the altered induction conditions. These gels did not support

the hypothesis that expression of Ct McsA and McsB in a *B. subtilis* expression system

would provide better expression, so a new method of expression would be needed to

obtain improved yields and soluble protein.
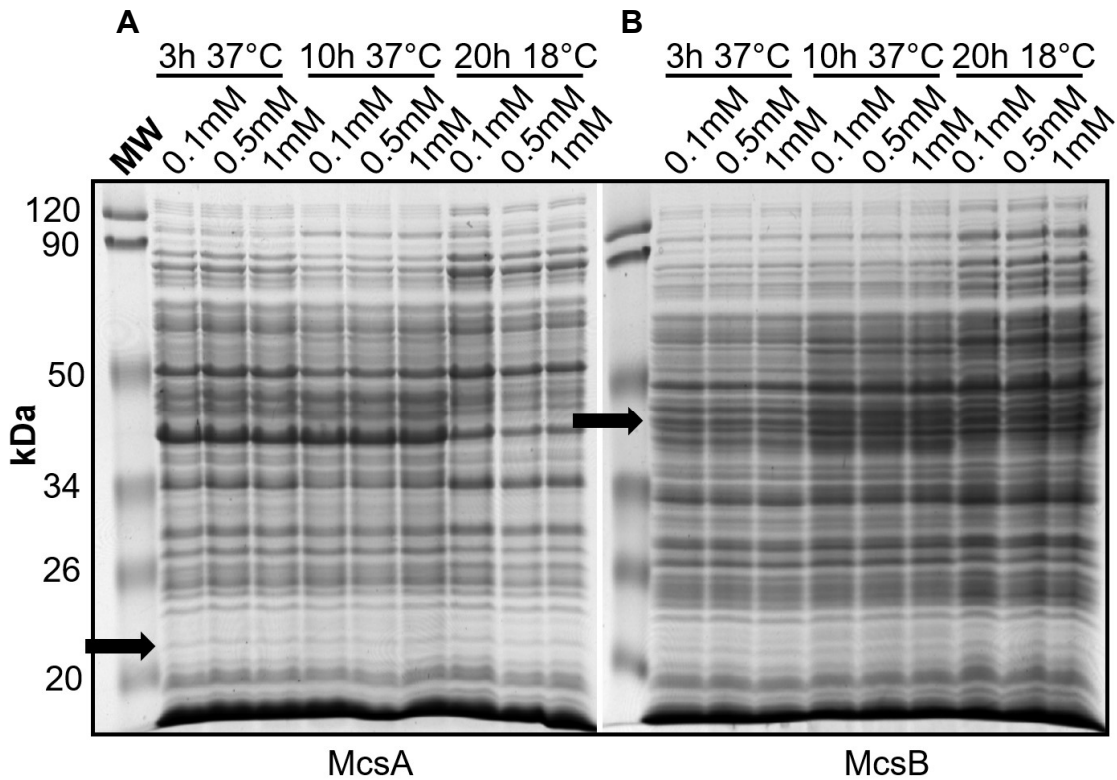
Figure 3.20. Induction trials of *Ct* McsA and McsB. Cultures were induced with either 0.1, 0.5, or 1 mM IPTG for either 3 hours at 37°C, 10 hours at 37°C, or 20 hours at 18°C Coomassie Brilliant Blue stained SDS-PAGE gels of (A) *Ct* McsA and (B) *Ct* McsB.

To improve upon expression and solubility, we assessed codon bias as a reason

for poor protein expression and solubility. Both sequences were codon optimized for

expression in either *E. coli* or *B. subtilis* using codon optimization tools provided by

NovoPro and Integrated DNA Technologies (IDT). NovoPro provided graphs showing

the improvement of sequences upon optimization, and the graphs were used to further

optimize sequences by hand. A representative graph of *Ct* McsA optimization for

expression in *E. coli* is shown in fig. 3.21. Codons that fell below 10% of relative

adaptiveness were replaced with codons that had ≥20% of relative adaptiveness as

determined by NovoPro. Examples of the improvement of relative adaptiveness is

shown with arrows. After creation of optimized *Ct* McsA and McsB sequences for *E. coli*

or *B. subtilis*, the respective gBlocks were ordered and cloned into protein expression

strains of *E. coli* using pLATE52 or *B. subtilis* using pHT08.
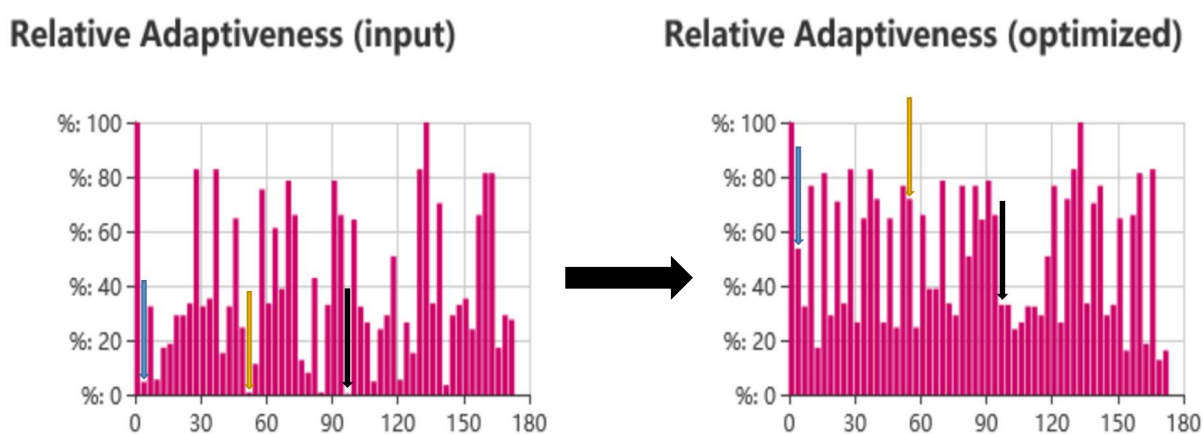
Figure 3.21. Representative codon optimization plot. Graphs were generated using the codon optimization tool offered by NovoPro. Similar colored arrows represent examples of codons that were corrected and the increase in percentage of relative adaptiveness.

The pLATE52 clones containing the codon optimized gBlocks of *Ct* McsA (g52A)

and McsB (g52B) were cloned and transformed into the *E. coli* ΔPAX strain for protein

expression. Fifty mL cultures of g52A and g52B were grown to an OD_{600nm} of 0.6-0.8

and induced with 1 mM IPTG for 2.5 hours at 37°C. Post-induction samples were taken

and run on a 12% SDS-PAGE gel (fig. 3.22). The Coomassie Brilliant Blue stained

SDS-PAGE gel showed the largest post-induction band seen thus far for McsB (except

when co-expressed in the pACYCDuet-1 vector with *mcsA* as seen in fig. 3.12C). We

attempted to confirm expression of both of the codon-optimized McsA and McsB

proteins via western blot with the mouse monoclonal α-6xHis antibody. Both the ClpX positive control and McsA were successfully visualized on the western blot, but McsB was not seen despite the prominent band observed on the Coomassie Brilliant Blue stained SDS-PAGE.
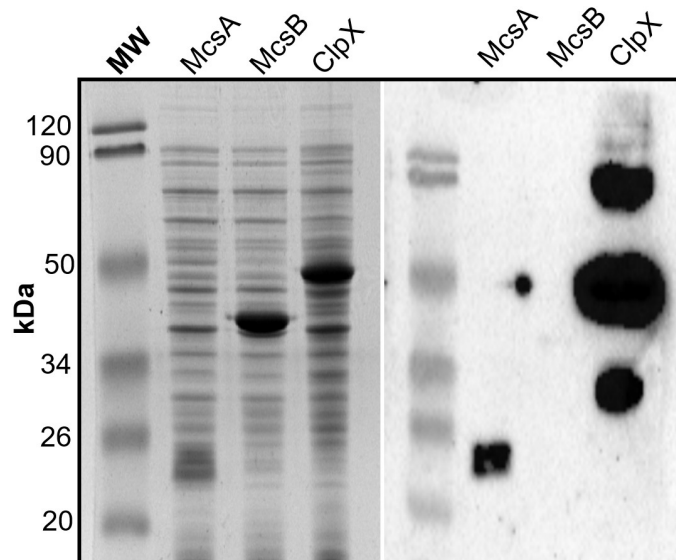
Figure 3.22. α-His western blot of McsA and McsB samples expressed from the codon optimized genes. Left is the Coomassie Brilliant Blue stained SDS-PAGE control for the western blot and on the right is the western blot with ClpX as a positive control.

Since previous α-His western blots to confirm expression of Ct McsB (fig. 3.21) and proteins expressed from *B. subtilis* (figures 3.18 and 3.19) failed, a urea denaturing purification was attempted. The advantage of this method is that even if the tag is buried in the native protein as previously suspected, the urea would denature the proteins so the HisPur cobalt resin would have access to the His tag on the proteins so they could be purified. The disadvantage of the urea approach is that the proteins are denatured so they cannot be used directly in activity assays. Fifteen mL cultures of g52B and pHT08 strains containing the codon optimized gBlocks of *Ct* McsA (g08A) and *Ct* McsB (g08B), and *Bs* McsA/B were grown to an OD_{600nm} of 0.6-0.8 and then induced with 1 mM IPTG

for 2.5 hours at 37°C. Cultures were spun down after induction and stored overnight at -80°C. The next day, cultures were purified via IMAC using HisPur cobalt resin. Pre-induction, post-induction, soluble, post-bind, elution, and resin samples from the purification were assessed on 12% SDS-PAGE gels and visualized using Coomassie Brilliant Blue staining (fig. 3.23). For g52B, a large amount of 6xHis-tagged McsB was recovered on the resin, thus supporting that the g52B clone was being expressed in *E. coli* and was ready for induction and solubility trials. For the proteins expressed in *B. subtilis* (p08B), there was significantly less protein recovered as seen on the g52B gel. However, there was enough protein recovered on the resin fractions for each protein (arrows) to support that the proteins were being expressed in *B. subtilis*. The urea denaturing purification demonstrated that the g52B, g08A/B, and *Bs* A/B expression strains were producing enough protein to initiate testing of optimal induction and solubility conditions.
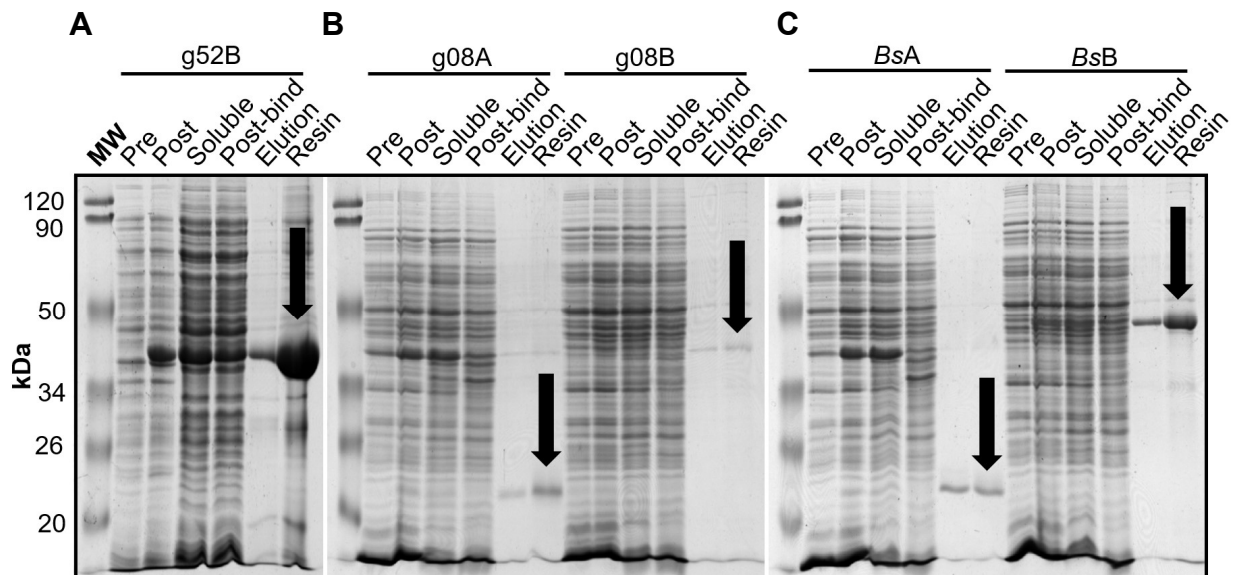
Figure 3.23. Urea denaturing purification SDS-PAGE gels for protein expressed from the g52B, g08 A/B, and *Bs* A/B strains. (A) g52B, (B) g08A and g08B, and (C) *Bs* A and B denaturing purification gels. Arrows point out the protein recovered from the HisPur Cobalt Resin.

After confirmation that the gBlock codon optimized pLATE52 McsA and McsB were being expressed (figs. 3.22 and 3.23A), induction trials were conducted to determine the optimal IPTG concentration and induction time and temperature. Fifty mL cultures of each strain were grown to an OD_{600nm} of 0.6-0.8, split into 15 mL aliquots, and induced with either 0.1, 0.5, or 1 mM IPTG at either 37°C for 2.5 hours, room temperature for 6 hours, or 18°C for 20 hours. After the induction time, post-induction samples were taken for assessment on SDS-PAGE via Coomassie Brilliant Blue staining. For both McsA and McsB, the strength of the band increased as induction time increased. Based on the gels in fig. 3.24, the optimal induction condition for both proteins was determined to be 0.5 mM IPTG for 20 hours at 18°C.
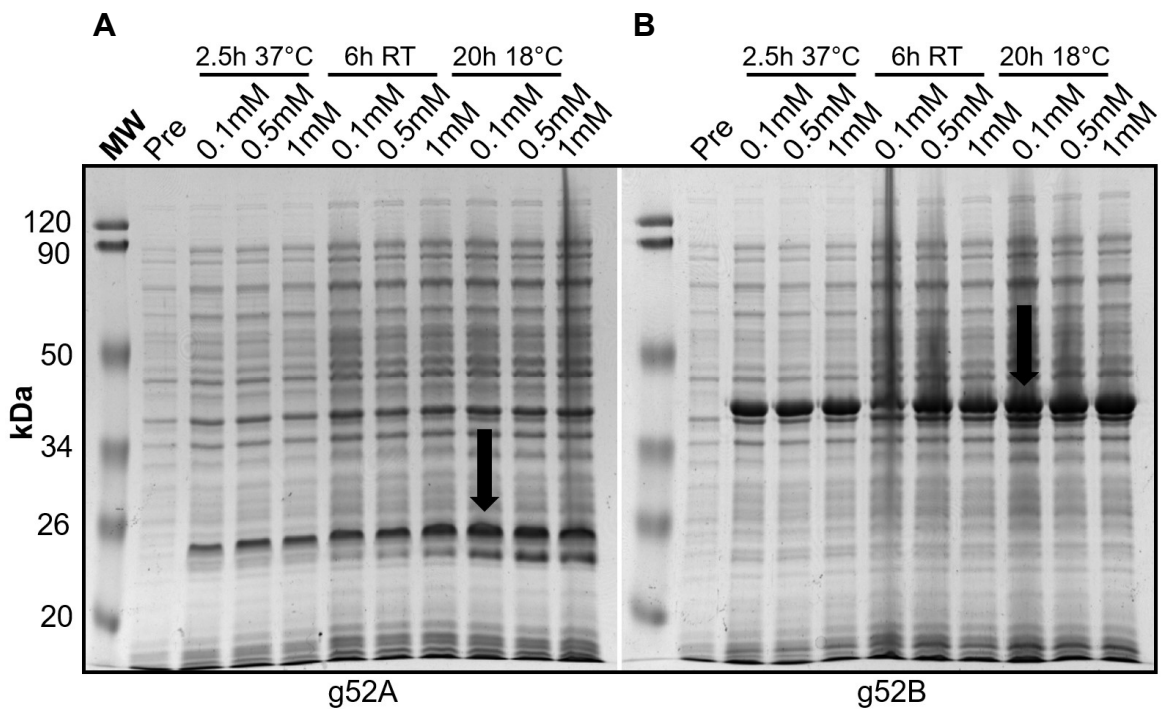
Figure 3.24. Induction trials of g52A and B. Cultures were induced with either 0.1, 0.5, or 1 mM IPTG for either 2.5 hours at 37°C, 6 hours at RT, or 20 hours at 18°C. (A) g52A and (B) g52B induction trials. Arrows represent the chosen induction condition.

After determining that 18°C for 20 hours with 0.5 mM IPTG was the optimal

induction condition, different lysis buffers were tested to determine optimal solubility.

Figure 3.25 shows representative gels based on solubility trials with these clones. In this

study, optimal solubility conditions were not able to be determined for either McsA or

McsB despite trying various different lysis buffer conditions.
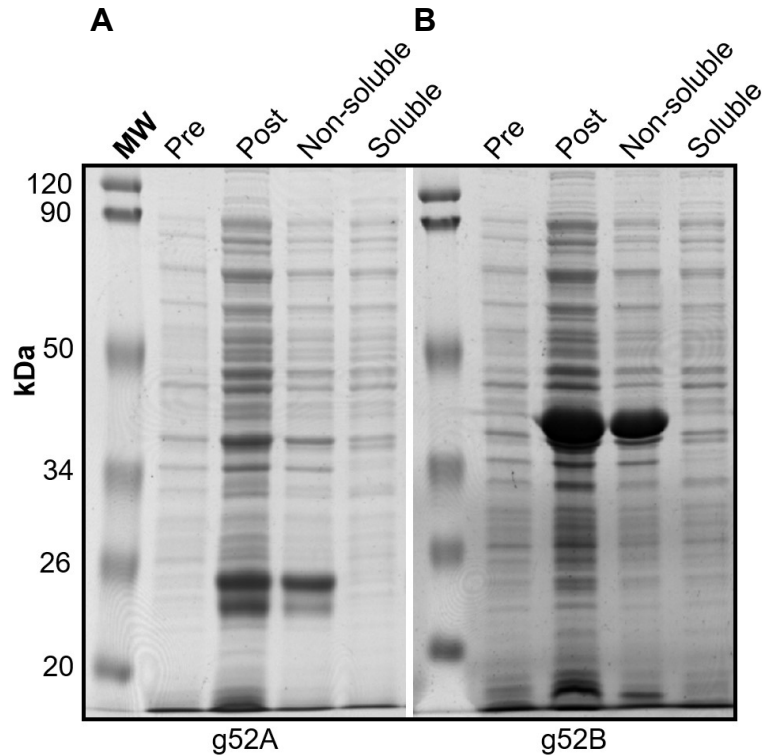
Figure 3.25. Representative gels of g52 A and B solubility trials. The first lane of each gel represents cultures prior to induction, the second lane represents cultures after induction, the third lane represents the non-soluble protein fraction, and the fourth lane represents the soluble protein fraction. (A) g52A and (B) g52B solubility trial SDS-PAGE gels.

Following confirmation that *Bs* McsA and McsB were being expressed in *B.*

subtilis (fig. 3.23C), induction trials were performed to determine optimal IPTG induction

concentration, temperature, and length of time. Fifty mL cultures of each strain were

grown to an OD_{600nm} of 0.6-0.8, split into 15 mL aliquots and induced with either 0.1,

0.5, or 1 mM IPTG at either 37°C for 2.5 hours, room temperature for 6 hours, or 18°C

for 20 hours. After induction, cultures were lysed using urea lysis buffer and IMAC resin was used to pull the induced protein out of the supernatant for assessment on SDS-PAGE (fig. 3.26). Without this extra step, it would be difficult to determine the optimal induction condition because as is seen in fig. 3.23C, the proteins were difficult to detect in the post-induction samples. *Bs* McsA had a similar induction band across all conditions tested. *Bs* McsB had the strongest induction band at 37°C for 2.5 hours with 1 mM IPTG. Since the induction condition impacted *Bs* McsB expression, but not *Bs* McsA, the optimal induction condition for both proteins was chosen to be 37°C for 2.5 hours with 1 mM IPTG guided by the results for *Bs* McsB.
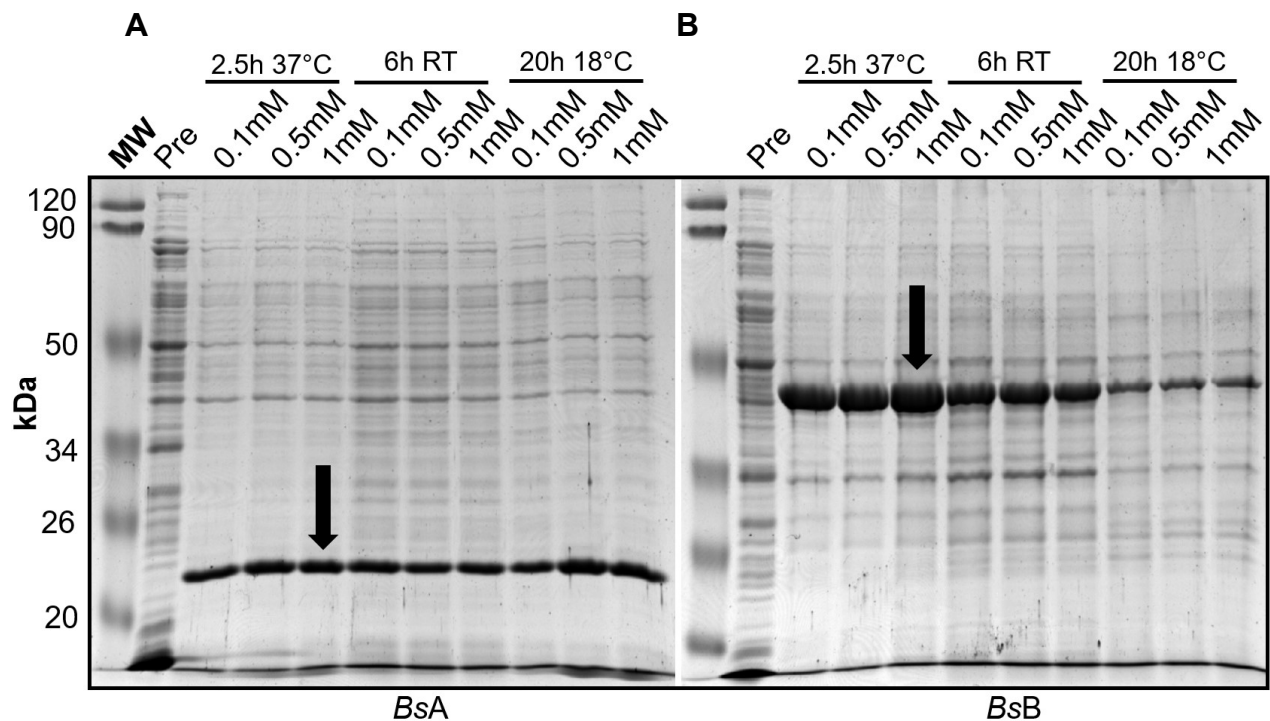

Figure 3.26. Induction trials of *Bs* McsA and McsB. Cultures were induced with either 0.1, 0.5, or 1 mM IPTG for either 2.5 hours at 37°C, 6 hours at RT, or 20 hours at 18°C. (A) *Bs* A and (B) *Bs* B induction trials. Arrows represent the chosen induction condition.

McsA Thermotolerance Growth Assay

In parallel with our attempts to express soluble *Ct* McsA and McsB in both *E. coli* and *B. subtilis*, we attempted to establish an *in vivo* assay that would establish functionality via complementation of a *B. subtilis* 168 Δ*mcsA* mutant with the *Ct mcsA*. Since the McsAB system is used in response to heat stress in *B. subtilis*, strains were grown at 53°C to test for complementation of the heat resistance phenotype (fig. 3.27). The *B. subtilis* strain expressing *Bs* McsA grew similarly to the WT strain supporting complementation although there was a slightly extended lag phase of the *Bs* McsA strain in the presence of IPTG. IPTG has been reported to cause growth delays when added to a culture in the lag phase (72). For *Ct* McsA without IPTG, the strain grew the same as the *B. subtilis* 168 Δ*mcsA*. However, the *Ct* McsA with IPTG strain grew moderately quicker, although it was still much slower in comparison to the WT and *Bs* McsA complemented strain. In conclusion, the expression of *Ct* McsA in *B. subtilis* does not improve thermotolerance.
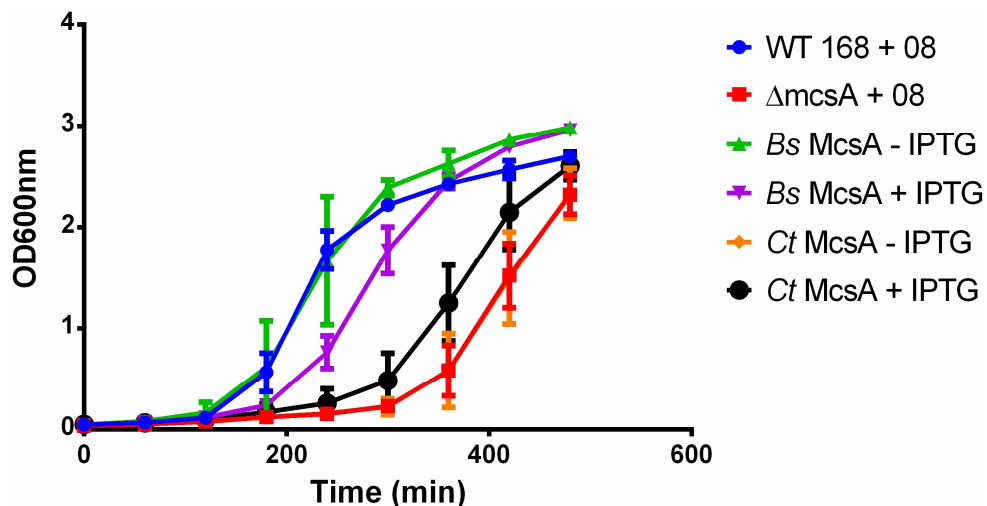
Figure 3.27. Thermotolerance Assay of *Bs* and *Ct* McsA. Cultures were grown with shaking for eight hours in a 53°C water bath with or without IPTG. OD_{600nm} readings taken every hour. The experiment was performed for eight hours and error bars report two independent experiments.

CHAPTER 4

DISCUSSION AND CONCLUSION

C. trachomatis is the most commonly reported cause of bacterial sexually

transmitted infections in the United States and is the leading cause of preventable

blindness worldwide. Although antibiotic resistance is not a current clinical problem for

chlamydial infections, the occurrence of asymptomatic infections that can lead to

complications including pelvic inflammatory disease and infertility coupled with drug

treatment failure emphasizes the need for a vaccine or specialized treatment options. In

addition, since infections are currently treated with broad spectrum antibiotics, it would

be preferred to find specific therapeutic targets in *Chlamydia* that would decrease the

incident of treatment failure and prevent induction of dysbiosis and the development of

non-chlamydial drug-resistance (14).

As *Chlamydia* undergo a biphasic developmental cycle between two distinct

forms (fig. 1.1) with unique protein profiles that presumably promote growth, replication,

and survival from host innate and adaptive immune response stressors, mechanisms

that regulate proteostasis are likely essential for survival in the host. The Clp systems

are a highly conserved system that functions in proteostasis by removing unwanted,

damaged, denatured, and aberrantly folded proteins that are harmful to the cell. Due to

the importance of the Clp systems for normal growth and stress responses, they have

been targets for drug development as novel approaches for treatment of bacterial

infections (54, 73). *Chlamydia* spp. encode two adaptor Clp components, ClpX and

ClpC, two protease components, ClpP1 and ClpP2, and protease targeting components

McsA and McsB (fig. 3.1). The maintenance of multiple *clp* genes in a minimal genome

organism suggests a critical role for the genes in promoting chlamydial fitness. *In vivo* support for the importance of the Clp system for chlamydial growth and development comes from our collaborative work showing that the expression of catalytically impaired forms of ClpP1 and ClpX or CRISPRi mediated knockdown of ClpP2 and ClpX significantly reduces chlamydial fitness (40, 60). These results support targeting the chlamydial Clp components as a therapeutic approach.

Typically, the ClpP drugs used are more effective against gram positive bacteria than gram negative bacteria due to permeability problems with the gram negative envelop making them narrow spectrum compounds (54). Our *in vivo* studies reported reduced chlamydial growth with ClpP-activators (55). While our *in vitro* data (fig. 3.5) are inconclusive regarding the mechanism of action of these compounds *in vivo*, the cell culture assays indicate that ClpP-drugs have potent anti-chlamydial properties. Our *in vitro* results also confirm that modification of the drugs can result in differential activity towards ClpPs from different species including *E. coli* (fig. 3.5A) and the human and mouse mitochondrial ClpP homolog (data not shown, reported in (55)). These data support that the Clp system could be leveraged to make a *Chlamydia*-specific drug.

To facilitate drug development and to better define the function of the Clp system in chlamydial growth, we sought to characterize the individual chlamydial Clp components and to reassemble the proteins into active complexes as required for drug testing and Clp-substrate identification. The latter point would be informative for selecting which components are the best druggable candidates for inhibiting bacterial growth. Based on prior studies with other Clp systems and work done on the chlamydial system as an undergraduate before initiating my thesis, we hypothesized that: 1) these

71

systems are essential for chlamydial development, 2) the ClpX/P2/P1 system will be important for degradation of proteins produced by *trans*-translation, and 3) the ClpC/P1/P2 and McsAB system will degrade phosphoarginine tagged proteins and will aid in redox signaling in *Chlamydia*. While not all of these hypotheses could be directly tested during my thesis, we are better positioned to perform this work in the near future.

ClpX/P2/P1

The ClpXP system can serve various functions in cells. A common function of ClpXP is degrading tagged proteins produced by *trans*-translation, which we hypothesized would also be one of its functions in *Chlamydia* which possess the *trans*-translation components (74). Before addressing its role in *Chlamydia*, we first sought to characterize the different components of the ClpX/P2/P1 system in *Chlamydia*. Based on work by both us and Pan *et al.* (48), the current model of the ClpX/P2/P1 system in *Chlamydia* is that the two ClpP paralogs, ClpP1 and ClpP2, form homo-heptamers that come together to form a functional hetero-tetradecamer protease (fig. 3.1B). This ClpP2/P1 complex alone can degrade smaller substrates, such as seen in the fluorescent peptide degradation assay (fig. 3.3), but upon association with the unfoldase ClpX, the system can recognize larger and specifically tagged substrates (fig. 3.10). Based upon the genomic organization, we hypothesized that ClpX will interact with the ClpP2 interface of the complex (fig. 3.1A). Although this question was not specifically pursued in this study, work by Pan *et al.* supports this hypothesis (48). In addition to the basic ClpX/P2/P1 system, we hypothesized based on other bacterial ClpXP systems and the presence of the ZBD motif (fig. 3.6) that the chlamydial ClpX will be able to work with different adaptor proteins to alter what ClpP2/P1 is able to degrade. One such

72

example is of the single domain response regulator CpdR and the phosphodiesterase PdeA involved in *Caulobacter crescentus* cell cycle regulation. Dephosphorylation of CpdR leads to degradation of PdeA by its ClpXP complex to help facilitate the transition between the dimorphic forms of *C. crescentus* (62, 75). Although adaptor proteins were not examined in this study, we hypothesize that their interaction with the chlamydial ClpX/P2/P1 system will be essential for its development and will be an interesting area of future study. To enable such studies, we purified and performed initial characterization of the Δ1-64 ClpX mutant that lacks the ZBD motif and should have reduced interactions with adaptor proteins. We confirmed that the protein could still oligomerize, hydrolyze ATP, and degrade an SsrA-tagged substrate (figs. 3.7, 3.9, and 3.10). Expression of this mutant protein in *C. trachomatis* by our collaborators will help to discern how important other adaptor proteins are towards ClpX function.

To enable for rigorous characterization of the chlamydial ClpX/P2/P1 system *in vitro*, we successfully purified ClpP1, ClpP2, ClpX, and various ClpX mutants in addition to ClpP from *E. coli* for use as a control protein (fig. 3.2). We also purified an SsrA-tagged GFP to test as a substrate of the system. To test for activity of the ClpP2/P1 complex, we utilized the Suc-Luc-Tyr-AMC fluorescent peptide degradation assay. The *E. coli* ClpP was highly active compared to the chlamydial version (fig. 3.5). On native-PAGE, ClpPec preferentially forms its active tetradecamer (40) as compared to the ClpP1 and ClpP2 of *Chlamydia* that preferentially forms its inactive heptamers, so this may explain the large differences in activity seen in this assay under the conditions tested. Nonetheless, ClpP2/P1 were able to degrade the peptide, and this effect was significantly increased upon the addition of sodium citrate which promotes

oligomerization. We further confirmed P1/P2 interactions using native-PAGE (fig. 3.4).

Distinct lower bands in the P1/P2 mixed lane that were at the same size of the

oligomers in the ClpP1 and ClpP2 only lanes suggested that the proteins are only able

to form homo-heptamers, and not hetero-heptamers as can be seen in some species of

cyanobacteria that express ClpP1 and ClpP2 homologs (76).

As work with other bacteria encoding ClpP suggested that drug-induced

hyperactivation of ClpP reduced growth, our collaborators at UNMC tested existing and

modified versions of ClpP activators against *C. trachomatis in vivo* (55). We then tested

a limited number of the compounds, guided by *in vivo* data, on the ClpP2/P1 complex *in

vitro* using the FITC-casein degradation assay (55). A number of the compounds led to

a decrease in inclusion size, altered inclusion morphology, and reduced IFUs. Based on

prior literature, we hypothesized that the decreased chlamydial growth observed was

due to activation of the ClpP2/P1 complex. However, no significant activation was seen

with any of the activators when used against the ClpP2/P1 complex using the *in vitro*

FITC-casein assay (fig. 3.5), suggesting that these activators might not be acting

through alteration of the ClpP complex activity. Activation was seen with certain

compounds when used with the ClpP of *E. coli*, so the FITC-casein degradation assay

will still be useful in testing future activating compounds. Although we hypothesized that

these compounds would activate the ClpP complex, the negative data for the FITC-

casein assay led us to test the compounds in the fluorescent peptide degradation assay

for ClpP inhibition, which was not observed (data not shown). The fluorescent peptide

degradation assay could be used to test for inhibitory compounds against the ClpP2/P1

complex since a decrease in activity could be determined, especially when used in the

presence of sodium citrate. The FITC-casein degradation assay would not be useful for testing inhibitors because ClpP2/P1 without an adaptor cannot degrade FITC-casein as seen in the DMSO control. Future work should also test compounds in the GFP degradation assay to assess inhibition in a configuration that is a better physiological mimic of what would occur *in vivo*. Taken altogether, the ClpP2/P1 complex of *Chlamydia* is functional *in vitro* when tested for fluorescent peptide degradation and when tested for oligomerization using the native-PAGE assay.

Before characterizing the chlamydial ClpX/P2/P1 system as whole, we sought to examine and characterize the motifs and activity of the unfoldase ClpX. When compared to the amino acid sequences of ClpX of five other bacteria, the chlamydial ClpX retained many conserved motifs (fig. 3.6). The following motifs are those that were mutated and examined for function in this study. Near the N-terminus, the chlamydial ClpX retains the ZBD needed to bind to adaptor proteins that enables the ClpP2/P1 complex to differentially degrade substrates as previously stated. ClpX also retains the Walker A and Walker B motifs needed for binding and hydrolysis of ATP, respectively. Conservation of this motif is essential since ClpX utilizes ATP to unfold large substrates that would not otherwise be degraded by the ClpP2/P1 complex. The chlamydial ClpX also retains IGF loops that enable binding to the ClpP2/P1 complex, an RKH motif for SsrA-tag recognition, and a pore 1 loop for substrate translocation from ClpX to the ClpP2/P1 complex. Regardless of the mutations mentioned here, we hypothesized that the ClpX proteins should be able to oligomerize into their functional hexamer and hexamer oligomerization was seen with every ClpX construct (fig. 3.7). Since the ClpX clones could all oligomerize, the ATPase activity of each was tested. The Malachite

Green BioMol Assay was initially use to measure the difference in release of inorganic phosphate due to ATP consumption between the wild-type and Walker B mutant ClpX (fig. 3.8). However, the small although significant difference in ATP consumption and the variability of the ClpXwt data was concerning because such a small difference becomes a problem when testing for the differential activity of ClpX mutants or of inhibitors or activators towards ClpX. Therefore, measurement of ATPase activity of the ClpX clones was switched over to the more sensitive kinase GLO assay. All ClpX clones containing the Walker B mutation had reduced ability to hydrolyze ATP as expected (fig. 3.9). The ClpXwt and ClpX I269E clones similarly utilized ATP; however, the ClpX Δ1-64 clone had increased ATP hydrolysis as compared to the wild-type. This result was not unexpected based on work by (59).

Since the activities of the ClpP2/P1 complex and ClpX could be demonstrated separately, we next confirmed that the protease complex and adaptor protein would work together. The SsrA-tagged GFP degradation assay was effective in demonstrating that the ClpX/P2/P1 system was functional (fig. 3.10). We also assessed whether a mutated SsrA-tag (VAA to VDD) would be ignored by ClpX as a negative control and obtained the expected result of a degradation-resistant GFP (data not shown). The ClpXwt protein had the highest rate of degradation and percent difference as compared to all other constructs tested. The ClpX Δ1-64 clones was also able to degrade GFP, however its rate of degradation was slower as compared to the wild-type. A previous study suggested that although ClpX Δ1-64 can still degrade SsrA-tagged GFP, its drop in efficiency as compared to the wild-type may suggest that the ZBD has some importance in the unfoldase activity because of a secondary binding site present in the

ZBD for the GFP-SsrA (59). As expected, no other constructs were able to degrade GFP: ClpX I269E due to its inability to bind to the ClpP2/P1 complex and all of the double mutants containing the Walker B motif mutation due to their inability to utilize ATP to linearize GFP for degradation in the protease complex. Inability of the I269E mutant to form the hetero-complex with ClpP2/P1 as suggested by lack of activity in the GFP assay should be further confirmed through the ATPase assay whereby ATP hydrolysis would remain unchanged in the presence of ClpP2/P1. Addition of the protease components typically reduces ATPase activity of ClpX unless a substrate is present (77). Complex formation could also be assessed using native-PAGE or gel filtration chromatography.

Unfortunately, single mutant constructs of R230A (inability to recognize SsrA-tag) and V156F (inability to translocate substrates to the ClpP2/P1 complex) were not created in time to be tested and included in this study. The R230A mutant should not engage the SsrA tag and will be helpful for assessing the importance of non-SsrA functions when expressed *in vivo* while the V156F mutant should not be able to translocate substrates into the ClpP2/P1 complex. The latter should be confirmed in the GFP degradation assay and this translocation mutant should be useful for identify ClpX substrates *in vivo* by functioning as a "substrate trap" that binds, but does not degrade substrates. While the single mutants were not tested, we hypothesize that they will generate similar results to their double mutant partners. Overall, our data demonstrates a functional ClpX/P2/P1 complex *in vitro* and the first characterization of conserved motifs in the chlamydial ClpX.

As our study mainly focuses on the *in vitro* characterization of the chlamydial ClpX/P2/P1 system, efforts to identify other substrates and adaptor proteins will be done *in vivo* by the Ouellette group at UNMC. Upon identification of other adaptors or substrates, it will be important to test these substrates in degradation assays to both further elucidate motif activity in ClpX and to confirm if identified proteins really are substrates of the ClpX/P2/P1 system. Labelling of substrate proteins with FITC as done for the casein assay (fig. 3.5) or simple Coomassie Brilliant Blue staining of SDS-PAGE resolved degradation products (55) should allow for analysis of degradation of bona-fide substrates. Further work will also be needed to identify specific activators (or inhibitors) due to previous failures to demonstrate activation of the ClpP2/P1 complex. However, we did identify and validated *in vivo* an inhibitor of ClpX/SsrA-mediated degradation that led to a significant reduction in chlamydial fitness further supporting the Clp system as a druggable target (60). Overall, basic characterization of the ClpX/P2/P1 system has shown that it functions in a similar manner to other ClpXP systems, although we predict that additional activities of the ClpX/P2/P1 system specific to *Chlamydia* are present and future work will be needed to test this hypothesis. In support of chlamydial specific functions, the mentioned ClpX inhibitor and overexpression of ClpX mutants led to an RB to EB developmental defect in a cell culture infection model (60).

ClpCP / McsAB

In *B. subtilis*, where this system is most well characterized, the ClpCP / McsAB system functions in the degradation of phosphoarginine-tagged proteins. Although it is an almost exclusively gram positive system, we hypothesize that it will function in a similar manner in *Chlamydia,* which is gram negative. The ClpC/P1/P2 complex should

function similarly to the ClpX/P2/P1 system in that the ClpP2/P1 complex serves as the proteolytic component and ClpC functions in unfolding and linearizing substrates in an ATP-dependent manner. Since we previously hypothesized that ClpX binds to the ClpP2 interface, we hypothesize that ClpC will bind to the ClpP1 interface, although this was not pursued in our study. In *B. subtilis*, McsA acts as the activator of the arginine kinase McsB and together they deliver doomed proteins to the ClpCP complex. Since gram negative bacteria do not have the McsAB system, we performed bioinformatic analysis of the chlamydial McsA and McsB to further test their assignments as homologous to the McsA and McsB proteins seen in gram positive bacteria (fig. 3.11). All McsA proteins contained a conserved UvrB/UvrC motif, which is associated with protein-protein interactions. The UvrABC endonuclease of *E. coli* is involved in excision repair of damaged nucleotides in DNA, but proteins UvrB and UvrC utilize this specific motif to interact with and activate each other and we predict this motif in McsA allows it to form either homo or hetero oligomers (70). When using MUSCLE to align the UvrB/UvrC motifs against the respective McsB of *Chlamydia* and *B. subtilis*, neither motif in the McsA proteins aligned with regions in the McsB proteins, suggesting that this motif in McsA may function in dimerization of McsA or interaction with other proteins in the cell. The *Ct* McsA retains all conserved cysteine residues and shares an additional cysteine with its close neighbor *C. pneumoniae* that is absent from the other bacteria assessed. Although we are unsure of the function of the "extra" cysteine residues, we hypothesize based on other McsA homologs that the conserved cysteines will function as redox-sensitive activators of McsB. In *Chlamydia*'s developmental cycle, EBs are generally oxidized while RBs are generally reduced. In the case of McsA, we

predict it will be inactive while oxidized (thus inactivating McsB) and active while reduced. Although no *in vitro* data was collected on the function of redox on McsA, *in vivo* our collaborator constructed a triple AxxA mutant in the conserved cysteine residues 11/14, 64/66, and 83/85 (highlighted in red on fig. 3.11A and circled in fig. 3.11B) in McsA and expressed it during infection. They demonstrated a lack of staining for an EB-associated marker HctB in the triple mutant expressing strain at the same time point where abundant HctB was detected in the wild-type strain. The results suggest a delay in progression through the developmental cycle in the presence of the redox insensitive McsA. Future work for McsA in relation to its role in redox signaling should be addressed both *in vitro* and *in vivo*. A click-PEG redox labelling system (78) to test the redox status of McsA as *Chlamydia* progresses through the development cycle would be informative and one could use the click-PEG system either *in vitro* or *in vivo* to discern which cysteines are oxidized and when oxidation occurs. The click-PEG system works by alkylating a reduced thiol with propargyl-maleimide and then conjugating it with an azide-PEG of high molecular weight (e.g. 5kDa) using copper-catalyzed Click chemistry leading to altered migration of labeled protein on SDS-PAGE. Two other potentially interesting aspects of the chlamydial McsA as compared to the other aligned McsA proteins are a missing stretch of 19 amino acids between ~80-100 (on the ruler on fig. 3.11A) and the insertion of 9 amino acids between positions ~135-145.

McsB proteins typically retain three conserved motifs (fig. 3.11C). First, the ADP binding site that enables ATP to be a phosphate donor, which corresponds with the activation of McsB via phosphorylation (as seen in the *B. subtilis* McsAB model). The

second motif is the phosphagen binding site. To satisfy short-term energy requirements, broadly classified, phosphagen kinases can catalyze the reversible transfer of a phosphate from phosphorylated guanidine molecules such as phosphoarginine or phosphocreatine to ADP. We hypothesize that the chlamydial McsB functions as an arginine kinase and has homology with the phosphagen kinases/phosphagen binding site owing to the similar mechanism of action and phosphorylation substrates used by both phosphagen kinases and arginine kinases. Finally, all of the McsB proteins share the substrate specificity loop for substrate binding. However, it should be noted that *Ct* McsB it is missing some key residues associated with other bacterial arginine kinases (71). While this does not exclude the chlamydial McsB from being an arginine kinase, it will be critical to confirm activity and to test if it can phosphorylate other residues instead or in addition to arginine.

To begin characterization of the chlamydial ClpC/P2/P1 / McsAB system *in vitro*, we first needed purified protein. Since ClpP1, ClpP2, and ClpC could already be purified, conditions for purification of McsA and McsB were the focus of Aim 2 of the thesis. For McsA, the only condition tested that produced soluble protein that could be purified was MBP-tagged McsA from the pMAL-c5X vector. Despite codon optimization and use of *B. subtilis* as an expression system, we were unable to generate soluble McsA that encoded a tag smaller than that of MBP. However, codon optimization of McsA and expression in *E. coli* produced promising induction trials for a His-tagged version, so solubility trials of this protein should still be pursued (fig. 3.24). If future attempts to produce soluble codon optimized McsA still fail, an optimal procedure to cleave the MBP tag from McsA has already been determined, so McsA alone could be

used in future activity assays. Removal of the MBP tag may prove critical as the large tag could interfere with McsA function by blocking protein-protein interactions.

Since we were unable to test McsA in an *in vitro* assay due to the inability to get purified McsB, we attempted a thermotolerance assay using both the *Bs* McsA as a control and *Ct* McsA since the McsAB system is used during the heat stress response in *B. subtilis*. Both the wild-type 168 and *Bs* McsA – IPTG grew at the same rate, with the *Bs* McsA + IPTG lagging slightly behind (fig. 3.27). This slight lag could just be due to adding IPTG at the start of growing the culture, which has been shown to cause a delay in growth (72). The *Bs* 168 Δ*mcsA* and *Ct* McsA – IPTG both grew at the same rate, while the *Ct* McsA + IPTG grew slightly faster. While the result of the *Ct* McsA + IPTG might suggest some complementation of the *B. subtilis* McsAB system, we were unable to determine a condition in which the *Ct* McsA complemented strain grew similarly to any of the strains containing the *Bs* McsA. Two potential explanations for this include: 1) the *Ct* McsA is not able to complement the *Bs* McsAB system or 2) there may not be complementation because the assay was done at 53°C, but *Chlamydia* typically grow at 37°C so the *Ct* McsA is simply unable to function at that high of a temperature. Therefore, a different complementation assay that does not include a high temperature condition such as transformation efficiency via natural competence should be attempted. For McsB, none of the conditions tested produced soluble protein that could be purified. However, codon optimized McsB produced the best induction condition seen throughout this entire study (fig. 3.24), so despite initial failures to get soluble protein, it should still be pursued for solubility and purification by varying lysis conditions.

In conclusion, our work has set the stage for more detailed characterization of the Clp system both *in vitro* and *in vivo*. We can now purify all components except McsB using *E. coli* as a surrogate host and have established assays to measure Clp functions including oligomerization, ATP hydrolysis (shown for ClpX, applicable to ClpC), and various degradation assays. Our assay "toolbox" will be critical for teasing apart the roles of different Clp-conserved motifs in Clp complex function and for the development of chlamydial-specific Clp-inhibitors and activators. In addition, our combined *in vitro* and *in vivo* data also highlight the critical role of the Clp system in chlamydial fitness and development, further supporting the system as a therapeutic target and its importance for chlamydial proteostasis.

REFERENCES

1. Everett KD. 2000. *Chlamydia* and *Chlamydiales*: more than meets the eye. Veterinary microbiology 75:109-126.
2. Elwell C, Mirrashidi K, Engel J. 2016. *Chlamydia* cell biology and pathogenesis. Nature Reviews Microbiology 14:385-400.
3. Rohde G, Straube E, Essig A, Reinhold P, Sachse K. 2010. Chlamydial zoonoses. Deutsches arzteblatt international 107:174.
4. Knittler MR, Sachse K. 2015. *Chlamydia psittaci*: update on an underestimated zoonotic agent. Pathogens and disease 73:1-15.
5. Di Pietro M, Filardo S, Romano S, Sessa R. 2019. *Chlamydia trachomatis* and *Chlamydia pneumoniae* interaction with the host: Latest advances and future prospective. Microorganisms 7:140.
6. Paavonen J, Eggert-Kruse W. 1999. *Chlamydia trachomatis*: impact on human reproduction. Human reproduction update 5:433-447.
7. Magill AJ, Ryan ET, Hill DR, Solomon T. 2012. Hunter's Tropical Medicine and Emerging Infectious Disease: Expert Consult-Online and Print. Elsevier Health Sciences.
8. Organization WH. 2016. Trachoma.
9. Pathela P, Blank S, Schillinger JA. 2007. Lymphogranuloma venereum: old pathogen, new story. Current infectious disease reports 9:143-150.
10. Hafner LM, Wilson DP, Timms P. 2014. Development status and future prospects for a vaccine against *Chlamydia trachomatis* infection. Vaccine 32:1563-1571.
11. Prevention CfDCa. 2018. Sexually Transmitted Disease Surveillance 2018.
12. Dugan J, Rockey DD, Jones L, Andersen AA. 2004. Tetracycline resistance in *Chlamydia suis* mediated by genomic islands inserted into the chlamydial inv-like gene. Antimicrobial agents and chemotherapy 48:3989-3995.
13. Somani J, Bhullar VB, Workowski KA, Farshy CE, Black CM. 2000. Multiple drug-resistant *Chlamydia trachomatis* associated with clinical treatment failure. The Journal of infectious diseases 181:1421-1427.
14. Mestrovic T, Ljubin-Sternak S. 2018. Molecular mechanisms of *Chlamydia trachomatis* resistance to antimicrobial drugs. Front Biosci 23:656-670.
15. Ory EM, Yow EM. 1963. The use and abuse of the broad spectrum antibiotics. JAMA 185:273-279.
16. Palmer HM, Young H, Winter A, Dave J. 2008. Emergence and spread of azithromycin-resistant *Neisseria gonorrhoeae* in Scotland. Journal of antimicrobial chemotherapy 62:490-494.
17. AbdelRahman YM, Belland RJ. 2005. The chlamydial developmental cycle. FEMS microbiology reviews 29:949-959.
18. Fields KA, Hackstadt T. 2002. The chlamydial inclusion: escape from the endocytic pathway. Annual review of cell and developmental biology 18:221-245.
19. Brunham RC, Rey-Ladino J. 2005. Immunology of *Chlamydia* infection: implications for a *Chlamydia trachomatis* vaccine. Nature reviews immunology 5:149-161.
20. Abdelrahman Y, Ouellette SP, Belland RJ, Cox JV. 2016. Polarized cell division of *Chlamydia trachomatis*. PLoS pathogens 12:e1005822.

21.   Hogan RJ, Mathews SA, Mukhopadhyay S, Summersgill JT, Timms P. 2004. Chlamydial persistence: beyond the biphasic paradigm. Infection and immunity 72:1843-1855.

22.   Wang X, Schwarzer C, Hybiske K, Machen TE, Stephens RS. 2014. Developmental stage oxidoreductive states of *Chlamydia* and infected host cells. MBio 5.

23.   Betts-Hampikian H, Fields K. 2011. Disulfide bonding within components of the *Chlamydia* type III secretion apparatus correlates with development. Journal of bacteriology 193:6950-6959.

24.   Liechti G, Kuru E, Hall E, Kalinda A, Brun Y, VanNieuwenhze M, Maurelli A. 2014. A new metabolic cell-wall labelling method reveals peptidoglycan in *Chlamydia trachomatis*. Nature 506:507-510.

25.   Fisher DJ, Adams NE, Maurelli AT. 2015. Phosphoproteomic analysis of the *Chlamydia caviae* elementary body and reticulate body forms. Microbiology 161:1648.

26.   Saka HA, Thompson JW, Chen YS, Kumar Y, Dubois LG, Moseley MA, Valdivia RH. 2011. Quantitative proteomics reveals metabolic and pathogenic properties of *Chlamydia trachomatis* developmental forms. Molecular microbiology 82:1185-1203.

27.   Skipp PJ, Hughes C, McKenna T, Edwards R, Langridge J, Thomson NR, Clarke IN. 2016. Quantitative proteomics of the infectious and replicative forms of *Chlamydia trachomatis*. PLoS One 11:e0149011.

28.   Scidmore MA, Rockey DD, Fischer ER, Heinzen RA, Hackstadt T. 1996. Vesicular interactions of the *Chlamydia trachomatis* inclusion are determined by chlamydial early protein synthesis rather than route of entry. Infection and immunity 64:5366-5372.

29.   Mogk A, Huber D, Bukau B. 2011. Integrating protein homeostasis strategies in prokaryotes. Cold Spring Harbor perspectives in biology 3:a004366.

30.   Santra M, Farrell DW, Dill KA. 2017. Bacterial proteostasis balances energy and chaperone utilization efficiently. Proceedings of the National Academy of Sciences 114:E2654-E2661.

31.   Sabate R, De Groot NS, Ventura S. 2010. Protein folding and aggregation in bacteria. Cellular and Molecular Life Sciences 67:2695-2715.

32.   Bhutani N, Udgaonkar JB. 2002. Chaperonins as protein-folding machines. Current Science:1337-1351.

33.   Merdanovic M, Clausen T, Kaiser M, Huber R, Ehrmann M. 2011. Protein quality control in the bacterial periplasm. Annual review of microbiology 65:149-168.

34.   Fenton WA, Horwich AL. 1997. GroEL-mediated protein folding. Protein science: a publication of the Protein Society 6:743.

35.   Lin Z, Madan D, Rye HS. 2008. GroEL stimulates protein folding through forced unfolding. Nature structural & molecular biology 15:303.

36.   Illingworth M, Hooppaw AJ, Ruan L, Fisher DJ, Chen L. 2017. Biochemical and genetic analysis of the *Chlamydia* GroEL chaperonins. Journal of bacteriology 199.

37.   Schramm FD, Schroeder K, Jonas K. 2020. Protein aggregation in bacteria. FEMS Microbiology Reviews 44:54-72.

38. Mogk A, Bukau B, Kampinga HH. 2018. Cellular handling of protein aggregates by disaggregation machines. Molecular cell 69:214-226.

39. Clausen T, Southan C, Ehrmann M. 2002. The HtrA family of proteases: implications for protein composition and cell fate. Molecular cell 10:443-455.

40. Wood NA, Chung KY, Blocker AM, de Almeida NR, Conda-Sheridan M, Fisher DJ, Ouellette SP. 2019. Initial characterization of the two ClpP paralogs of *Chlamydia trachomatis* suggests unique functionality for each. Journal of bacteriology 201.

41. Tsilibaris V, Maenhaut-Michel G, Van Melderen L. 2006. Biological roles of the Lon ATP-dependent protease. Research in microbiology 157:701-713.

42. Cha SS, An YJ, Lee CR, Lee HS, Kim YG, Kim SJ, Kwon KK, De Donatis GM, Lee JH, Maurizi MR. 2010. Crystal structure of Lon protease: molecular architecture of gated entry to a sequestered degradation chamber. The EMBO journal 29:3520-3530.

43. Gur E, Sauer RT. 2008. Recognition of misfolded proteins by Lon, a AAA+ protease. Genes & development 22:2267-2277.

44. Hani FM. 2020. Using a collection of nonfunctional missense mutants to examine how molecular chaperones and proteases maintain protein homeostasis.

45. Christensen SK, Maenhaut-Michel G, Mine N, Gottesman S, Gerdes K, Van Melderen L. 2004. Overproduction of the Lon protease triggers inhibition of translation in *Escherichia coli*: involvement of the *yefM-yoeB* toxin-antitoxin system. Molecular microbiology 51:1705-1717.

46. Hedstrom L. 2002. Serine protease mechanism and specificity. Chemical reviews 102:4501-4524.

47. Gatsogiannis C, Balogh D, Merino F, Sieber SA, Raunser S. 2019. Cryo-EM structure of the ClpXP protein degradation machinery. Nature structural & molecular biology 26:946-954.

48. Pan S, Malik IT, Thomy D, Henrichfreise B, Sass P. 2019. The functional ClpXP protease of *Chlamydia trachomatis* requires distinct clpP genes from separate genetic loci. Scientific reports 9:1-14.

49. Akopian T, Kandror O, Raju RM, UnniKrishnan M, Rubin EJ, Goldberg AL. 2012. The active ClpP protease from *M. tuberculosis* is a complex composed of a heptameric ClpP1 and a ClpP2 ring. The EMBO journal 31:1529-1541.

50. Thompson MW, Maurizi MR. 1994. Activity and specificity of *Escherichia coli* ClpAP protease in cleaving model peptide substrates. Journal of Biological Chemistry 269:18201-18208.

51. Kirstein J, Molière N, Dougan DA, Turgay K. 2009. Adapting the machine: adaptor proteins for Hsp100/Clp and AAA+ proteases. Nature Reviews Microbiology 7:589-599.

52. Alexopoulos JA, Guarné A, Ortega J. 2012. ClpP: a structurally dynamic protease regulated by AAA+ proteins. Journal of structural biology 179:202-210.

53. Baker TA, Sauer RT. 2012. ClpXP, an ATP-powered unfolding and protein-degradation machine. Biochimica et Biophysica Acta (BBA)-Molecular Cell Research 1823:15-28.

54. Ye F, Li J, Yang C-G. 2017. The development of small-molecule modulators for ClpP protease activity. Molecular BioSystems 13:23-31.

55. Seleem MA, Rodrigues de Almeida N, Chhonker YS, Murry DJ, Guterres ZdR, Blocker AM, Kuwabara S, Fisher DJ, Leal ES, Martinefski MR. 2020. Synthesis and Antichlamydial Activity of Molecules Based on Dysregulators of Cylindrical Proteases. Journal of medicinal chemistry 63:4370-4387.

56. Keiler KC. 2008. Biology of trans-translation. Annu Rev Microbiol 62:133-151.

57. Keiler KC, Feaga HA. 2014. Resolving nonstop translation complexes is a matter of life or death. Journal of bacteriology 196:2123-2130.

58. Moore SD, Sauer RT. 2007. The tmRNA system for translational surveillance and ribosome rescue. Annu Rev Biochem 76:101-124.

59. Wojtyra UA, Thibault G, Tuite A, Houry WA. 2003. The N-terminal zinc binding domain of ClpX is a dimerization domain that modulates the chaperone function. Journal of Biological Chemistry 278:48981-48990.

60. Wood NA, Blocker AM, Seleem MA, Conda-Sheridan M, Fisher DJ, Ouellette SP. 2019. The AAA+ ATPase ClpX Is Critical for Growth and Development of *Chlamydia trachomatis*. bioRxiv:868620.

61. Mahmoud SA, Chien P. 2018. Regulated proteolysis in bacteria. Annual review of biochemistry 87:677-696.

62. Vass RH, Zeinert RD, Chien P. 2016. Protease regulation and capacity during *Caulobacter* growth. Current opinion in microbiology 34:75-81.

63. Krüger E, Völker U, Hecker M. 1994. Stress induction of *clpC* in *Bacillus subtilis* and its involvement in stress tolerance. Journal of bacteriology 176:3360-3367.

64. Schumann W. 2003. The *Bacillus subtilis* heat shock stimulon. Cell stress & chaperones 8:207.

65. Elsholz AK, Michalik S, Zühlke D, Hecker M, Gerth U. 2010. CtsR, the Gram-positive master regulator of protein quality control, feels the heat. The EMBO Journal 29:3621-3629.

66. Claywell JE, Fisher DJ. 2016. CTL0511 from *Chlamydia trachomatis* is a type 2C protein phosphatase with broad substrate specificity. Journal of bacteriology 198:1827-1836.

67. Fisher DJ, Fernández RE, Maurelli AT. 2013. *Chlamydia trachomatis* transports NAD via the Npt1 ATP/ADP translocase. Journal of bacteriology 195:3381-3386.

68. Jung H, Choi Y, Lee D, Seo JK, Kee J-M. 2019. Distinct phosphorylation and dephosphorylation dynamics of protein arginine kinases revealed by fluorescent activity probes. Chemical Communications 55:7482-7485.

69. Moolenaar GF, Franken KL, van de Putte P, Goosen N. 1997. Function of the homologous regions of the *Escherichia coli* DNA excision repair proteins UvrB and UvrC in stabilization of the UvrBC–DNA complex and in 3′-incision. Mutation Research/DNA Repair 385:195-203.

70. Sohi M, Alexandrovich A, Moolenaar G, Visse R, Goosen N, Vernede X, Fontecilla-Camps JC, Champness J, Sanderson MR. 2000. Crystal structure of *Escherichia coli* UvrB C-terminal domain, and a model for UvrB-UvrC interaction. FEBS letters 465:161-164.

71. Suskiewicz MJ, Hajdusits B, Beveridge R, Heuck A, Dai Vu L, Kurzbauer R, Hauer K, Thoeny V, Rumpel K, Mechtler K. 2019. Structure of McsB, a protein kinase for regulated arginine phosphorylation. Nature chemical biology 15:510-518.

72. Malakar P, Venkatesh K. 2012. Effect of substrate and IPTG concentrations on the burden to growth of *Escherichia coli* on glycerol due to the expression of Lac proteins. Applied microbiology and biotechnology 93:2543-2549.

73. Compton CL, Schmitz KR, Sauer RT, Sello JK. 2013. Antibacterial activity of and resistance to small molecule inhibitors of the ClpP peptidase. ACS chemical biology 8:2669-2677.

74. Thomson NR, Holden MT, Carder C, Lennard N, Lockey SJ, Marsh P, Skipp P, O'Connor CD, Goodhead I, Norbertzcak H. 2008. *Chlamydia trachomatis*: genome sequence analysis of lymphogranuloma venereum isolates. Genome research 18:161-171.

75. Jenal U. 2009. The role of proteolysis in the *Caulobacter crescentus* cell cycle and development. Research in microbiology 160:687-695.

76. Stanne TM, Pojidaeva E, Andersson FI, Clarke AK. 2007. Distinctive types of ATP-dependent Clp proteases in cyanobacteria. Journal of Biological Chemistry 282:14394-14402.

77. Joshi SA, Hersch GL, Baker TA, Sauer RT. 2004. Communication between ClpX and ClpP during substrate processing and degradation. Nature structural & molecular biology 11:404-411.

78. van Leeuwen LA, Hinchy EC, Murphy MP, Robb EL, Cochemé HM. 2017. Click-PEGylation–a mobility shift approach to assess the redox state of cysteines in candidate proteins. Free Radical Biology and Medicine 108:374-382.

APPENDIX A

E. COLI AND *B. SUBTILIS* STRAINS WITH PLASMID, ANTIBIOTIC RESISTANCE, AND DESCRIPTION

Clone	Background strain	Resistance	Description
pLATE31 *clpPec*	*E. coli* XL-1 Blue	Amp	Cloning
pLATE31 *clpP1*	*E. coli* XL-1 Blue	Amp	Cloning
pLATE31 *clpP2*	*E. coli* XL-1 Blue	Amp	Cloning
pLATE31 *clpC*	*E. coli* XL-1 Blue	Amp	Cloning
pLATE31 *clpX*	*E. coli* XL-1 Blue	Amp	Cloning
pLATE31 *clpX* E187A	*E. coli* XL-1 Blue	Amp	Cloning
pLATE31 *clpPec*	*E. coli* BL21 (DE3)	Amp	Protein expression
pLATE31 *clpP1*	*E. coli* BL21 (DE3)	Amp	Protein expression
pLATE31 *clpP2*	*E. coli* BL21 (DE3)	Amp	Protein expression
pLATE31 *clpC*	*E. coli* BL21 (DE3)	Amp	Protein expression
pLATE31 *clpX*	*E. coli* BL21 (DE3)	Amp	Protein expression
pLATE31 *clpX* E187A	*E. coli* BL21 (DE3)	Amp	Protein expression
pLATE31 *clpX* I269E	*E. coli* DH5α	Amp	Cloning
pLATE31 *clpX* R230A/E187A	*E. coli* DH5α	Amp	Cloning
pLATE31 *clpX* V165F/E187A	*E. coli* DH5α	Amp	Cloning
pLATE31 *clpX* Δ1-64	*E. coli* DH5α	Amp	Cloning
pLATE31 *clpX* I269E/E187A	*E. coli* DH5α	Amp	Cloning
pLATE31 *clpPec*	*E. coli* ΔPAX	Amp, cm, kan	Protein expression
pLATE31 *clpP1*	*E. coli* ΔPAX	Amp, cm, kan	Protein expression
pLATE31 *clpP2*	*E. coli* ΔPAX	Amp, cm, kan	Protein expression
pLATE31 *clpC*	*E. coli* ΔPAX	Amp, cm, kan	Protein expression
pLATE31 *clpX*	*E. coli* ΔPAX	Amp, cm, kan	Protein expression
pLATE31 *clpX* E187A	*E. coli* ΔPAX	Amp, cm, kan	Protein expression

pLATE31 *clpX* I269E	*E. coli* ΔPAX	Amp, cm, kan	Protein expression
pLATE31 *clpX* R230A/E187A	*E. coli* ΔPAX	Amp, cm, kan	Protein expression
pLATE31 *clpX* V165F/E187A	*E. coli* ΔPAX	Amp, cm, kan	Protein expression
pLATE31 *clpX* Δ1-64	*E. coli* ΔPAX	Amp, cm, kan	Protein expression
pLATE31 c*lpX* I269E/E187A	*E. coli* ΔPAX	Amp, cm, kan	Protein expression
pGex-6p-1 *gfp* VAA full	*E. coli* BL21 (DE3)	Amp	Cloning
pGex-6p-1 *gfp* VAA truncated	*E. coli* BL21 (DE3)	Amp	Cloning
pGex-6p-1 *gfp* VDD full	*E. coli* BL21 (DE3)	Amp	Cloning
pGex-6p-1 *gfp* VDD truncated	*E. coli* BL21 (DE3)	Amp	Cloning
pGex-6p-1 *gfp* VAA full	*E. coli* BL21 (DE3)	Amp	Protein expression
pGex-6p-1 *gfp* VAA truncated	*E. coli* BL21 (DE3)	Amp	Protein expression
pGex-6p-1 *gfp* VDD full	*E. coli* BL21 (DE3)	Amp	Protein expression
pGex-6p-1 *gfp* VDD truncated	*E. coli* BL21 (DE3)	Amp	Protein expression
pGex-6p-1 *gfp* VAA full	*E. coli* ΔPAX	Amp, cm, kan	Protein expression
pGex-6p-1 *gfp* VAA truncated	*E. coli* ΔPAX	Amp, cm, kan	Protein expression
pGex-6p-1 *gfp* VDD full	*E. coli* ΔPAX	Amp, cm, kan	Protein expression
pGex-6p-1 *gfp* VDD truncated	*E. coli* ΔPAX	Amp, cm, kan	Protein expression
pLATE52 *gfp* VAA full	*E. coli* DH5α	Amp	Cloning
pLATE52 *gfp* VAA truncated	*E. coli* DH5α	Amp	Cloning
pLATE52 *gfp* VDD full	*E. coli* DH5α	Amp	Cloning
pLATE52 *gfp* VDD truncated	*E. coli* DH5α	Amp	Cloning
pLATE52 *gfp* VAA full	*E. coli* ΔPAX	Amp, cm, kan	Protein expression
pLATE52 *gfp* VAA truncated	*E. coli* ΔPAX	Amp, cm, kan	Protein expression
pLATE52 *gfp* VDD full	*E. coli* ΔPAX	Amp, cm, kan	Protein expression

pLATE52 *gfp* VDD truncated	*E. coli* ΔPAX	Amp, cm, kan	Protein expression
pACYCDuet-1 *Ct mcsA*	*E. coli* XL-1 Blue	Cm	Cloning
pACYCDuet-1 *Ct mcsB*	*E. coli* XL-1 Blue	Cm	Cloning
pACYCDuet-1 *Ct mcsA and mcsB*	*E. coli* XL-1 Blue	Cm	Cloning
pLATE 31 *mcsA*	*E. coli* XL-1 Blue	Amp	Cloning
pLATE 31 *mcsB*	*E. coli* XL-1 Blue	Amp	Cloning
pLATE 31 *mcsB* and pACYCDuet-1 Ct *mcsA*	*E. coli* BL21 (DE3)	Cm and amp	Protein expression
pACYCDuet-1 *Ct mcsA*	*E. coli* BL21 (DE3)	Cm	Protein expression
pACYCDuet-1 *Ct mcsB*	*E. coli* BL21 (DE3)	Cm	Protein expression
pACYCDuet-1 *Ct mcsA and mcsB*	*E. coli* BL21 (DE3)	Cm	Protein expression
pLATE 31 *mcsA*	*E. coli* BL21 (DE3)	Amp	Protein expression
pLATE 31 *mcsB*	*E. coli* BL21 (DE3)	Amp	Protein expression
pGex-6p-1 *Ct mcsA*	*E. coli* XL-1 Blue	Amp	Cloning
pGex-6p-1 *Ct mcsB*	*E. coli* XL-1 Blue	Amp	Cloning
pMAL-c5X *Ct mcsB*	*E. coli* XL-1 Blue	Amp	Cloning
pMAL-c5X *Ct mcsA*	*E. coli* XL-1 Blue	Amp	Cloning
pGex-6p-1 *Ct mcsA*	*E. coli* ΔPAX	Amp, cm, kan	Protein expression
pGex-6p-1 *Ct mcsB*	*E. coli* ΔPAX	Amp, cm, kan	Protein expression
pMAL-c5X *Ct mcsA*	*E. coli* ΔPAX	Amp, cm, kan	Protein expression
pMAL-c5X *Ct mcsB*	*E. coli* ΔPAX	Amp, cm, kan	Protein expression
pHT08	*E. coli* DH5α	Amp	Cloning
pHT08	*B. subtilis* 168	Cm	Protein expression
pHT08 *Ct mcsA*	*E. coli* DH5α	Amp	Cloning
pHT08 *Ct mcsB*	*E. coli* DH5α	Amp	Cloning
pHT08 *Ct mcsA*	*B. subtilis 168 ΔmcsA*	Cm, kan	Protein expression
pHT08	*B. subtilis 168 ΔmcsA*	Cm, kan	Protein expression
pHT08 *Ct mcsB*	B. subtilis 168 *ΔmcsB*	Cm, kan	Protein expression
pHT08	B. subtilis 168 *ΔmcsB*	Cm, kan	Protein expression

pHT08 *Bs mcsA*	*E. coli* DH5α	Amp	Cloning
pHT08 *Bs mcsB*	*E. coli* DH5α	Amp	Cloning
pHT08 *Bs mcsA*	*B. subtilis 168 ΔmcsA*	Cm, kan	Protein expression
pHT08 *Bs mcsB*	B. subtilis 168 *ΔmcsB*	Cm, kan	Protein expression
pLATE52 codon opt. gBlock of *Ct mcsA*	*E. coli* DH5α	Amp	Cloning
pLATE52 codon opt. gBlock of *Ct mcsB*	*E. coli* DH5α	Amp	Cloning
pLATE52 codon opt. gBlock of *Ct mcsA*	*E. coli* ΔPAX	Amp, cm, kan	Protein expression
pLATE52 codon opt. gBlock of *Ct mcsB*	*E. coli* ΔPAX	Amp, cm, kan	Protein expression
pHT08 codon opt. gBlock of *Ct mcsA*	*E. coli* DH5α	Amp	Cloning
pHT08 codon opt. gBlock of *Ct mcsB*	*E. coli* DH5α	Amp	Cloning
pHT08 codon opt. gBlock of *Ct mcsA*	B. subtilis 168 *ΔmcsA*	Cm, kan	Protein expression
pHT08 codon opt. gBlock of *Ct mcsB*	B. subtilis 168 *ΔmcsB*	Cm, kan	Protein expression

APPENDIX B

BUFFER LIST

Buffer	Components
ClpP lysis / wash buffer	25 mM Tris Base [pH 7.5], 150 mM NaCl, 10 mM Imidazole, 10% glycerol
ClpP elution buffer	25 mM Tris Base [pH 7.5], 150 mM NaCl, 300 mM Imidazole, 10% glycerol
ClpP storage buffer	25 mM Tris Base [pH 7.5], 150 mM NaCl, 10% glycerol
ClpX lysis / wash buffer	25 mM Tris Base [pH 7.5], 300 mM NaCl, 10 mM Imidazole
ClpX elution buffer	25 mM Tris Base [pH 7.5], 300 mM NaCl, 300 mM Imidazole
ATPase assay buffer	25 mM HEPES [pH 7.2], 200 mM KCl, 20 mM $MgCl_2$, 10% glycerol
GFP lysis buffer	50 mM NaH_2PO_4 [pH 8], 300 mM NaCl, 20 mM Imidazole, protease inhibitor
GFP wash buffer	50 mM NaH_2PO_4 [pH 8], 300 mM NaCl, 20 mM Imidazole
GFP elution buffer	50 mM NaH_2PO_4 [pH 8], 300 mM NaCl, 300 mM Imidazole
GFP storage buffer	50 mM NaH_2PO_4 [pH 8], 300 mM NaCl, 10% glycerol
pACYCDuet-1 McsA lysis buffer	50 mM NaH_2PO_4 [pH 7.8], 300 mM NaCl, 10 mM Imidazole, 0.1% Triton X-100, 10% glycerol, 1 mg/mL lysozyme, protease inhibitor
pACYCDuet-1 McsA wash buffer	50 mM NaH_2PO_4 [pH 7.8], 300 mM NaCl, 10 mM Imidazole, 0.1% Triton X-100, 10% glycerol
pACYCDuet-1 McsA elution buffer	50 mM NaH_2PO_4 [pH 7.8], 300 mM NaCl, 300 mM Imidazole, 0.1% Triton X-100, 10% glycerol
pACYCDuet-1 McsA storage buffer	20 mM HEPES [pH 7.4], 200 mM KCl, 10% glycerol
McsA lysis buffer	50 mM NaH_2PO_4 [pH 7.8], 300 mM NaCl, 10 mM Imidazole, 0.1% Triton X-100, 10% glycerol, 1 mM DTT, 1 mg/mL lysozyme, protease inhibitor
McsA wash buffer	50 mM NaH_2PO_4 [pH 7.8], 300 mM NaCl, 10 mM Imidazole, 0.1% Triton X-100, 10% glycerol, 1 mM DTT
McsA elution buffer	50 mM NaH_2PO_4 [pH 7.8], 300 mM NaCl, 1 mM DTT, 10 mM maltose, 10% glycerol
McsA storage buffer	50 mM NaH_2PO_4 [pH 7.8], 300 mM NaCl, 10% glycerol
Cleavage buffer	20 mM Tris-HCl [pH 8], 100 mM NaCl, 2 mM CaCl2
Buffer E	50 mM Tris-HCl [pH 8], 200 mM KCl, 1 mM DTT

Buffer F	50 mM Tris-HCl [pH 8], 200 mM KCl, 1 mM DTT, 200 mM trisodium citrate
Buffer PZ	25 mM HEPES [pH 7.6], 200 mM KCl, 5 mM MgCl2, 1 mM DTT, 10% glycerol
Oligomerization Buffer	25 mM Tris Base [pH 7.5], 5 mM KCl, 5 mM $MgCl_2$, 1 mM DTT, 10% glycerol
Native Running Buffer	30 g Tris base, 144 g glycine, dH2O to 1 L
Native Sample Buffer	5 mM Tris [pH 6.8], 38 mM glycine, 0.06% bromophenol blue
2xYT medium*	2xYT: in 500 mL → 8 g tryptone, 5 g yeast extract, 2.5 g NaCl
10X S-base*	2 g $(NH_4)_2SO_4$, 14 g K_2HPO_4, 6 g KH_2PO_4, 1 g sodium citrate, add ddH_2O to 100 mL and autoclave, add 0.1 mL of filter sterilized 1 M $MgSO_4$
HS medium*#	66.5 mL ddH_2O, 10 mL 10X S-base, 2.5 mL 20% glucose, 5 mL 0.1% L-tryptophan, 1 mL 2% casamino acids, 5 mL 10% yeast extract, 10 mL 8% arginine / 0.4% histidine
LS medium*#	80 mL ddH_2O, 10 mL 10X S-base, 2.5 mL 20% glucose, 0.5 mL 0.1% L-tryptophan, 0.5 mL 2% casamino acids, 5 mL 2% yeast extract, 0.25 mL of 1 M $MgCl_2$, 0.05 mL of 1 M $CaCl_2$
Bacillus subtilis Electroporation Buffer*	0.5 M trehalose, 0.5 M sorbitol, 0.5 M mannitol, 0.5 mM $MgCl_2$, 0.5 mM K_2HPO_4, pH 7.4, molecular grade water
Bacillus subtilis Electroporation Recovery Buffer*#	2xYT broth containing 0.5 M sorbitol and 0.38 M mannitol
Bacillus subtilis 5X SDS Lysis Buffer	20 mM Tris, 15% w/v sucrose
Bacillus subtilis SDS Sample Buffer	50 mM Tris [pH 6.8], 100 mM DTT, 30% v/v glycerol, 10% w/v SDS, 0.02% Bromophenol Blue
Urea Lysis Buffer	50 mM Tris [pH 7.4], 7 M Urea, 300 mM NaCl, 10 mM Imidazole
Urea Elution Buffer	50 mM Tris [pH 7.4], 7 M Urea, 300 mM NaCl, 150 mM Imidazole

*Bacillus subtilis Pgrac01 Expression Vectors manual from MoBiTec
#Autoclave all components separately then combine, filter sterilize L-tryptophan

Vector / Insert	Sequence (5'-3')
pLATE31 *clpPec* F	AGAAGGAGATATAACTATGTCATACAGCGGCGAACGAG
pLATE31 *clpPec* R	GTGGTGGTGATGGTGATGGCCATTACGATGGGTCAGAATCGAATCG
pLATE31 *clpP1* F	AGAAGGAGATATAACTATGCCTGAAGGGGAAATGATGCATAAG
pLATE31 *clpP1* R	GTGGTGGTGATGGTGATGGCCCAAGTCGTTAAAAGAGAAGAGAATCCC
pLATE31 *clpP2* F	AGAAGGAGATATAACTATGACGTTGGTACCATACGTTGTTGAAG
pLATE31 *clpP2* R	GTGGTGGTGATGGTGATGGCCAGACGCAATACTCTTATCTTTTGTC
pLATE31 *clpC* F	AGAAGGAGATATAACTATGTTTGAGAAGTTTACCAATCGCGCAAAGCAAG
pLATE31 *clpC* R	GTGGTGGTGATGGTGATGGCCTGATTCATCAGCTGTAATAG
pLATE31 *clpX* F	AGAAGGAGATATAACTATGACAAAAAAAAATCTTGCGGTCTGTTC
pLATE31 *clpX* R	GTGGTGGTGATGGTGATGGCCAGCAATCGCCTCTGGTGATTTC
pLATE31 *clpX* Δ1-64 F	AGAAGGAGATATAACTATGAGAGTGTTAACCCCTAAAG
pLATE52 *gfp* F	GGTTGGGAATTGCAAAGTAAAGGAGAAGCACTTTTCACTGGAG
pLATE52 *gfp* VAA full R	GGAGATGGGAAGTCATTATTAAGCAGCTACGCGTAGATC
pLATE52 *gfp* VAA trunc R	GGAGATGGGAAGTCATTATTAAGCAGCTACCTTGTATAGTTCATC
pLATE52 *gfp* VDD full R	GGAGATGGGAAGTCATTATTAATCATCTACGCGTAGATCTTCGAGATC
pLATE52 *gfp* VDD trunc R	GGAGATGGGAAGTCATTATTAATCATCTACCTTGTATAGTTCATCCATGC
pGex-6p-1 *gfp* F	CTGGGATCCAGTAAAGGAGAAGCACTTTTCAC
pGex-6p-1 *gfp* VAA full R	AACCGGCCGTTAAGCAGCTACGCGTAGATCTTCG
pGex-6p-1 *gfp* VAA trunc R	CGAGTCGACTTAAGCAGCTACCTTGTATAGTTCATCCATG
pGex-6p-1 *gfp* VDD full R	AACCGGCCGTTAATCATCTACGCGTAGATCTTCG
pGex-6p-1 *gfp* VDD trunc R	CGAGTCGACTTAATCATCTACCTTGTATAGTTCATCCATGCCATGTGTAATC

pLATE31 *mcsB* F	AGAAGGAGATATAACTATGCTCCCTAATCATATTCTTAC
pLATE31 *mcsB* R	GTGGTGGTGATGGTGATGGCCGATTCGAATAATCAGTCGCTC TGCC
pLATE31 *mcsA* F	AGAAGGAGATATAACTATGGATCATACAGAAGAGTCTCCTGC TCTTTG
pLATE31 *mcsA* R	GTGGTGGTGATGGTGATGGCCGGGAGCATCGGTAGTATTCT G
pGex-6p-1 *mcsA* F	CTGGGATCCGATCATACAGAAGAGTCTCCTGCTCTTTG
pGex-6p-1 *mcsA* R	CCGCTCGAGTCAGGGAGCATCGGTAGTATTC
pGex-6p-1 *mcsB* F	CTGGGATCCCTCCCTAATCATATTCTTAC
pGex-6p-1 *mcsB* R	CCGCTCGAGTCAGATTCGAATAATCAGTCG
pMAL-c5X *mcsA* F	TGGGCGGCCGCGATCATACAGAAGAGTCTCCTGCTCTTTG
pMAL-c5X m*csA* R	TTCGGATCCTCAGGGAGCATCGGTAGTATTC
pMAL-c5X *mcsB* F	TGGGCGGCCGCCTCCCTAATCATATTCTTACTGC
pMAL-c5X *mcsB* R	TTCGGATCCTCAGATTCGAATAATCAG
pACYCDuet-1 *mcsA* F	CCAGGATCCAGATCATACAGAAGAGTCTCCTGCTCTTTG
pACYCDuet-1 *mcsA* R	TATGCGGCCGCTTAGGGAGCATCGGTAGTATTC
pACYCDuet-1 *mcsB* F	ATACATATGCTCCCTAATCATATTCTTACTGCTATC
pACYCDuet-1 *mcsB* R	AGACTCGAGGATTCGAATAATCAGTCGCTC
pHT08 sequencing primer F	CCTCGTTTCCACCGGAATTAGCTTG
pHT08 sequencing primer R	GCCGATATTAGCCTCGTATG
pHT08 *Ct mcsA* F	CACGGATCCGATCATACAGAAGAGTCTCCTGCTCTTTG
pHT08 *Ct mcsA* R	TGCCCCGGGTTAGGGAGCATCGGTAGTATTCTG
pHT08 *Ct mcsB* F	CACGGATCCCTCCCTAATCATATTCTTACTGCTATCG
pHT08 *Ct mcsB* R	TGCCCCGGGTTAGATTCGAATAATCAGTCGCTCTGCCTGG

pHT08 *Bs mcsA* F	CACGGATCCTTGATTTGTCAAGAGTGCCACGAGAG
pHT08 *Bs mcsA* R	TGCCCCGGGTTACTCCTGTTCCTCCTCACTATC
pHT08 *Bs mcsB* F	CACGGATCCTCGCTAAAGCATTTTATTCAG
pHT08 *Bs mcsB* R	TGCCCCGGGTCATATCGATTCATCCTCCTGTC
Codon opt. pLATE52 *Ct mcsA* F	CGGTTGGGAATTGCAAGATCACACCGAGGAATCTCCTGCTCTG
Codon opt. pLATE52 *Ct mcsA* R	CGGAGATGGGAAGTCATTAAGGGGCATCGGTCGTGTTCTGG
Codon opt. pLATE52 *Ct mcsB* F	TCCGGTTGGGAATTGCAACTGCCGAACCACATCCTG
Codon opt. pLATE52 *Ct mcsB* R	CGGAGATGGGAAGTCATTAGATGCGGATGATCAGACG

VITA

Graduate School
Southern Illinois University

Amanda M. Blocker

a.blocker23@yahoo.com

Southern Illinois University Carbondale
Bachelor of Science, Microbiology, May 2019

Special Honors and Awards:
   Master's Fellowship, Southern Illinois University, 2019

Thesis Paper Title:
   Characterization of Proteostasis Mechanisms in *Chlamydia trachomatis*

Major Professor: Dr. Derek J. Fisher

Publications:
1. Wood, N. A., Chung, K. Y., Blocker, A. M., de Almeida, N. R., Conda-Sheridan, M., Fisher, D. J., & Ouellette, S. P. (2019). Initial characterization of the two ClpP paralogs of *Chlamydia trachomatis* suggests unique functionality for each. *Journal of bacteriology*, *201*(2).
2. Wood, N. A., Blocker, A. M., Seleem, M. A., Conda-Sheridan, M., Fisher, D. J., & Ouellette, S. P. (2020). The ClpX and ClpP2 Orthologs of *Chlamydia trachomatis* Perform Discrete and Essential Functions in Organism Growth and Development. *Mbio*, *11*(5).
3. Seleem, M. A., Rodrigues de Almeida, N., Chhonker, Y. S., Murry, D. J., Guterres, Z. D. R., Blocker, A. M., ... & Conda-Sheridan, M. (2020). Synthesis and Antichlamydial Activity of Molecules Based on Dysregulators of Cylindrical Proteases. *Journal of medicinal chemistry*, *63*(8), 4370-4387.